Bergslagen, etapp 2

Investigation of layered gabbroic intrusions, Bergslagen

Dick Claeson & Daniel Sopher

mars 2021

SGU-rapport 2021:18

SGU Geological Survey of Sweden

Cover photo: Layered gabbroic rock at Pappas kullar, the Flinten intrusion (6723543/554218).
Photographer: Dick Claeson.

Author: Dick Claeson, Daniel Sopher
Reviewed by: Magnus Ripa, Johan Jönberger
Head of unit: Ildikó Antal Lundin

Editor: Lina Rönnåsen

Geological Survey of Sweden
Box 670, 751 28 Uppsala, Sweden
phone: 018-17 90 00
e-mail: sgu@sgu.se

www.sgu.se

TABLE OF CONTENTS

SAMMANFATTNING

Projektet *Bergslagen, etapp 2 – regional* ingår i SGUs systematiska geologiska undersökningar av prospekteringsintressanta områden, där delprojektet Basiska intrusioner ingår (se www.sgu.se under Mineralnäring/Mineralinformation/Kartering i Bergslagen).

Bergslagen är en av Sveriges viktigaste malmprovinser där gruvdrift har pågått i mer än 1 000 år. Utöver att vara en region med många järn-, basmetall- och ädelmetallfyndigheter, har Bergslagen också potential för innovationskritiska metaller och mineral. Behovet av metaller och mineral ökar och har aldrig varit större än vad det är idag. Inom EU finns ett särskilt intresse för så kallade ”kritiska material” som bland annat behövs i grön teknik som elbilar, batterier, vindkraftverk och solceller. Även efterfrågan på andra metaller ökar. Klimatförändringar och energiomställningen utgör en utmaning för råvaruförsörjningen.

I samband med SGUs undersökningar av berggrunden i Ludvikaområdet så konstaterades kraftigt förhöjda halter av innovationskritiska metaller inom platinagruppen (PGE) i mineraliseringen i en äldre nickel- och koppargruva vid Brunnsjöberget, Hedemora (Claeson m.fl. 2018, 2019). Förekomst av basmetaller är av avgörande betydelse för att man ska kunna få ekonomi för en eventuell brytning av de mer sällsynta metallerna. Sedan tidigare var det känt att man vid intrusionen Flinten funnit anomala halter PGE i lokala block men inte i fast klyft (Filén m.fl. 1989, Filén 1990).

Mot denna bakgrund beslutades om en mindre insats för att studera några förekomster av basiska intrusioner och analysera berggrunden med hjälp av geofysik och litogeokemi samt utföra fältuppföljningar inom Bergslagen. Ytterligare förekomster i äldre gruvområden har besökts och genom litogeokemisk provtagning analyserats med avseende på ett stort antal grundämnen.

Syftet med projektet är att uppdatera de lokala berggrundsgeologiska och geofysiska databaserna, vilka kan utgöra planerings- och resurshushållningsunderlag för prospekteringsföretag, kommuner och länsstyrelser med flera i Bergslagen. Databaserna från projektet kommer att omfatta kartor, hällobservationer, litogeokemi, mineralfyndigheter, petrofysiska egenskaper och geofysiska markmätningar. Projektarbetet startade i början på året 2019 och avslutas i början av 2021.

Sommaren och hösten 2019 utfördes geologiska och geofysiska fältundersökningar vid den lagrade basiska intrusionen Flinten, samt litogeokemisk provtagning vid gruvor i gabbroida bergarter vid Kuså och Gaddebo. Under november–december 2019 gjordes flyggeofysiska TEM-mätningar med helikopter över Flinten med omgivning. Under en vecka i maj 2020 genomfördes geologiska och geofysiska fältundersökningar vid den lagrade basiska intrusionen Fullen och två närliggande basiska kroppar vid Furulund och Skållberget i trakterna av Hofors. Petrofysiska mätningar på delar av de insamlade bergarterna utfördes vid SGUs laboratorium under 2019 och 2020.

Denna rapport redovisar huvudsakligen nytillkommen information från fältsäsongen 2019 och 2020, modellering från de markgeofysiska mätningarna, petrofysiska mätningar, de helikopterburna TEM-mätningarna och litogeokemiska analysresultat.

De basiska intrusionerna i Bergslagen visar lovande potential för att både basmetaller, som till exempel nickel och koppar, tillsammans med PGE kan förekomma i ekonomiskt signifikanta koncentrationer. Det är dock inte mycket känt om omfattningen av mineraliseringar eller extraherbarheten för vissa mineral eller grundämnen i dessa. Trots att ingen gruvdrift av PGE har skett i Bergslagenregionen visar denna studie att det finns potential, både i större lagrade intrusioner och i sulfidgruvor med nickel och koppar i Bergslagen. De kända Ni-Cu-sulfidgruvorna finns ofta i mindre, gabbroiska kroppar och uppvisar således ingen uppenbar relation till större lagrade intrusioner. Dock är geometrin för dessa magmatiska system fortfarande okänd och därför är det okänt om de kan ha någon koppling till större magmatiska kroppar på större djup i krustan.

Inom denna studie har geometrin för den magmatiska lagringen inom både Flinten- och Fullen-intrusionerna tolkats, baserat främst på data från magnetfältet som uppmätts med flyg och observationer vid hällblottningar. Dessutom har de magmatiska bergartslagrens magnetiska egenskaper modellerats i två dimensioner och i fallet med Flinten-intrusionen även i 3-dimensioner. Magnetiska mätningar gjorda över ett litet fokusområde vid Fullen-intrusionen visar utmärkt korrelation mellan de magnetiska anomaliernas orientering och magmatisk lagring i hällarna, vilket ger ett gott stöd för tolkningarna. Vid Flinten-intrusionen visar observationerna och de magnetiska mätningarna från ett litet fokusområde ett mer komplext förhållande. Detta indikerar att även om lagringsgeometrin som tolkas från de flygmätta data vid Flinten sannolikt är representativ i stor skala, kan den ha en mer komplex geometri när man studerar i en mindre skala. Karaktäriseringen av lagringen av dessa intrusioner, om än i stor skala, kan vara användbar information för framtida geofysiska och geologiska undersökningar. Till exempel tillhandahåller de ett verktyg för att förutsäga orienteringen av eventuella potentiella sulfidmineraliseringar i form av lager, vilka kan associeras med till exempel PGE och andra ädla metaller. Detta kan även vara användbart för att utforma och optimera framtida undersökningsmetoder, såsom markbaserade elektromagnetiska mätningar.

Baserat på de luftburna och markbaserade elektromagnetiska mätningarna som presenteras i denna rapport har flera zoner med lägre resistivitetsvärden än deras omgivningar markerats. I vissa fall verkar dessa zoner ligga nästan parallellt med den tolkade riktningen för den magmatiska lagringen. Sådana områden kan vara av intresse för vidare utredning.

En tolkning av Flinten-intrusionens struktur presenteras i denna studie, baserat på den observerade lagringens riktning, luftburna magnetiska mätningar och gravitationsdata. I denna tolkning är intrusionen uppdelad i fem regioner, vilka tolkas representera enskilda delintrusioner. Baserat på deras geofysiska egenskaper kan dessa regioner ordnas i två grupper (tre norra regioner och två södra regioner), där delintrusionerna inom varje grupp tolkas som mer eller mindre samtida. Två- och tredimensionell modellering av gravitation och magnetiska data stöder denna tolkning. Denna karakterisering kan vara intressant att utforska vidare, eftersom den kan indikera systematiska skillnader i kemi och fysikaliska egenskaper inom de olika delarna av Flinten-intrusionen. Det är dock viktigt att notera att innan en sådan tolkning kan underbyggas bättre skulle mycket mer data, till exempel litogeokemiska och petrofysiska prover, behöva samlas in och analyseras.

Ytterligare undersökningar av de basiska intrusionerna inom Bergslagen kan bestå av omfattande markgeofysiska mätningar, omfattande litogeokemiska provtagningar och analyser, bestämning av mineraler och deras sammansättning, textur, strukturgeologi och när en potentiell sulfidmineralisering lokaliseras även kärnborrning. Sådana undersökningar utfördes dock inte som en del av detta projekt på grund av kostnader och tidsbegränsningar.

Den finansiella kostnaden för denna första bedömning av den ekonomiska potentialen för lagrade intrusioner i Bergslagenregionen har varit relativt låg. Trots detta har metoderna och tillvägagångssättet som tillämpats i denna studie visat sig vara effektiva för att karakterisera strukturen, de kemiska och fysiska egenskaperna hos de undersökta intrusionerna och skulle därför vara bra att använda i framtida undersökningar av basiska intrusioner, inom Sverige eller någon annanstans. Denna studie ger också ett exempel på vad som kan uppnås när omfattande data från SGUs befintliga databaser utnyttjas tillsammans med nya data, från relativt småskaliga men fokuserade markbaserade undersökningar.

Lägesbestämningar har gjorts i koordinatsystemet Sweref 99 TM.

Uppdatering av SGUs databaser (malmkemi, bergartskemi, geofysiska data) sker kontinuerligt allt eftersom resultat från nya analyser och mätresultat kommer in från SGUs Bergslagsprojekt.

ABSTRACT

Presently, global demand for innovation-critical metals, such as PGEs, is high and continues to grow. The Geological Survey of Sweden (SGU) has conducted a study to investigate the potential for PGE as well as base metal deposits in basic intrusions within the Bergslagen region, Sweden. The study focuses on the Flinten and Fullen intrusions but also addresses a series of abandoned mines within other basic intrusions, such as the Kuså gruvor and Gaddebo gruvor.

As part of this study, new field investigations were performed during 2019 and 2020, which included geological observations, collection of petrophysical and lithogeochemical samples and outcrop measurements of natural gamma radiation and magnetic susceptibility. Furthermore, magnetic field and VLF measurements were collected along a series of profiles. New airborne geophysical data collected over the Flinten and Fullen intrusions as well as gravity measurements are also included in the study. These data have been processed, interpreted, and modelled in 2- and 3-dimensions to characterise the structure, properties, and geochemistry of the different intrusions.

The study shows promising indications that both base metals and PGEs occur in economic concentrations within the basic intrusions within the Bergslagen region. A clear relationship between the anomalies in the airborne magnetic field data and magmatic layering observed at outcrop appears to exist. Hence, the large-scale geometry of the layering in the Flinten and Fullen intrusions has been interpreted. Based on the data in this study the Flinten intrusion is interpreted to consist of several sub-intrusions. Based on the airborne and ground-based geophysical data, several regions with low resistivity, which lie subparallel to the interpreted magmatic layering have been identified at the Fullen and Flinten intrusions, which could be interesting for further investigation.

INTRODUCTION

The “Basic intrusions” sub-project is included within the Bergslagen project (stage 2 – regional), which forms part of SGU's systematic geological investigation of areas of interest for exploration (see www.sgu.se at Mineral resources/Geological information for mineral exploration/Mapping in Bergslagen).

The Bergslagen region is one of Sweden's most important ore provinces where mining has been performed for more than 1 000 years. As well as being rich in iron, base metal, and precious metal deposits, the Bergslagen region also has the potential to host innovation-critical metal and mineral deposits. The global demand for these resources has never been higher than it is today and is likely to increase in the future. Within the EU, there is a special interest in the so-called “critical materials” that are needed in green technology such as electric cars, batteries, wind turbines and solar cells. Presently, one of the important challenges for the innovations required to address climate change and to provide alternative energy solutions for society is the supply of raw materials.

In connection with SGU's investigations of the bedrock in the Ludvika area, elevated contents of innovation-critical metals within the platinum group elements (PGE) were found in an old nickel and copper mine at Brunnsjöberget, Hedemora (Claeson et al. 2018, 2019). Furthermore, previous prospecting efforts at the Flinten intrusion identified anomalous levels of PGEs, albeit within local boulders of basic intrusive rock (i.e. not sampled from outcrop) (Filén et al. 1989, Filén 1990). In addition, a better understanding of the potential for base metal deposits within basic intrusions in the Bergslagen region is required. As the presence of base metals in association with rarer metals (important for green technology), can be an important factor in making the extraction of these rarer metals economically viable.

In the light of the above, it was decided that a small effort would be made to perform a focused study of the Flinten and Fullen intrusions within the Bergslagen region. This would include geophysical and lithogeochemical measurements, as well as geological field observations (fig. 1). Minor sampling for lithogeochemical analysis of additional deposits and abandoned mines, within basic intrusions elsewhere within the Bergslagen region, was also part of the project.

The purpose of the project is to update the geological and geophysical databases within and around these basic intrusions. These data can be valuable for planning and resource management, for exploration companies, municipalities, county administrative boards and other parties interested in the Bergslagen region. The databases from the project will include maps, rock observations, lithogeochemical data, data from mineral deposits, petrophysical data, and ground-based geophysical measurements. The project work started at the beginning of the year 2019 and will end in early 2021.

All position information within the study is provided in the Sweref 99 TM coordinate system.

SGU's databases (including bedrock observations, lithogeochemical and geophysical databases) are updated continuously as new results become available from SGU's Bergslagen project.

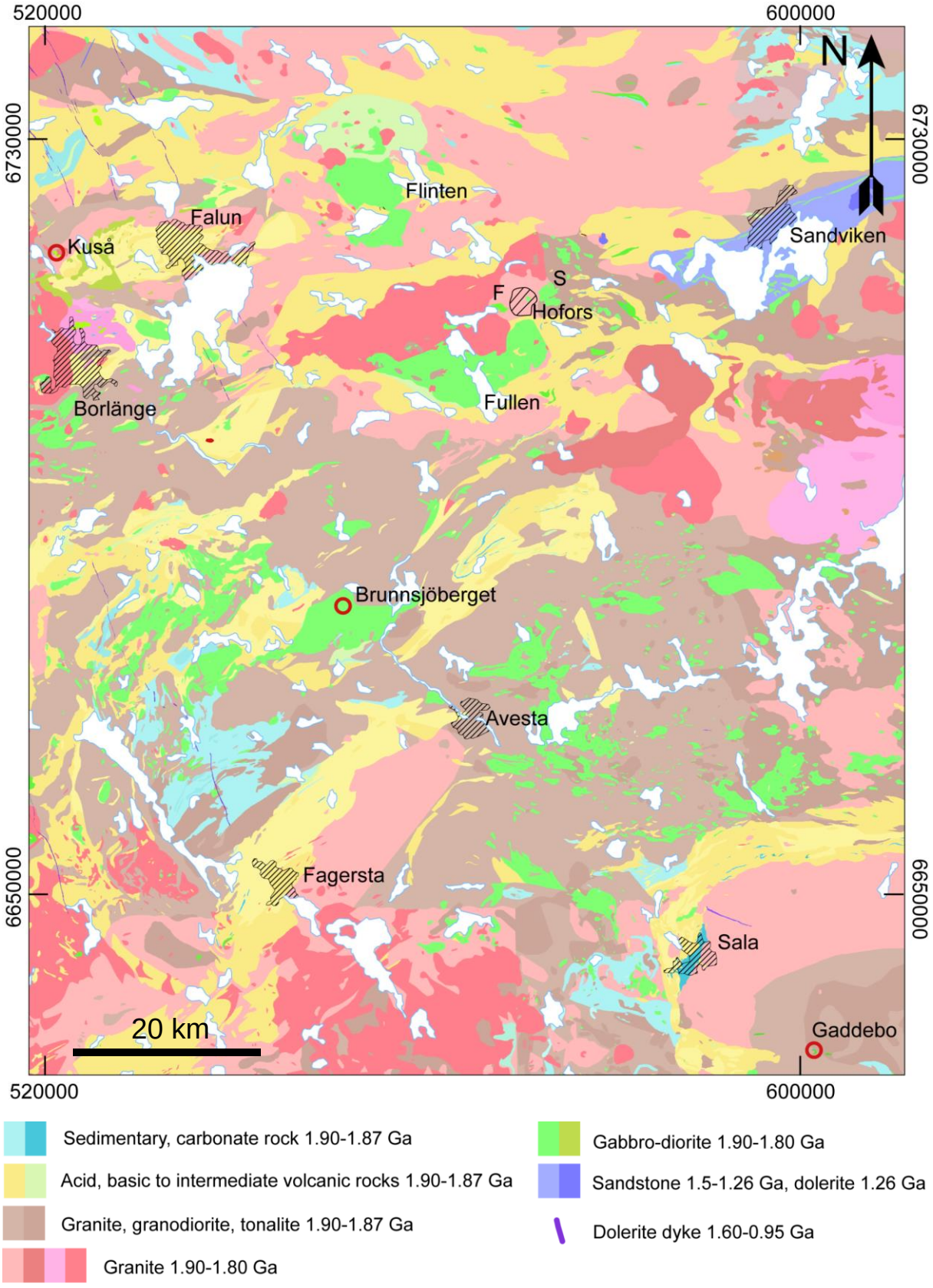

Figure 1. Geological map of the central-northern part of the Bergslagen region, which includes the basic intrusions investigated in this study (simplified from SGU's database). Most rocks are metamorphic except for the youngest. The locations of the Flinten and Fullen intrusions are shown. Red circles indicate the position of sulphide mines within basic intrusions, which were sampled for geochemical analysis. The two intrusions, close to the town of Hofors, labelled with letters F and S show the locations of the Furulund and Skållberget intrusions, respectively.

GEOLOGICAL FIELD WORK

The Flinten intrusion

The Flinten intrusion has been the subject of earlier investigations and exploration efforts of various kinds (e.g. Hammergren 1982, Filén et al. 1989, Lindholm 1990). It is a layered basic intrusion with more or less well-developed modal layering (fig. 2A–B). Cumulate rocks are clearly observable at most of the outcrops visited, however, it is not always possible to discern layering or structures related to magmatic segregation and fractionation. Ultramafic to leucogabbroic layers with different proportions of dark and light-coloured minerals, constitute the macroscopically observable forms of layering. At some of the visited outcrops, light-coloured cumulates of troctolite are present, a rock dominated by plagioclase and olivine with minor pyroxene and amphibole. In the cumulate layers, more diffuse aggregates of light-coloured minerals are sometimes seen in darker layers. These could be interpreted as regions of late crystallised magma, forming mainly within layers dominated by dark-coloured minerals as a post-cumulus product. However, the aggregates can also appear in adjacent layers, indicating that fluid phases moved around within the cumulate rocks before the intrusion completely solidified (fig. 2C). Cumulates of gabbro pegmatite to coarse-grained gabbro with cm-sized crystals also occur at some outcrops (fig. 2D). In general, however, the rocks are medium-grained to coarse-grained at the outcrops which were investigated. At some outcrops, large variations in the composition of the cumulate rocks are seen, varying from anorthosite to leucogabbro, to gabbro and to ultramafic cumulates Here they can appear partly as layers and partly with more chaotic geometries. These different varieties can sometimes coexist, often displaying coarse-grained portions (fig. 2E–H).

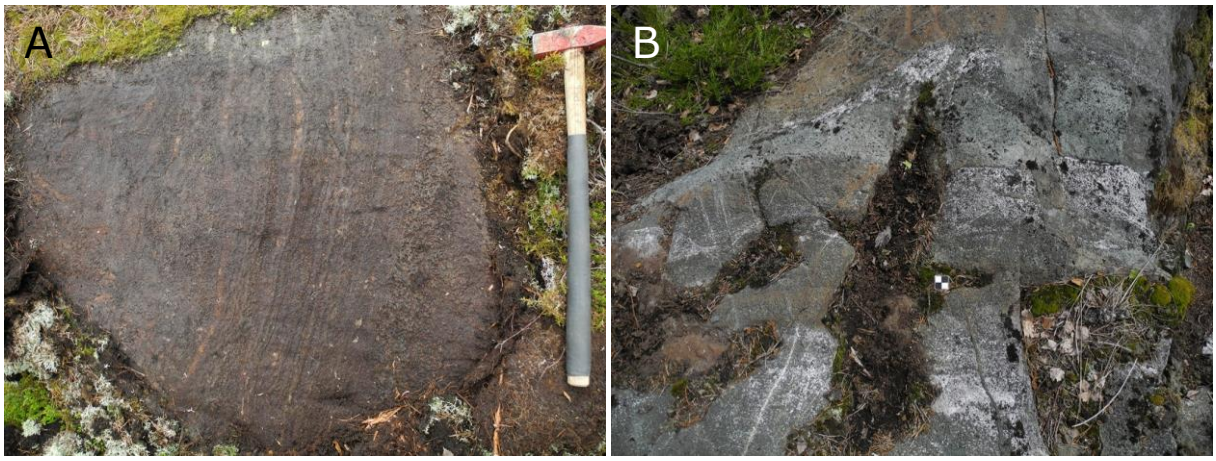

Figure 2. Obvious modal layering. **A.** Small-scale repetition of layers with different mineral compositions, often centimetre wide (6723758/555933). **B.** Several decimetre wide cumulate layers with different proportions of light- and dark-coloured minerals respectively (6723608/554213). Photos: Dick Claeson.

Figure 2 continued. C. Cumulate layer with diffuse accumulations of light-coloured minerals in relation to the darker, pockets of late crystallised magma, mainly within the layer, but also seen in the adjacent layer (6723581/554446). **D.** Cumulate of gabbro pegmatite to coarse-grained gabbro (6723898/555826). A large variation in compositions (E–H), from anorthosite, over leucogabbro and gabbro to ultramafic cumulates, where they appear partly as layers and partly more chaotic with different varieties alternating, often with coarse-grained parts. **E.** Leucogabbro and ultramafic cumulates. **F.** Close-up of coarse-grained leucogabbro. **G.** Coarse-grained ultramafic cumulate with portions of anorthosite. **H.** Close-up of anorthosite in ultramafic cumulate (E–H images at 6723997/555808). Photos: Dick Claeson.

Figure 3. A. Biotite oikocryst-bearing ultramafic cumulate at Vargberget östra (6723231/552845). **B.** Pyrrhotite in fractures of ultramafic cumulate at Vargberget västra (6723454/552390). **C.** Thin sulphide mineralised portions, possibly fracture-fillings, **D.** close-up of C. (6723794/554310). Photos: Dick Claeson.

There are two known mineralised parts of the Flinten intrusion where some mining activity has occurred, a closed mine called Vargberget östra and a prospecting pit called Vargberget västra. The rocks at Vargberget östra consist typically of an ultramafic cumulate with minor gabbroic cumulate rocks. Here biotite occurs as oikocrysts (several cm in size) and the rock surface has cavities due to the preferential weathering of these oikocrysts (fig. 3A). This is the only sampled rock at Flinten that had any anomalous concentrations of PGE and it is an early-formed cumulate without obvious crystals of sulphide minerals (see sample 9 in section *Lithogeochemistry*). Vargberget västra on the other hand has pyrrhotite within both gabbroic and ultramafic parts and is a late-formed cumulate (fig. 3B, see sample 10 in section *Lithogeochemistry*). Other observations of sulphide minerals, apart from within boulders, were thin, sulphide mineralised portions, possibly fracture-fillings, at a few outcrops (fig. 3C–D). Such an occurrence in a melanocratic gabbro was sampled and analysed. The results showed elevated concentrations of Cu, Ni, and Co but not elements of the platinum group (see sample 14 section *Lithogeochemistry*).

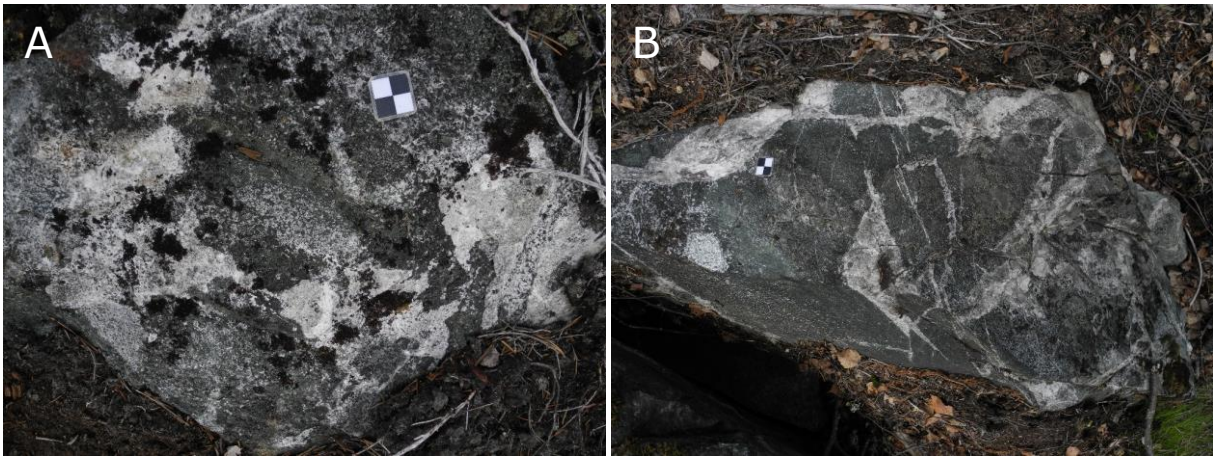

Figure 4. Different behaviour of trondhjemite at Flinten. **A.** Ductile and with contacts indicating that they are comagmatic (6723543/554218). **B**. A brittle appearance with fracture-fillings and parts of the cumulate as fragments (6723608/554213). Photos: Dick Claeson.

Trondhjemite is seen as almost white areas at outcrops and as wide fracture-fillings at several sites (fig. 4A). The trondhjemite is most likely comagmatic with the gabbro in which it occurs. These rocks are late derivatives formed by fractional crystallisation and accumulation of the basic magma, which are subsequently distributed within fracture systems within the previously formed cumulate gabbroic rocks. The fractures which the trondhjemite has filled, most likely formed at a time when the cumulates were to a large extent rigid. The cumulates were then ruptured due to movements within the magma chamber or due to contraction during solidification of the intrusion (fig. 4B).

In parts of the intrusion, fragments of what appears to be previously solidified mafic magma can be observed. These fragments probably formed and solidified within a large (primary) magma chamber and were later broken up and transported in connection with movement of magma through supply channels (fig. 5A). At other outcrops, it is difficult to determine whether these fragments are fine-grained parts of consanguine gabbroid rocks or xenoliths (probably volcanic) unrelated to the intrusion (fig. 5B). At some outcrops classic magma mingling and mixing structures can be observed. Here fragments with very different appearances can be seen, however, they are interpreted here to all originate from the same mafic magma source (fig. 5C–D).

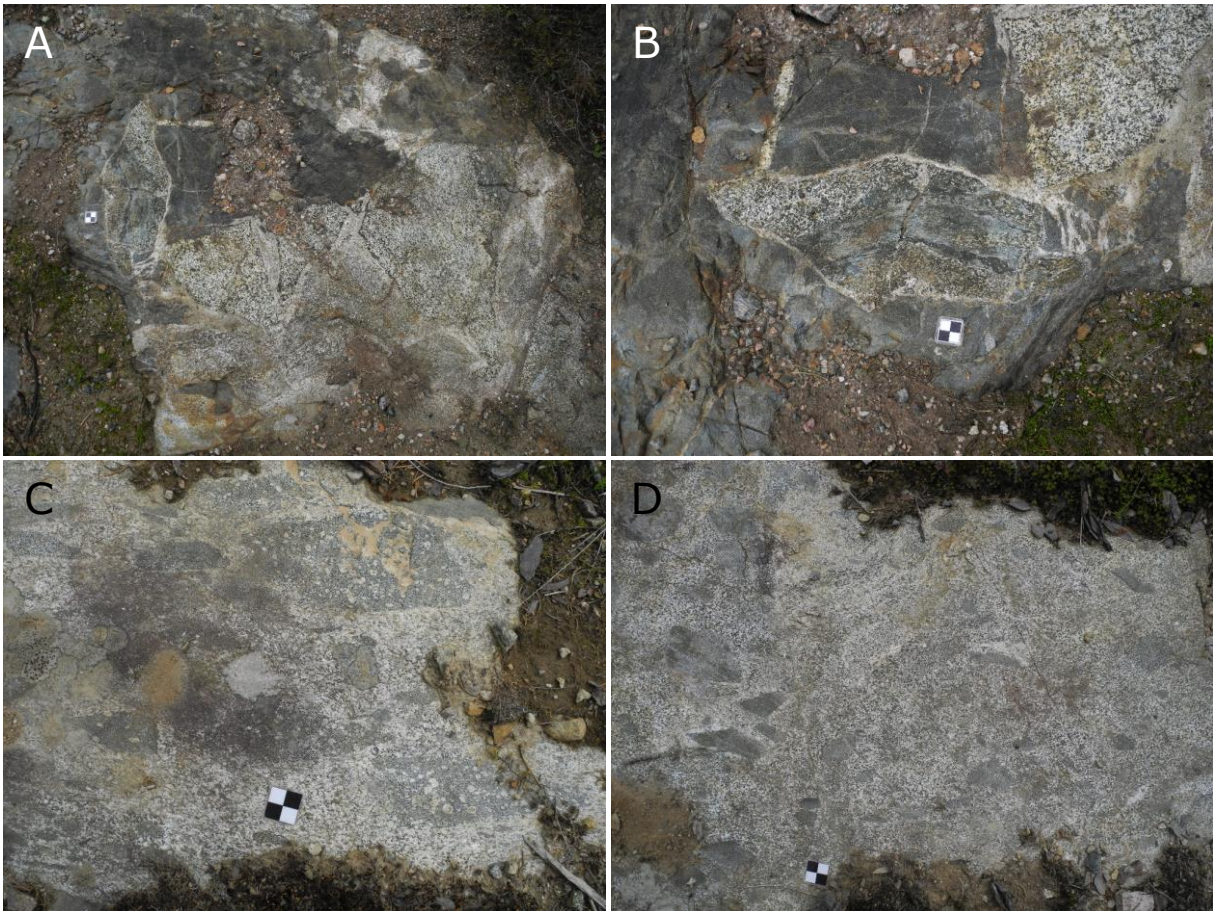

Figure 5. A. Fragments that likely formed and solidified within the main magma chamber, which have subsequently been broken up, **B.** close-up of gabbroid fragment with fine-grained basic fragment (images at 6724267/554180). Fragments with classic magma mingling and mixing structures, very different appearance but probably all components derived from the mafic magma, **C.** round contacts, with ocelli of plagioclase, **D.** angular and round contacts of dark fragments (images at 6725424/553676). Photos: Dick Claeson.

Deformation can be seen at some outcrops, that may be of a regional nature, but overall, the layered sequences are intact and not characterised by any extensive deformation. Most of the minor deformation which can be observed in outcrop is probably related to contraction during the final phase of the solidification process within the magma chamber. However, the presence of small local brittle and ductile deformation zones is also likely. This is consistent with the interpretation of the regional magnetic field data (see section *Geophysical work,* fig. 24), which suggests that the level of deformation within the mafic rocks of the Flinten intrusion is relatively low, when compared to the surrounding area. Alteration is noted at some outcrops within the intrusion, occurring mainly in amphibole and plagioclase-bearing cumulates. In these cases, the appearance of the rocks which have undergone alteration provides a strong contrast to that of unaltered rocks. Here, the primary minerals, mostly black pyroxene and olivine, are replaced with greenish amphibole. The altered rocks are deformed in some places (fig. 6A). However, it is not known whether these features are related to the initial magmatic and cooling event or to later metamorphic overprinting. Perhaps the most notable deformation zone within the intrusion, is present to the north of Sparvguldsberget and has a northeast to southwest direction. This deformation zone can clearly be observed in the apparent resistivity map of the Flinten intrusion (see section *Geophysical work,* marked with an X in fig. 26). Based on observations from outcrops and from the Sparvguld borehole, located at 6725901/554780, this deformation affects dioritoid to gabbroid rocks (fig. 6B) and skarn-bearing metavolcanic rocks present in this area (Hammergren 1982).

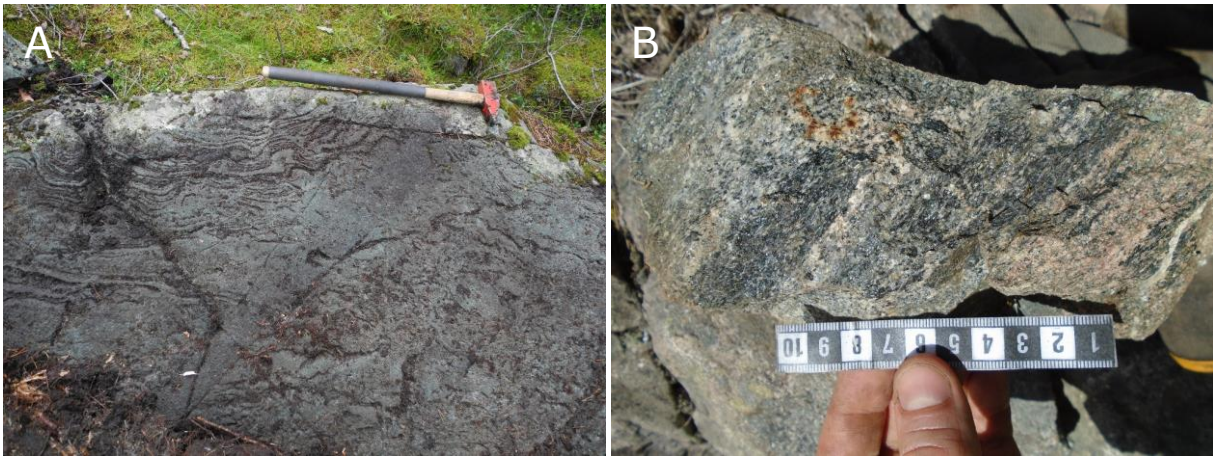

Figure 6. A. Altered and deformed cumulate rock (6723885/555980). Photo: Dick Claeson. **B.** Deformed dioritoid to monzogabbro in deformation zone (6725352/553594). Photo: Daniel Sopher.

The samples analysed for lithogeochemical composition show a large variation, which is interpreted to be related to magmatic differentiation and the formation of cumulates in a large magma chamber (see section *Lithogeochemistry*). Based on work from this study, it is interpreted that the Flinten intrusion consists of several magma chambers and that the intrusion is formed by at least three relatively independent parts present at the surface. These independent parts are likely to be fed from a common magma chamber, positioned lower in the crust (see section *Geophysical work,* specifically figs. 25 and 49). Exactly how these parts were formed, in what order, and if differences in the magma that fed these parts exists, are questions which require greater resources than were available for this study.

The Fullen, Skållberget and Furulund intrusions close to Hofors

The Fullen intrusion has been the target of various investigations and exploration efforts in the past (e.g. Filén et al. 1988, Filén 1990). It is a layered, basic intrusion which often exhibits well-developed modal layering (fig. 7A–B). Cumulate rocks are clear characteristics of most of the outcrops visited, however, it is not always possible to discern layering or structures related to magmatic segregation and fractionation. At some locations cumulates can range from leucocratic, to melanocratic and ultramafic over a single outcrop, representing modal variations of light-coloured and dark minerals (fig. 7C–E). In some cases, the layering is associated with changes in the grain-size distribution (fig. 7F). The contrast between different layers can sometimes be conspicuous, relating to changes in colour, grain size, or modal composition (fig. 7G–I). Contacts between different layers can be razor sharp or more gradual (fig. 7C, G). Often all or several of the above layering structures were present at the outcrops which were investigated. Conversely, in rare cases no signs of layering were present, where the texture of the rock exhibited a massive appearance, in some cases over the entire outcrop (fig. 7J). Regions of relatively high and low magnetic susceptibility could also be measured at a given outcrop, which in some cases, could be correlated with visible indications of layering.

Figure 7. A. Well-developed modal layering resulting in alternating gabbro and melagabbro to ultramafic cumulates (6705360/563131). **B.** Layering in terms of different compositions and grain size (6705833/561615). **C.** Layering as modal variations of light-coloured and dark minerals (6705360/563131). **D.** Layering of leucocratic and melanocratic gabbro (6704609/562635). **E.** Layering of gabbro and ultramafic cumulates (6704609/562635). **F.** Variable grain-size distribution resulting in layering (6705833/561615). Photos: Dick Claeson.

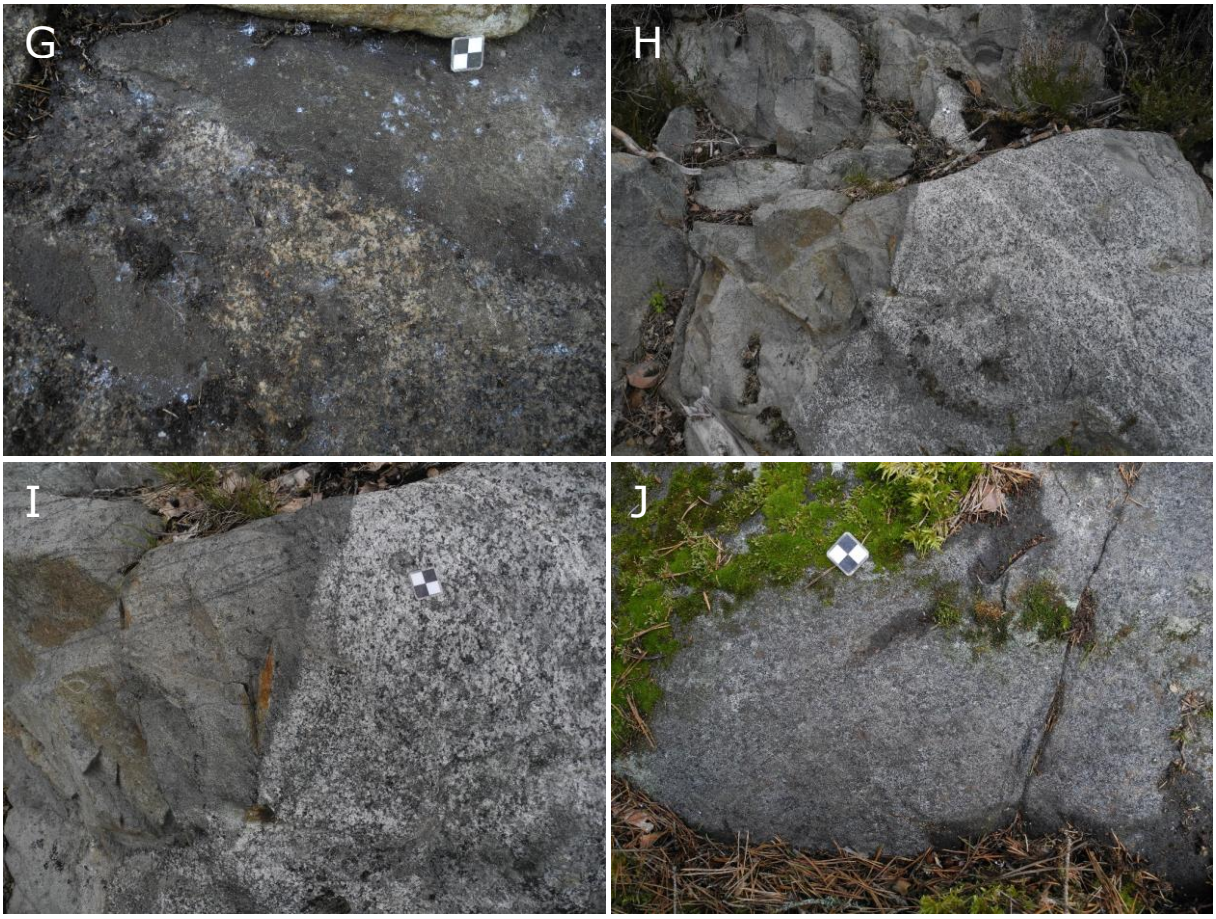

Figure 7 continued. G. Razor sharp contacts between different layers (6706968/562785). **H.** Conspicuous contrast between different layers (6705408/563185). **I.** Close-up of contact in H. **J.** Massive gabbro (6706050/570996). Photos: Dick Claeson.

A few occurrences of rocks that are enclave-bearing were seen and may indicate that magma mingling between consanguineous batches occurred (fig. 8A). Note the lack of any features indicating a major difference in temperature, e.g. chilled margins, between the rocks and how the contacts are interfingering and lobate (fig. 8A). Amphibole-filled fractures were present almost orthogonal to the layering at some outcrops, probably formed during late crystallisation and contraction of the cumulates (fig. 8B).

Some outcrops have gabbro with distinct parts which contain plagioclase phenocrysts (fig. 8C). Pegmatite gabbro is observed over large areas as well as in small portions or pockets of late-stage crystallisation in cumulates (fig. 8D–E).

Trondhjemite was seen at a few outcrops as fracture-filling (fig. 9A–B). This type of rock is most likely comagmatic with the gabbro within which they occur, formed by fractional crystallisation of the basic magma and later injected into the fracture systems within the cumulates.

At some outcrops xenoliths of rhyolite are seen and these are clearly older rocks than the gabbro they occur in at the Fullen intrusion (fig. 9C).

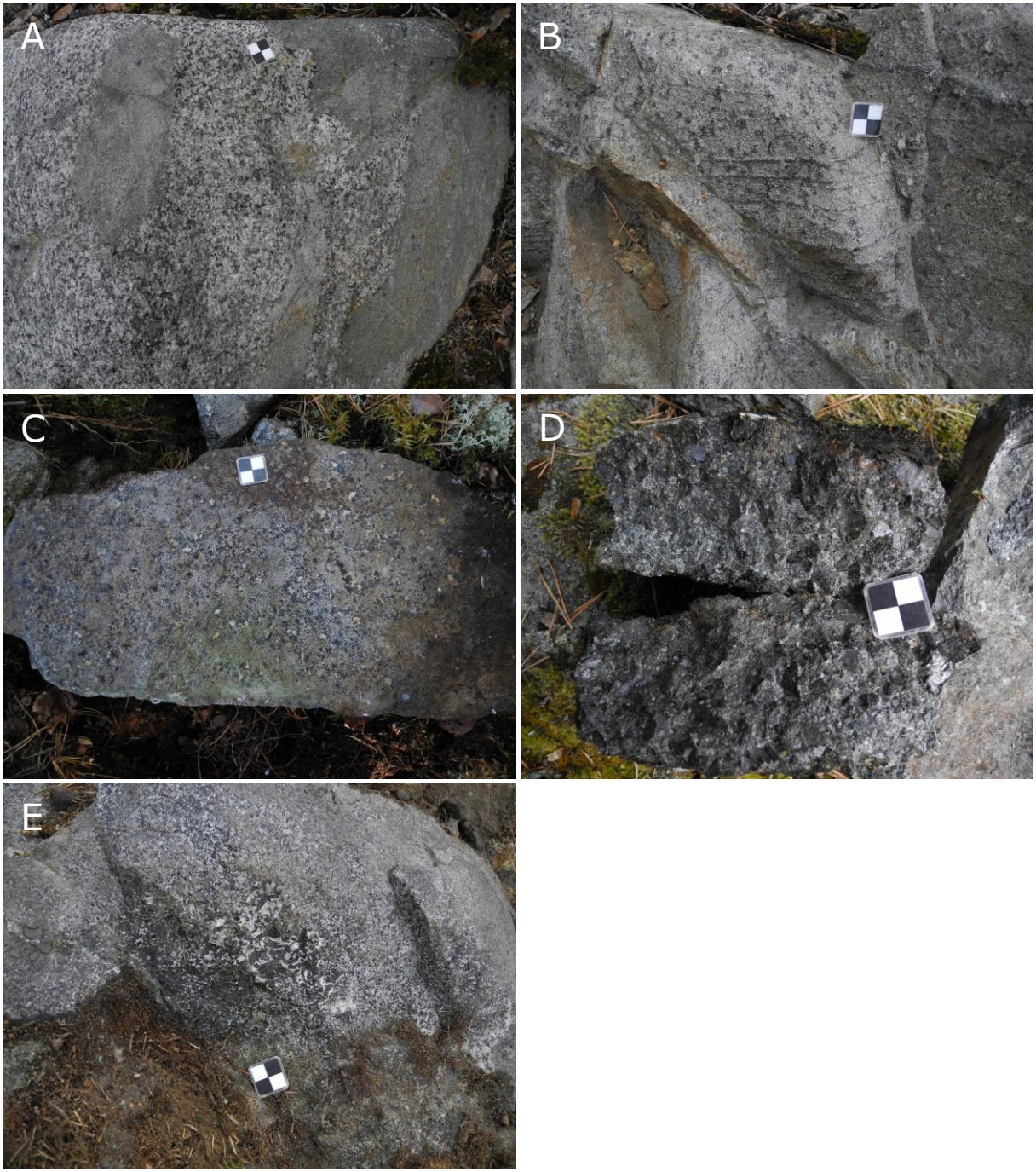

Figure 8. A. Enclave-bearing cumulate indicates magma mingling, note absence of chilled margins and the interfingering and lobate contacts (6705408/563185). **B.** Amphibole-filled fractures almost orthogonal to layering (6705408/563185). **C.** Plagioclase porphyric gabbro (6706968/562785). **D.** Pegmatite gabbro from a layer (6706365/559244). **E.** Pocket of pegmatite gabbro formed during late-stage crystallisation in cumulate (6705833/561615). Photos: Dick Claeson.

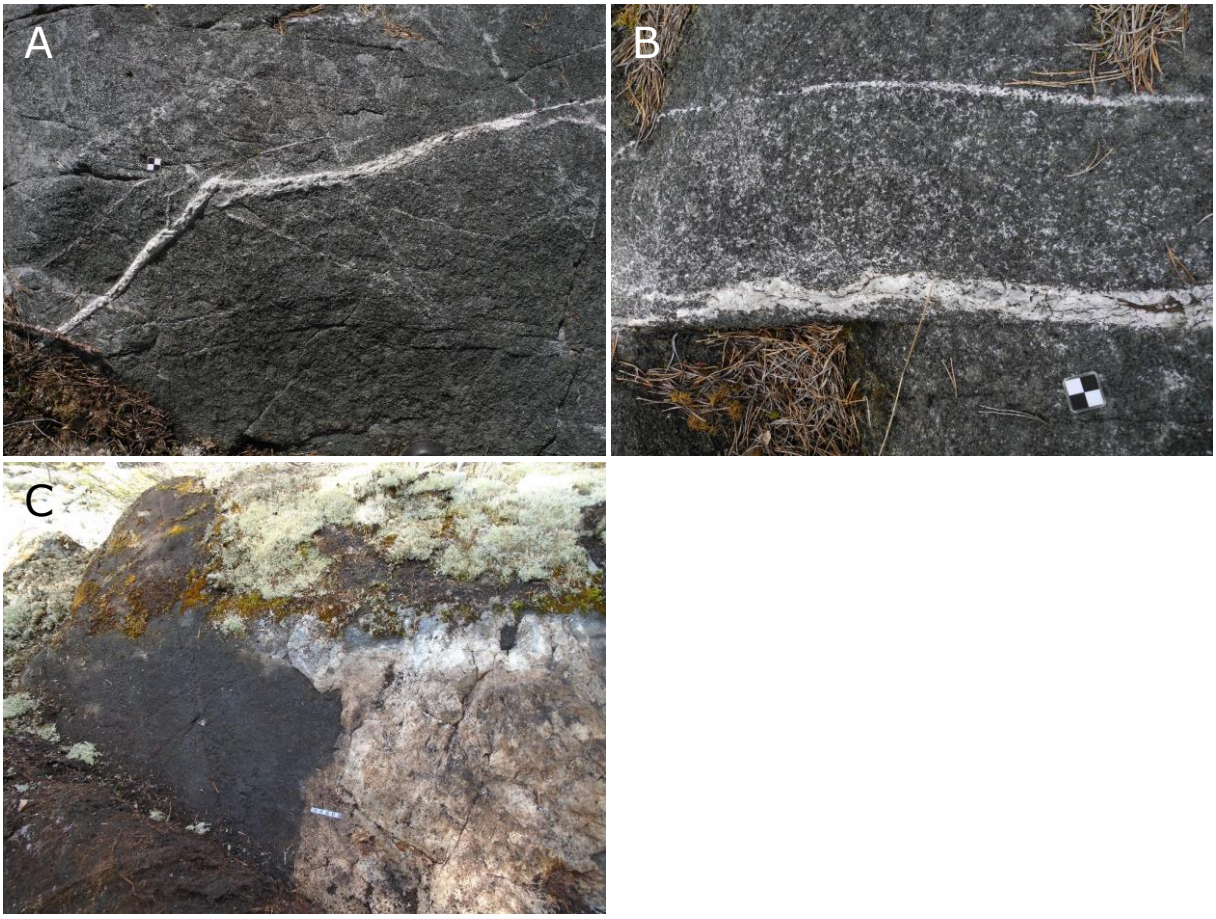

Figure 9. A. Trondhjemite is seen in few outcrops as fracture-fillings, **B.** close-up (images at 6705644/568847). Photos: Dick Claeson. **C.** Xenolith of rhyolite in layered gabbro cumulate (6707680/570040). Photo: Daniel Sopher.

Two intrusions, located to the east (Skållberget) and west (Furulund) of Hofors, respectively, were visited and a single sample was collected from each intrusion (fig. 1). The intrusion at Skållberget shows layering features (fig. 10A). The sampled ultrabasic cumulate has in places weak dissemination of pyrrhotite and chalcopyrite (fig. 10B).

The intrusion at Furulund consists mostly of ultramafic cumulates, where a major portion of the rocks are altered and now have serpentine instead of olivine in their groundmass (fig. 10E). If plagioclase is present at all in these rocks, it occurs as an interstitial, late-crystallising mineral (fig. 10D). Layering is present but not easily detected on all surfaces (fig. 10C). The Karlsborg mine, which was quarried between 1962 and 1974 (Wik et al. 2009, fig. 10F), is located within the Furulund intrusion. Today the Karlsborg mine appears as a small, partly water-filled hole.

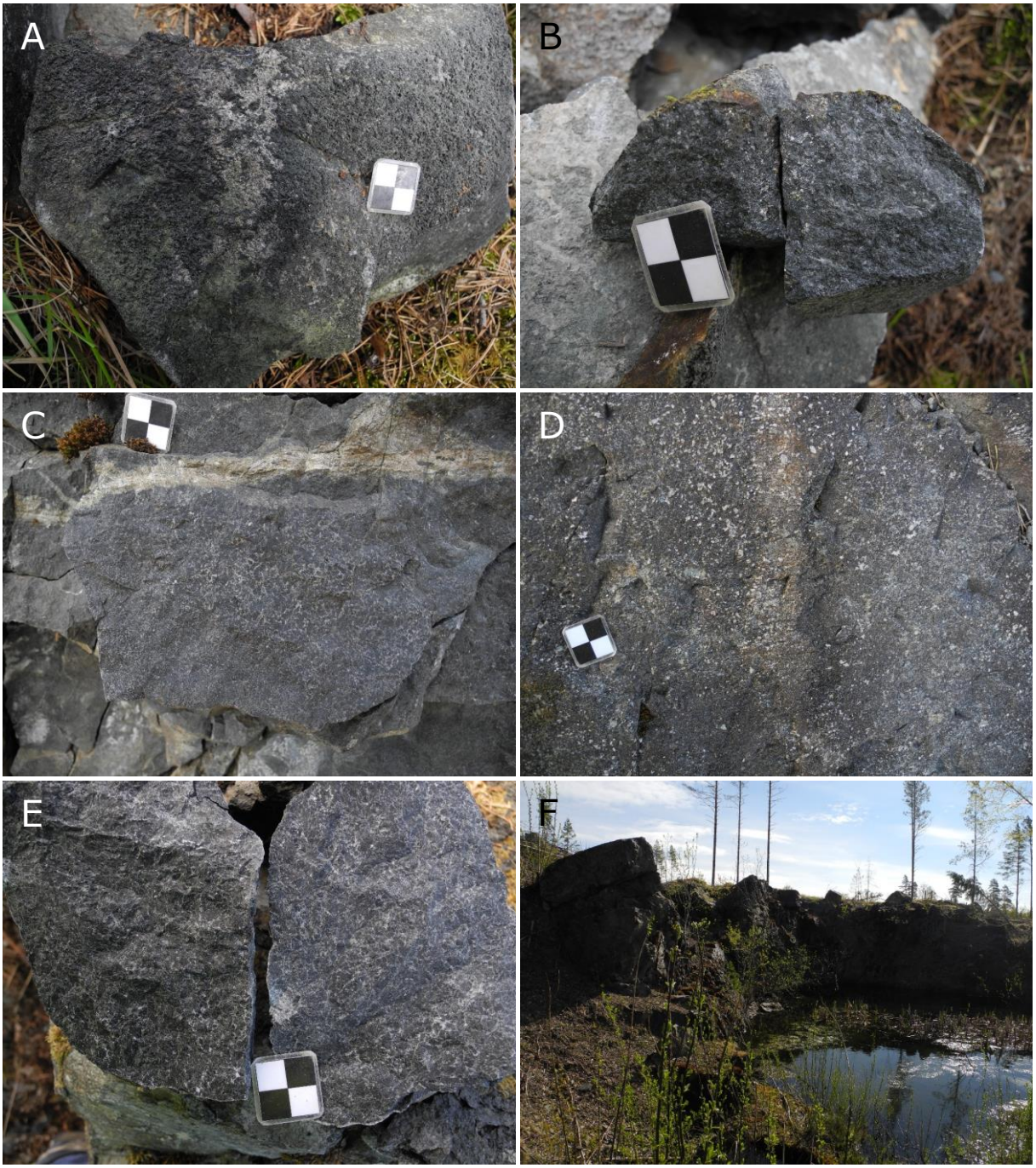

Figure 10. A. The intrusion at Skållberget shows layering features (6713678/573892). **B.** An ultrabasic cumulate at Skållberget, which has in places weak dissemination of pyrrhotite and chalcopyrite (6713678/573892). **C.** Layering is present but not easily detected on all surfaces at the Karlsborg mine, Furulund (6712495/568024). **D.** If plagioclase is present at all in the ultramafic cumulate, it occurs as an interstitial, late-crystallising mineral (6712495/568024). **E.** Altered ultramafic cumulate at the Karlsborg mine, Furulund with serpentine replacing olivine (6712495/568024). **F.** Karlsborg mine, Furulund (6712495/568024). Photos: Dick Claeson.

Sulphide mines at Kuså and Gaddebo

The nickel and copper mines at Kuså and Gaddebo were visited and sampled for lithogeochemical analysis in 2019.

The Kuså mine and its surroundings have been described in several papers (e.g. Löfstrand 1903, Geijer 1917, Kulling & Hjelmqvist 1948, Grip 1961, Magnusson 1973, Nilsson 1985, Ripa et al. 2017). The Kuså mine includes three smaller mines which were visited in this study, these were the Kuså gruva 2 mine, the Muttogruvan 2 mine and the Illingsbergsgruvan mine. The waste rock at the Kuså gruva 2 mine consists of gabbroic rocks and large amounts of sulphide minerals (fig. 11A). The sulphide minerals which were identified were chalcopyrite, pyrrhotite, and pyrite. Occasionally, "skillersten" and oikocrysts of amphibole in gabbroid to hornbländite were present. The mineral sperrylite ($PtAs_2$) has been reported from the Kuså mine (Zakrzewski 1989). At the Muttogruvan 2 mine, there were significantly smaller amounts of sulphide-rich waste rock when compared to the Kuså gruva 2 mine, which contained chalcopyrite and pyrrhotite (fig. 11B). The waste rock was mixed with gabbroid. The third mine in the Kuså area, the Illingsbergsgruvan, had sulphide-rich gabbroid among the waste rock (fig. 11C). The sulphide minerals consist mainly of chalcopyrite, pyrrhotite, and single crystals of covellite. Irregular occurrence of "skillersten" and centimetre-sized oikocrysts of amphibole were noted in the gabbro rocks.

The Gaddebo mines were in production between 1870–1871 and subsequently several investigations have been carried out (e.g. Löfstrand 1903, Grip 1961, Wik et al. 2006). At the Gaddebo mines, the waste rock consists of gabbroid with sulphide-rich parts (fig. 11D–E). The sulphide minerals chalcopyrite and pyrrhotite occur as lumps or as aggregates. However, these minerals can also be disseminated within the gabbroid (fig. 11D–E).

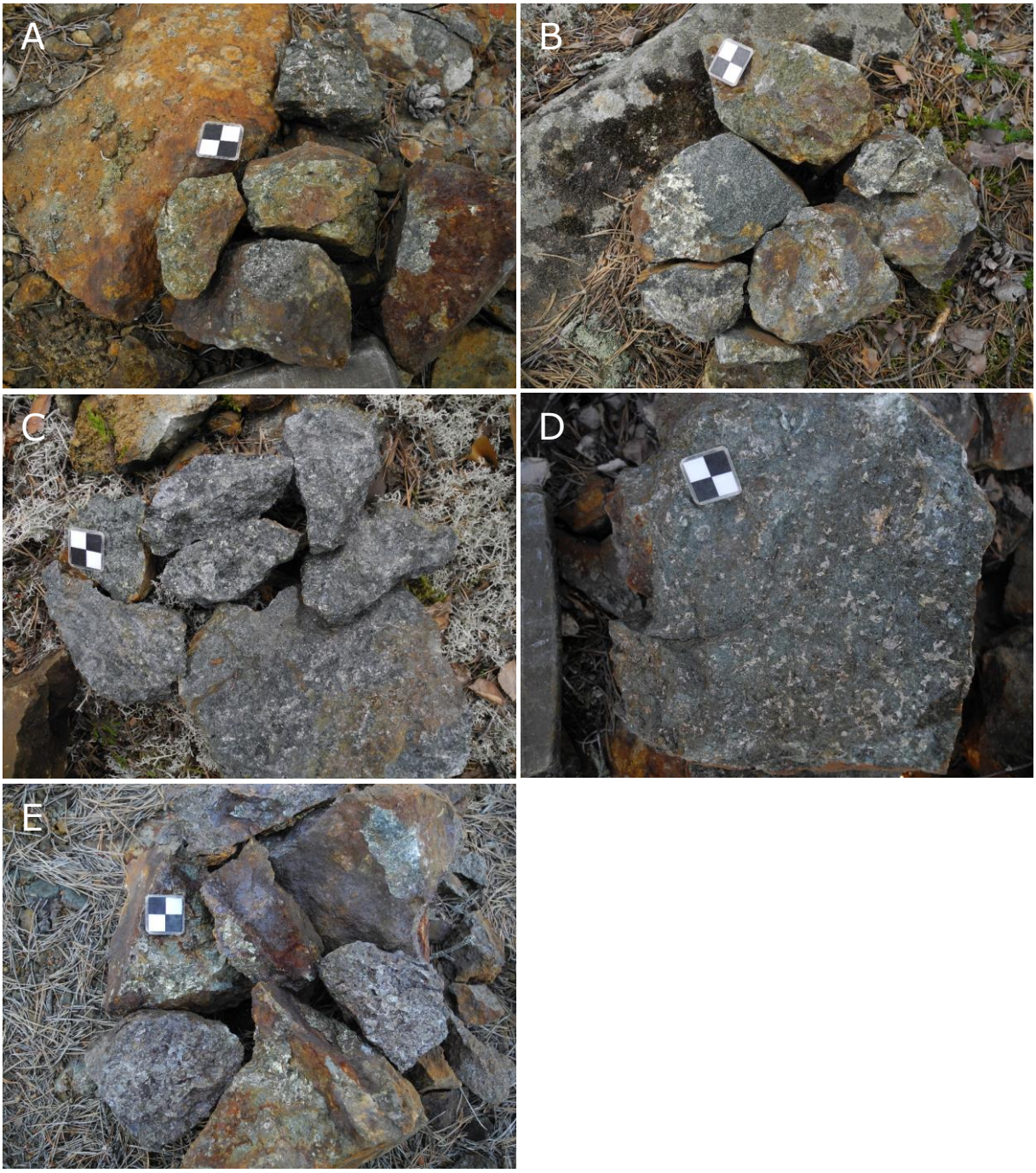

Figure 11. A. Waste rock at Kuså gruva 2 of gabbroic rocks with sulphide minerals (6717698/521472). **B.** Gabbroid at Muttogruvan 2 with chalcopyrite and pyrrhotite (6717501/521587). **C.** Sulphide-rich gabbroid in waste rock from Illingsbergsgruvan (6717451/521806). **D.** The waste rock at Gaddebo gruvor consists of gabbroid with sulphide-rich parts (6633246/601595). **E.** The most common sulphide minerals are chalcopyrite and pyrrhotite, both as aggregates and disseminated (6633246/601595). Photos: Dick Claeson.

GEOPHYSICAL WORK

The physical properties of mafic intrusions often contrast significantly with the physical properties of the surrounding rocks. As well as this, strong contrasts in physical properties can also occur in association with the internal structure of mafic intrusions. Hence, geophysical methods can be a useful tool when investigating layered mafic-ultramafic intrusions as well as the potential for associated mineralisation.

There are numerous examples of other studies which have used geophysical methods to investigate layered intrusions. McEnroe et al. (2009) performed a detailed investigation of the magnetic properties of the Bjerkreim-Sokndal norite, layered intrusion in Norway. Here the complex magnetic pattern observed from airborne and ground magnetic data is attributed to variations in the magnetic minerals within the different layers. The pattern is complicated by cycles of magma recharge, which alter the composition of the magma chamber over time. Ferré et al. (2009) show examples of how the magnetic properties vary through layers within several mafic-ultramafic intrusions from Africa. In this study, differentiation within the magma chamber combined with magma recharge is also invoked as the mechanism for altering the amount of magnetic minerals within different layers of the intrusions. Ferré et al. (2009) identify magnetite as the most important magnetic mineral within their case studies, however they note that pyrrhotite in association with other sulphide minerals can also be important for the magnetic response. Maes et al. (2007) use anisotropy of magnetic susceptibility (AMS) measurements to gain insight into the formation of a stratabound zone enriched in Au and PGE, within the Sonju Lake layered intrusion, USA. Finn et al. (2015) use a range of geophysical methods including magnetotellurics (MT), gravity, and magnetics to generate models to characterize the South African Bushveld layered mafic intrusion in 3D. Ferris et al. (1998) used 2D modelling to investigate the structure of the Dufek intrusion in Antarctica, based on aeromagnetic data. PGE deposits, which can occur within layered mafic intrusions, often have physical properties which contrast to the surrounding mafic rocks. Electrical resistivity is an important example of such a property. As PGE deposits often occur in association with sulphide minerals, they can have far lower electrical resistivity values than the surrounding mafic rocks (King 2007, Finn et al. 2013).

Previous geophysical investigations have been carried out at the Flinten intrusion, which included acquisition and interpretation of ground VLF (very low frequency) and magnetic data, interpretation of airborne data and collection of petrophysical samples (Granar & Henkel 1981). Many of these investigations were focused on a region with anomalously low resistivity. Based partially on these results, the Sparvguld borehole (shown in figure 12) was drilled to investigate this anomaly (Hammergren 1982). However, no sulphide mineralisation was encountered and instead a water-bearing deformation zone was intersected, within a sequence of predominantly felsic rocks.

As part of the project, additional geophysical data were collected from the Flinten and Fullen intrusions during the summers of 2019 and 2020 (fig. 12). This included geophysical observations which were made at outcrops. These observations included magnetic susceptibility measurements (at least 8 measurements for each rock type present at a given outcrop), acquisition of 51 petrophysical samples and 19 measurements of natural gamma radiation (at 8 unique locations). Furthermore, several ground-based profiles were collected at the two sites including 16 profiles were the magnetic field was measured and six profiles were the electrical conductivity was measured using the VLF method. In addition, new measurements collected by SGU within the Bergslagen area in association with other projects between 2019 and 2020 were utilised in this study. This included new airborne measurements of the magnetic field and natural gamma radiation. Electrical conductivity was also measured using the VLF method (dual transmitters). In the late autumn of 2019 airborne transient electromagnetic (ATEM) measurements were also

performed over the Flinten intrusion and surrounding area. Furthermore, additional gravity measurements were made at the Flinten intrusion.

The objectives of the geophysical investigations within this project were as follows:

- To increase the amount of geophysical and petrophysical data available for these two intrusions in SGU's databases.
- To perform an assessment of the petrophysical properties of these two intrusions.
- To improve the understanding of the large-scale structure and geometry of these intrusions.
- To gain a better understanding of the internal structure of these intrusions, specifically, the magmatic layering.
- To highlight any indications of mineralisation based on the geophysical data.

To address these objectives within this study, the available petrophysical data as well as the newly acquired airborne and gravity data are presented, discussed, and interpreted. Furthermore, 2D and 3D geophysical modelling of the Fullen and Flinten intrusions are also presented and discussed.

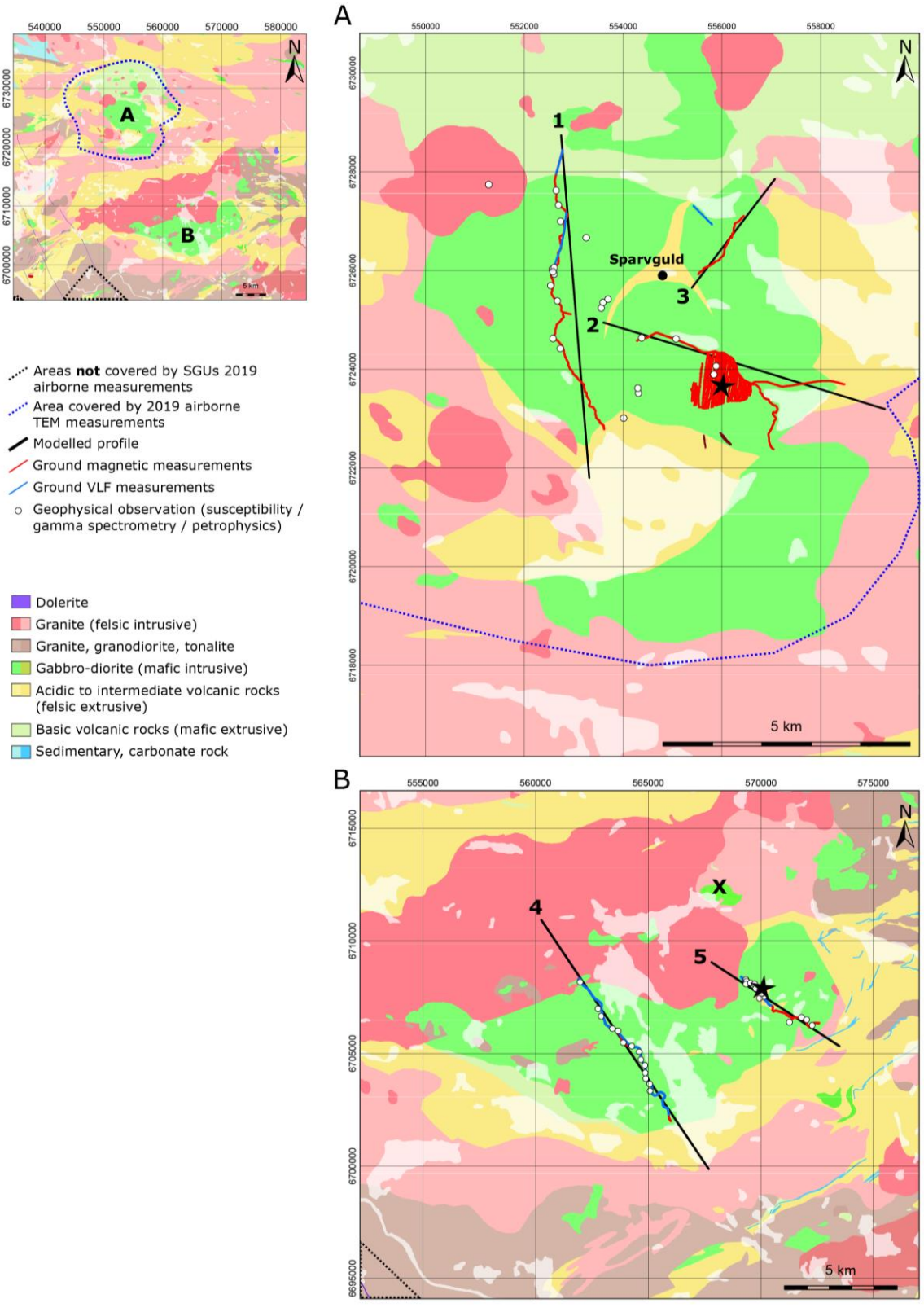

Figure 12. Maps detailing the two intrusions where geophysical investigations were performed. The small map in the top left corner shows a large-scale map detailing the relative position of the two mafic intrusions shown in more detail in A. and B. The location of new ground-based data acquired within the project as well as the 2D profiles which are modelled are shown on the maps. **A.** Map of the Flinten intrusion. **B.** Map of the Fullen intrusion. The X denotes the location of the abandoned Karlsborg mine, within the Furulund intrusion, where serpentinised ultramafic rocks occur. The black stars in A. and B. denote the location where 2D ground magnetic measurements were conducted. The location of the Sparvguld borehole is labelled in A.

Petrophysical measurements

Before attempting to interpret the geophysical data, it is important to develop an understanding of the physical properties of the different rock types which occur in the vicinity of the two intrusions. In this section, a statistical analysis of the newly acquired and pre-existing petrophysical data is presented and discussed.

Petrophysical measurements from the Flinten intrusion

Figure 13 describes the locations of the available petrophysical data for the Flinten intrusion and defines the area considered in the petrophysical analysis. Here it can be observed that, within the central area of the Flinten intrusion (approximately at coordinates 6725000/555000), that there are relatively large amounts of petrophysical data available. However, within the intrusive mafic rocks outside of the central area there are far fewer petrophysical samples available. Similarly, there are relatively few petrophysical samples available for the felsic extrusive and intrusive rocks in the surrounding area. In contrast to the petrophysical measurements, there are relatively large amounts of outcrop magnetic susceptibility measurements in the surrounding felsic rocks. The extrusive mafic rocks to the north of the Flinten intrusion are poorly sampled, when compared to the other rock types in the study area.

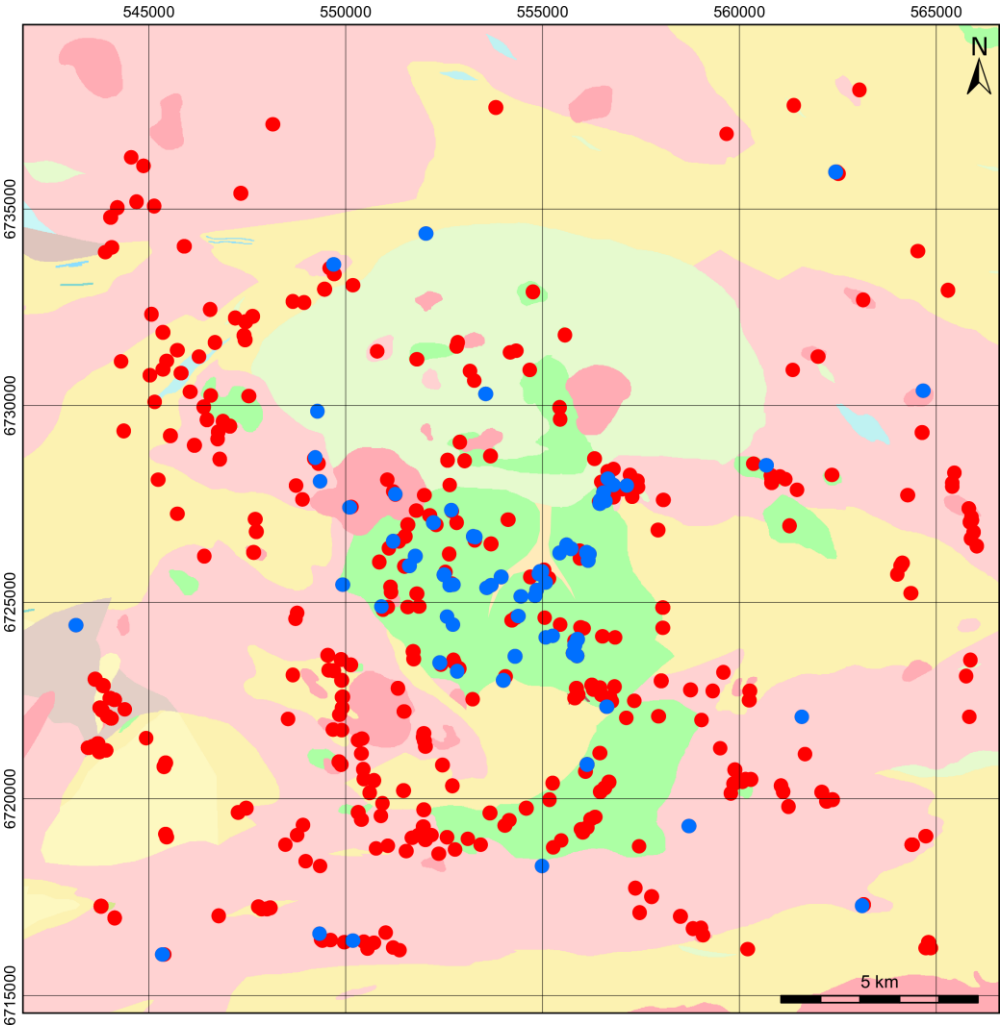

Figure 13. Map detailing the data used in the Flinten petrophysical analysis. The red dots indicate where magnetic susceptibility has been measured at outcrop, while the blue dots indicate locations where petrophysical samples have been acquired. See figure 12 for the legend for the bedrock geology map.

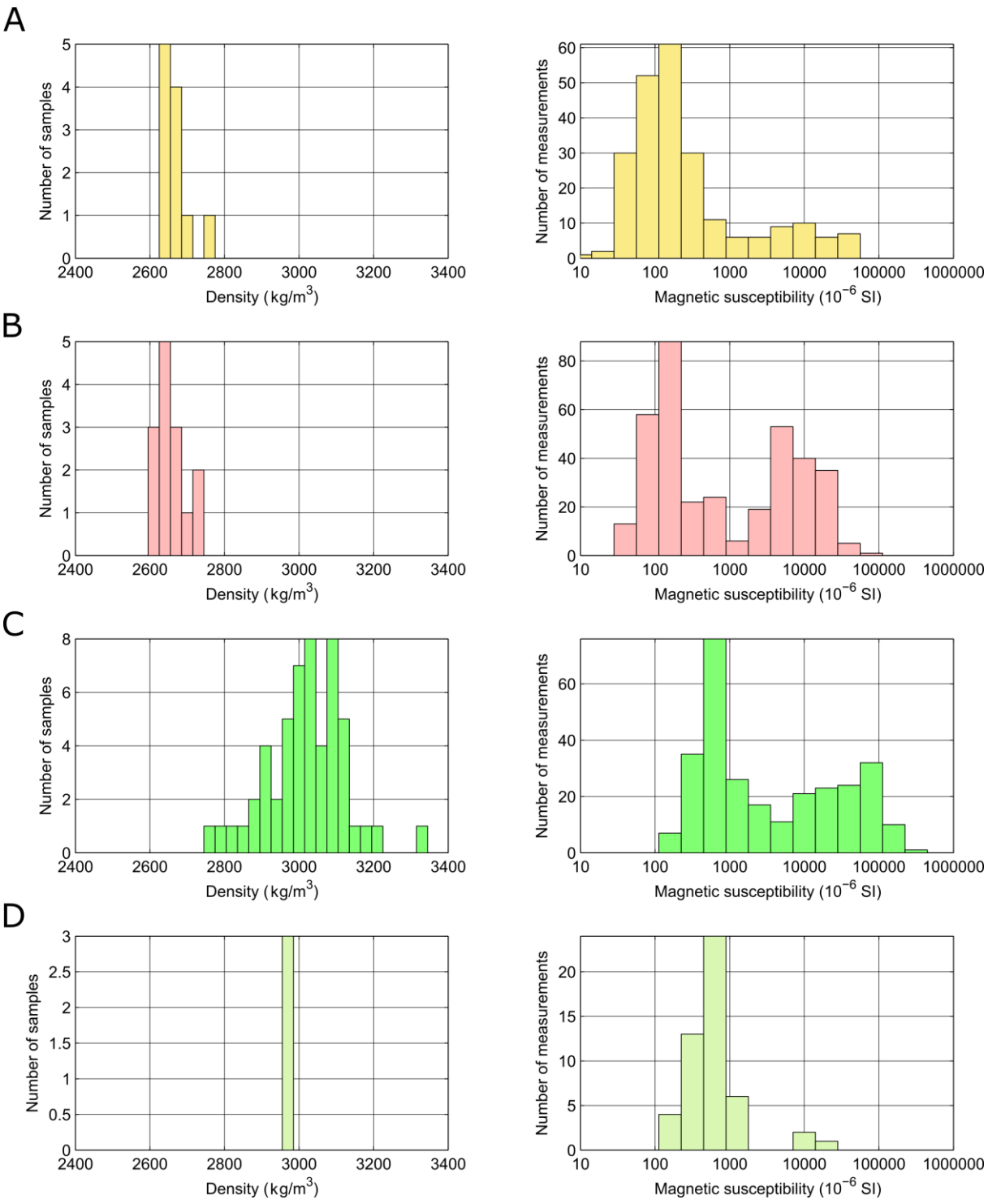

Figure 14. Histograms showing the distribution of density (left) measured on petrophysical samples and magnetic susceptibility (right) measured on petrophysical samples and at outcrop, for four different rock types in the Flinten area. **A.** Graphs for extrusive felsic rocks. **B.** Graphs for intrusive felsic rocks. **C.** Graphs for intrusive mafic rocks. **D.** Graphs for extrusive mafic rocks.

Figure 14 shows histograms describing the distributions of density and magnetic susceptibility for the four major rock types in the Flinten study area. Figure 15 shows cross plots of density and magnetic susceptibility for the same groups. Summary statistics for these groups can also be found in table 1. Here it can be observed that the felsic extrusive and felsic intrusive rocks have average densities of 2 670 and 2 660 kg/m^3, respectively.

Table 1. Summary statistics for the petrophysical data from the Flinten study area. The upper part of the table (with blue striped shading) shows the statistics for all available data, from the four major rock types considered. The lower part of the table (with green striped shading) provides statistics for more detailed classifications of mafic intrusive rocks. Note that only samples collected during this project are included in these more detailed classifications.

Rock Type	Density (kg/m³)			Susceptibility (10^{-6} SI)				Q			
	Samples	Mean	Std. dev.	Samples	Min	Max	Median	Samples	Min	Max	Median
Felsic extrusive	11	2670	36	231	10	50000	200	11	0.07	2	0.13
Felsic intrusive	14	2660	37	364	30	80000	490	11	0.04	7.04	0.10
Mafic intrusive	53	3020	107	283	150	387000	1580	51	0.04	91.3	0.63
Mafic extrusive	3	2960	8	50	200	20000	600	1	0.77	0.77	0.77
Diorite-Gabbro	2	2770	17	2	440	483	461	2	1.06	1.24	1.15
Troctolite	2	2830	13	2	1160	1470	1310	2	2.78	6.76	4.77
Gabbro	10	3030	57	10	640	138000	18200	10	0.12	91.3	1.64
Gabbro-Ultramafic	3	3170	154	3	127000	387000	131000	3	0.05	2.92	0.39
Ultramafic	1	3180	NA	1	156000	156000	156000	1	0.04	0.04	0.04

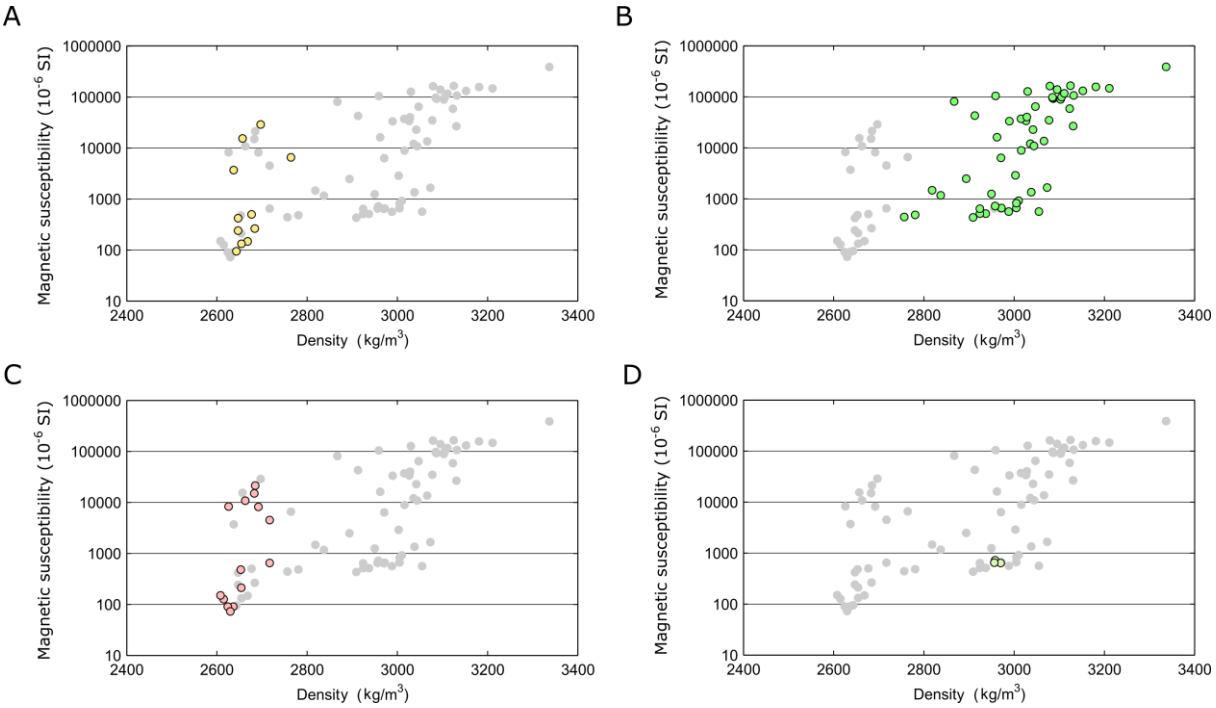

Figure 15. Cross plots showing the density and magnetic susceptibility values for petrophysical samples from four different rock types from the Flinten area. In each graph the coloured dots indicate the data from a specific rock type, while the grey dots show all the available petrophysical data for the Flinten area. **A.** Graph for extrusive felsic rocks. **B.** Graph for intrusive mafic rocks. **C.** Graph for intrusive felsic rocks. **D.** Graph for extrusive mafic rocks.

The extrusive and intrusive mafic rocks have far higher average densities of 2 960 and 3 020 kg/m^3, respectively. With regards to the magnetic properties of the felsic rocks, both intrusive and extrusive rock types have a peak susceptibility value at 100 × 10^{-6} SI, which is most likely due to the presence of iron-bearing paramagnetic minerals. The susceptibility distribution for intrusive felsic rocks (granite; and to a lesser extent extrusive felsic rocks) has a second peak value at approximately 3 000 × 10^{-6} SI. This could be due to the presence of a significant proportion of biotite in some cases but could also be due to the presence of small amounts of magnetic minerals. The average magnetic susceptibility values of the extrusive and intrusive mafic rocks are higher than the felsic rocks. For both mafic rock types, a peak susceptibility value can be observed at approximately 1 000 × 10^{-6} SI, which most likely represents significant quantities of iron-bearing paramagnetic minerals. A significant proportion of the

susceptibility values for the intrusive mafic rocks lie above 10 000 × 10^{-6} SI, which is most likely due to the presence of magnetic minerals.

Figure 16 shows a cross plot of magnetic susceptibility and density for intrusive mafic rocks from the Flinten study area. Here the data are subdivided to investigate the properties of the different types of intrusive mafic rocks. Summary statistics for these data can also be found in table 1. It can be observed that the samples classified as diorite-gabbro and troctolite have relatively low-density values. This is most likely due to the larger proportion of feldspar, and in the case of diorite-gabbro, potentially small quantities of quartz. A general increase in density is observed as the amount of feldspar in the different rock types decreases (e.g. from troctolite to gabbro and finally ultramafic). With these samples, a general increase in magnetic susceptibility is also observed, moving from the more feldspar-rich rock types (e.g. diorite-gabbro and troctolite) to the gabbro and ultramafic rocks. This is most likely due an overall increase in iron-bearing paramagnetic minerals and magnetic minerals.

As part of the petrophysical analysis the remnant magnetisation of the different rock types was investigated. Figure 17 shows cross plots of the Q value and remanent magnetisation (J) versus magnetic susceptibility. The Q value describes the ratio between the remanent and induced components of the magnetisation, where a Q value above 1 indicates that the remnant component of the overall magnetisation is greater than the induced component. Here it can be observed that remanent magnetisation is significant for the intrusive mafic rocks from the Flinten study area, where a significant proportion of the samples exhibit a Q value above 1. An approximately linear trend also appears to exist between remanent magnetisation and magnetic susceptibility (fig. 17). Remnant magnetisation for the other rock types considered in this study are also shown in figure 17 (as grey dots). The Q values in these rock types are typically not above 1.

Figure 17 also shows a rose diagram of the azimuth of the remanent magnetisation for intrusive mafic rocks from the Flinten study area. The dominant azimuth for the remanent magnetisation is north-northeast. Inclination values (not shown here) for the remanent magnetisation are also typically above 50°. Hence it appears that in most cases, the remanent magnetisation has a similar orientation to the Earth's current magnetic field.

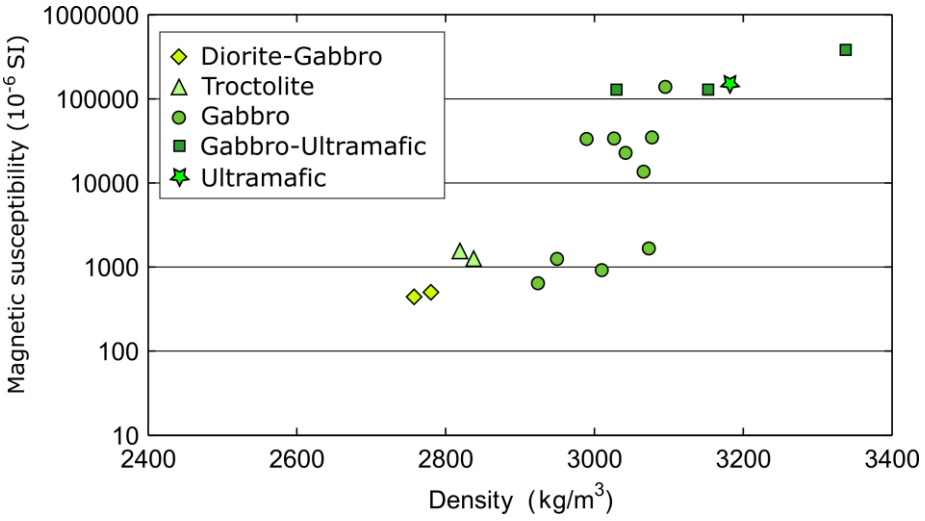

Figure 16. Cross plot showing the density and magnetic susceptibility values for petrophysical samples for intrusive mafic rocks from the Flinten intrusion. Only values for petrophysical data collected during this project are shown. The data are grouped into five different categories, which are represented with different symbols and colours.

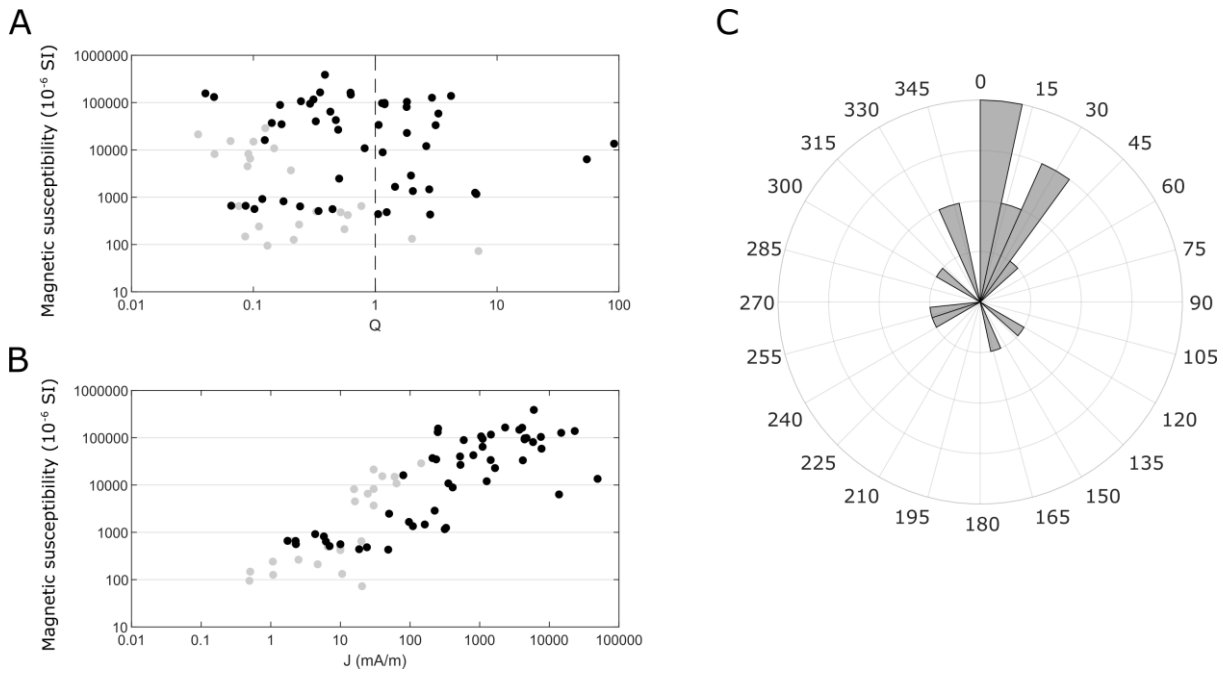

Figure 17. Graphs describing the remanent magnetisation of intrusive mafic rocks from the Flinten intrusion. **A.** A cross plot showing the Q value versus the magnetic susceptibility. **B.** A cross plot showing the remanent magnetisation (J) versus the magnetic susceptibility. In both A and B, data from intrusive mafic rocks are shown as black dots. Data from the other rock types in the study area are shown as grey dots. **C.** A rose diagram showing the azimuth of the remanent magnetisation for intrusive mafic rocks.

Petrophysical measurements from the Fullen intrusion

As part of this study a petrophysical analysis was also carried out for the Fullen intrusion and surrounding area. Figure 18 shows the available data which was considered in the petrophysical analysis as well as the area over which the data was collected.

Figure 20 shows histograms of the available density and magnetic susceptibility data from the Fullen study area. Figure 19 shows cross plots of magnetic susceptibility versus density for the Fullen petrophysical data. Table 2 shows summary statistics for the four different rock type classifications used in figures 19 and 20. In general, the density and magnetic susceptibility distributions for the Fullen intrusion are similar to those from the Flinten intrusion. Here felsic extrusive and intrusive rocks have an average density of 2 640 kg/m^3, while mafic extrusive and intrusive rocks have average densities of 3 000 and 2 970 kg/m^3, respectively. The distributions of magnetic susceptibility are also similar to those observed in the Flinten intrusion. However, in contrast to the data from the Flinten area, the felsic extrusive and intrusive rocks appear to have a larger proportion of samples with a relatively high susceptibility value. Hence in the Fullen data the second maximum on the histogram (at approximately 3 000 × 10^{-6} SI) is larger than in the Flinten data. Similarly, the average magnetic susceptibility values of the mafic rocks are also higher for the Fullen intrusion when compared to the Flinten intrusion. This difference in magnetic susceptibility values between the Flinten and Fullen study areas is also reflected in the summary values in table 2. A number of samples from the mafic intrusive rocks from the Fullen area have anomalously low densities, which are highlighted in figures 19 and 20. These samples were collected from the abandoned Karlsborg mine, within the Furulund intrusion, west of the town of Hofors (fig. 10F). In this area ultramafic rocks occur which have been serpentinised (see figure 12 for location), hence the overall density of these ultramafic rocks has been reduced due to the alteration process (hydration).

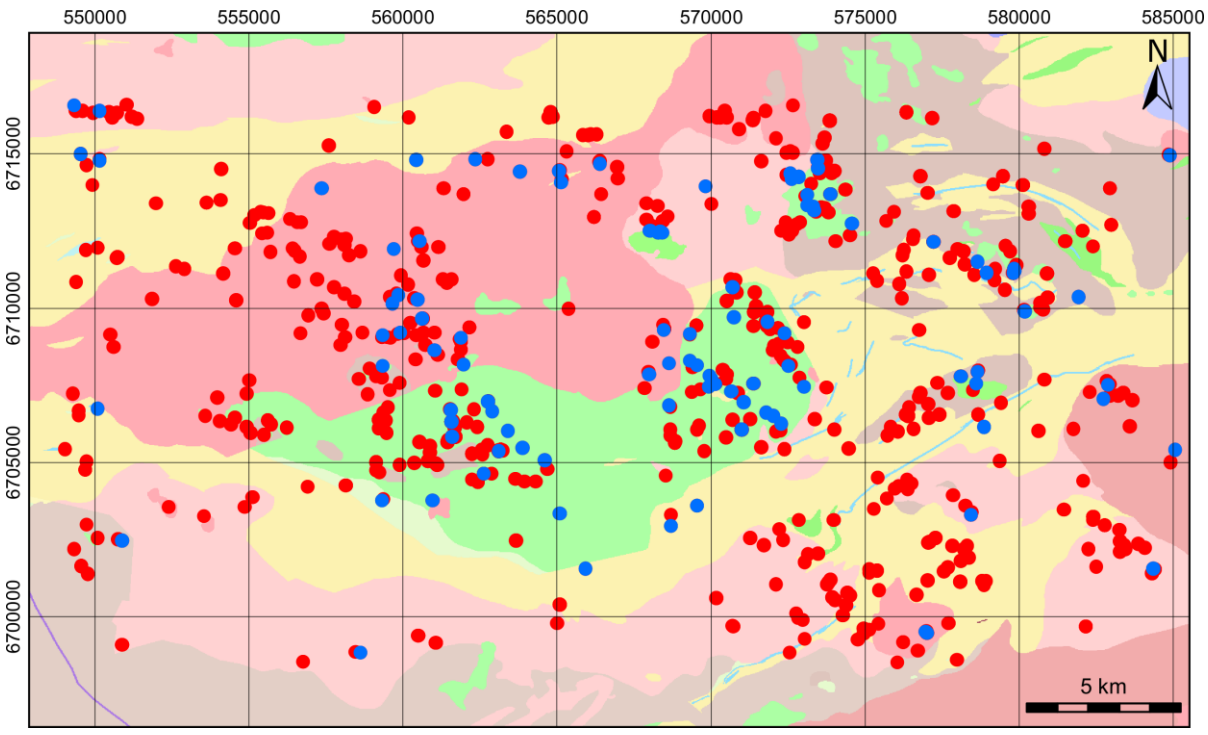

Figure 18. Map detailing the data used in the Fullen petrophysical analysis. The red dots indicate where magnetic susceptibility has been measured at outcrop, while the blue dots indicate locations where petrophysical samples have been acquired. See figure 12 for the legend for the bedrock geology map.

Table 2. Summary statistics for the petrophysical data from the Fullen study area. The upper part of the table (with blue striped shading) shows the statistics for all available data, from the four major rock types considered. The lower part of the table (with green striped shading) provides statistics for more detailed classifications of mafic intrusive rocks. Note that only samples collected during this project are included in these more detailed classifications.

Rock Type	Density (kg/m³)			Susceptibility (10^{-6} SI)				Q			
	Samples	Mean	Std. dev.	Samples	Min	Max	Median	Samples	Min	Max	Median
Felsic extrusive	9	2640	29	196	48	500000	400	6	0.06	8.81	1.23
Felsic intrusive	34	2640	51	723	10	80000	2000	28	0.03	12.5	0.23
Mafic intrusive	84	2970	77	605	10	700000	8000	80	0.02	186	0.40
Mafic extrusive	1	3000	NA	64	200	400000	600	1	0.77	0.77	0.77
Leucogabbro	1	2800	NA	1	728	728	728	1	2.35	2.35	2.35
Gabbro	20	3010	60	20	611	196000	38200	20	0.02	19.1	0.34
Gabbro-Ultramafic	1	3040	NA	1	34900	34900	34900	1	0.13	0.13	0.13
Ultramafic	1	2760	NA	1	189000	189000	189000	1	1.24	1.24	1.24

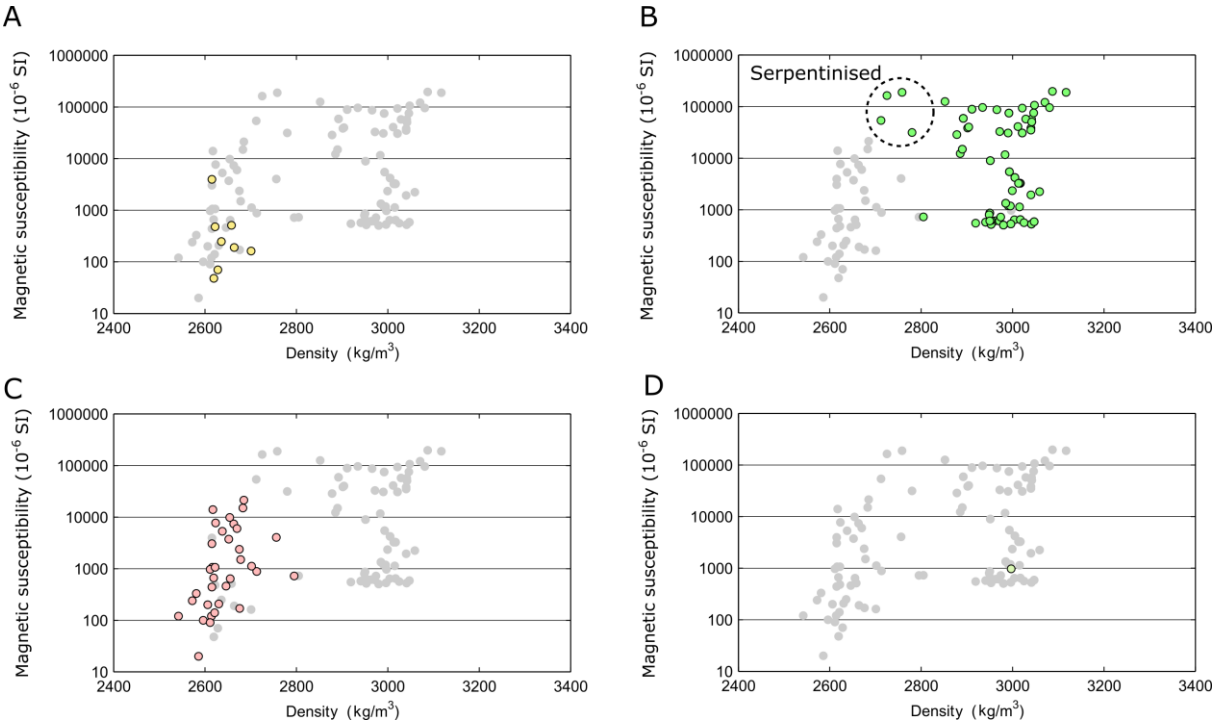

Figure 19. Cross plots showing the density and magnetic susceptibility values for petrophysical samples from four different rock types from the Fullen area. In each graph the coloured dots indicate the data from a specific rock type, while the grey dots show all the available petrophysical data for the Fullen area. **A.** Graph for extrusive felsic rocks. **B.** Graph for intrusive mafic rocks. **C.** Graph for intrusive felsic rocks. **D.** Graph for extrusive mafic rocks.

Figure 21 shows a cross plot of magnetic susceptibility and density for petrophysical samples from the Fullen study area, subdivided into different types of intrusive mafic rocks. Summary statistics for these data can also be found in table 2. A single sample collected from a rock type classified as leucogabbro exhibits a relatively low density and magnetic susceptibility when compared to the other rock types. This is most likely due to the relatively large amounts of feldspar present within this sample. The majority of the samples are from gabbro. Here a bimodal distribution in magnetic susceptibility can be observed (as in figs. 19 and 20). The higher susceptibility values (of approximately 100 000 × 10^{-6} SI) likely reflect layers of gabbro which contain appreciable amounts of magnetic minerals (such as magnetite). A single sample of ultramafic rock taken from the Karlsborg mine (within the Furulund intrusion) exhibits a relatively high magnetic susceptibility but low density, due to serpentinisation.

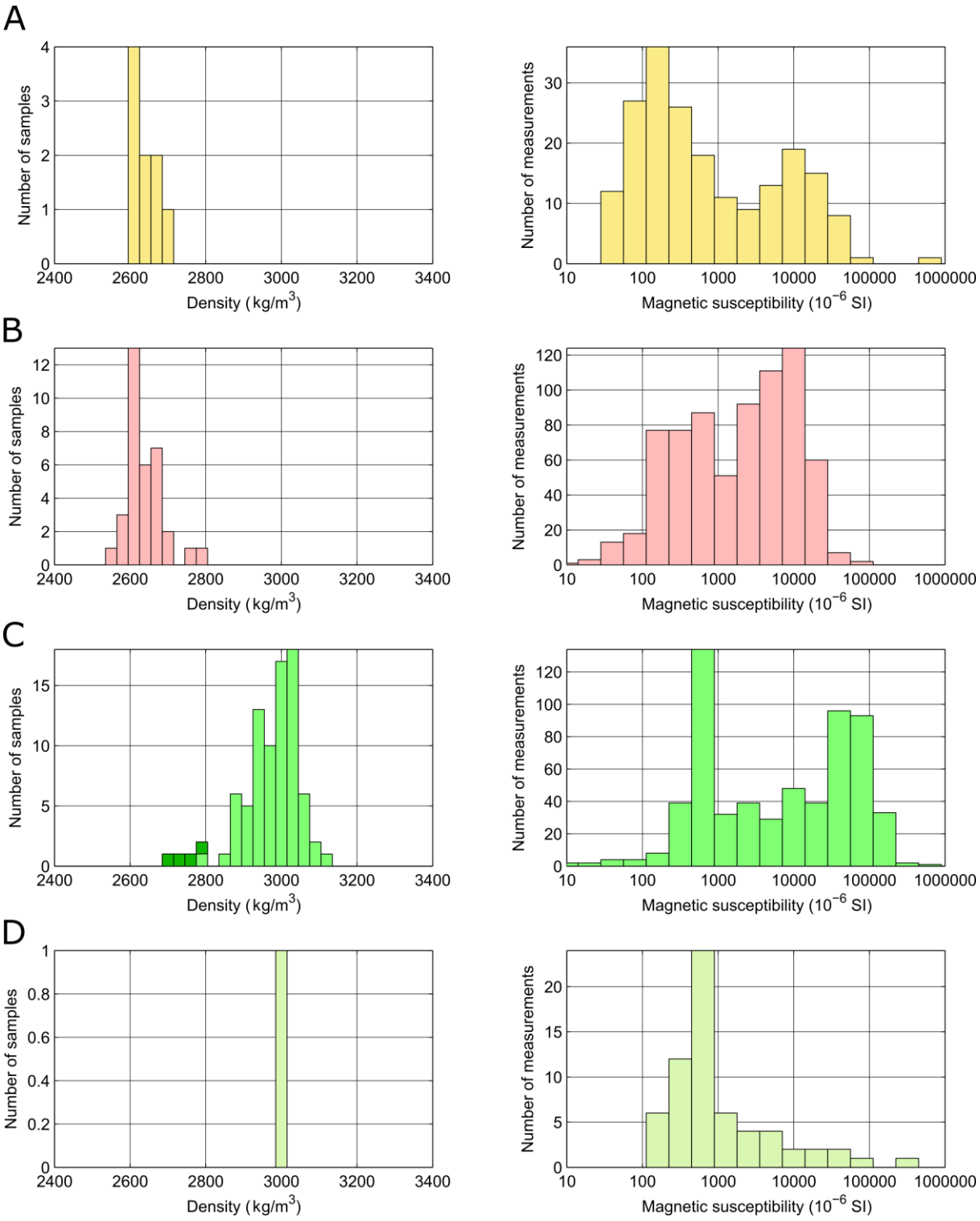

Figure 20. Histograms showing the distribution of density (left) measured on petrophysical samples and magnetic susceptibility (right) measured on petrophysical samples and at outcrop, for four different rock types in the Fullen area. **A.** Graphs for extrusive felsic rocks. **B.** Graphs for intrusive felsic rocks. **C.** Graphs for intrusive mafic rocks. Note that the samples shaded in dark green with very low densities are ultramafic rocks which have been serpentinised. **D.** Graphs for extrusive mafic rocks.

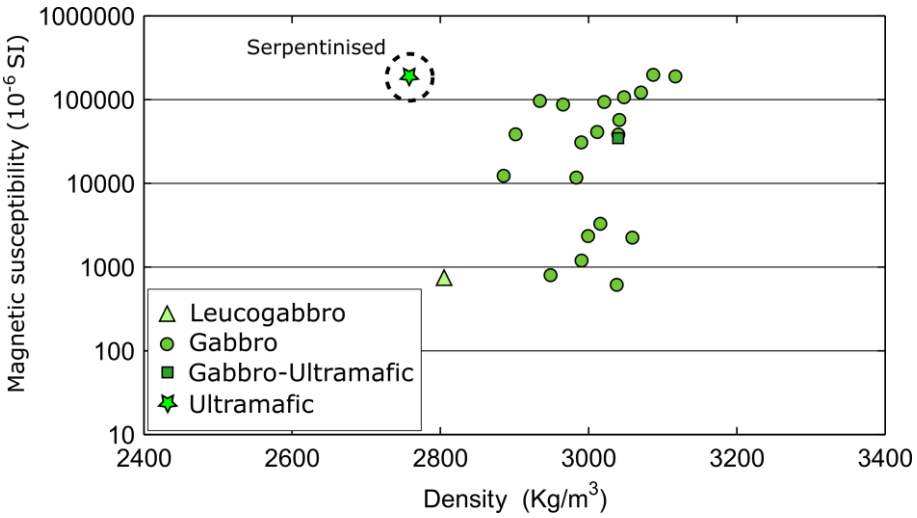

Figure 21. Cross plots showing the density and magnetic susceptibility values for petrophysical samples for intrusive mafic rocks from the Fullen study area. Only values for petrophysical data collected during this project are shown. The data are grouped into four different categories, which are represented with different symbols and colours.

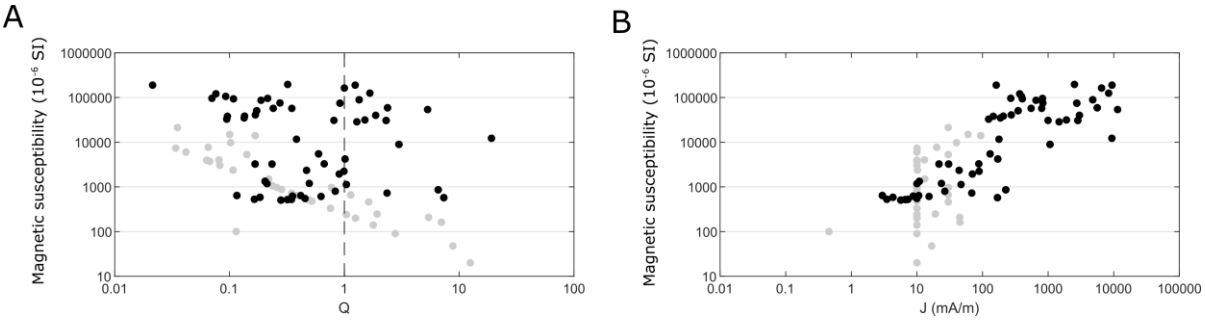

Figure 22. Graphs describing the remanent magnetisation of intrusive mafic rocks from the Fullen intrusion. **A.** A cross plot showing the Q value versus the magnetic susceptibility. **B.** A cross plot showing the remanent magnetisation (J) versus the magnetic susceptibility. In both A and B, data from intrusive mafic rocks are shown as black dots. Data from the other rock types in the study area are shown as grey dots. The strange appearance of the grey dots in this case is due to rounding of the data within the database to a certain number of significant figures.

Figure 22 shows cross plots of the Q value and remanent magnetisation (J) versus magnetic susceptibility for intrusive mafic rock types. As in the Flinten study area it can be observed that remanent magnetisation is significant in the Fullen mafic intrusive rocks where a significant proportion of the samples have a Q value above 1. Due to limitations of the available data no rose diagram is presented describing the azimuth of the remanent magnetisation for the intrusive mafic rocks from the Fullen area. However, from the limited data available, the azimuth of the remanent magnetisation appears to be aligned, to a large extent, with the azimuth of the Earth's magnetic field. However, the limited data show that the inclination of the remanent magnetisation is somewhat variable. Table 3 summarises all the petrophysics results for samples collected during this project.

Table 3. Summary of all new petrophysical data collected.

Sample ID	Easting (m)	Northing (m)	Location	Description	Density (kg/m³)	Magnetic susceptibility (10^{-6} SI)	J (mA/m)
DCL190001A	555092	6724088	Flinten	troctolite	2837	1165	315
DCL190007A	555826	6723898	Flinten	gabbro-pegmatite to gabbro	3042	22795	1660
DCL190009A	552845	6723231	Flinten, Vargberget östra	ultramafic rock	3030	126847	14825
DCL190010A	552390	6723454	Flinten, Vargberget västra	gabbro to ultramafic rock	3152	131172	250
DCL190019A	556188	6726211	Flinten	ultramafic cumulate, skillersten	3181	156354	253
DCL190022A	554859	6725302	Flinten	gabbro to ultramafic cumulate	3337	387550	5997
DCL190026A	555272	6724137	Flinten	gabbro	3066	13520	49357
DCL190027A	553298	6726649	Flinten	gabbro	3010	916	4
DCL190029A	552754	6725436	Flinten	gabbro	3026	33692	1437
DSR192007A	554381	6724635	Flinten	gabbro	3077	34828	237
DSR192008A	555073	6724608	Flinten	pegmatite	2597	-5	18
DSR192009A	554014	6723001	Flinten	felsic extrusive	2654	132	11
DSR192011A	554300	6723613	Flinten	troctolite	2818	1467	163
DSR192012A	552733	6724415	Flinten	gabbro	3073	1661	97
DSR192013A	552584	6724623	Flinten	gabbro	3095	138474	23200
DSR192014A	552695	6727326	Flinten	gabbro	2924	640	6
DSR192016A	553255	6726660	Flinten	gabbro	2990	33246	4165
DSR192018A	553594	6725352	Flinten	diorite to gabbro	2780	483	24
DSR192019A	553699	6725417	Flinten	diorite to gabbro	2756	439	19
DSR192021A	555884	6724056	Flinten	gabbro	2950	1244	329
DSR192023A	551276	6727739	Flinten	granite	2630	73	20
DCL190023A	521472	6717698	Kuså gruva 2	sulphide mineralisation in gabbro	3146	13668	14693
DCL190025A	521806	6717451	Illingsbergsgruvan	sulphide mineralisation in gabbro	3197	10900	329213
DCL190030A	601595	6633246	Gaddebo gruvor	sulphide mineralisation in gabbro	3315	49587	62497
DCL201001A	561590	6706322	Fullen	gabbro	3021	93226	404
DCL201001B	561590	6706322	Fullen	gabbro	3016	3281	88
DCL201002A	562785	6706968	Fullen	gabbro	3040	38023	146
DCL201004A	563131	6705360	Fullen	gabbro to ultramafic	3040	34900	187
DCL201005A	559244	6706365	Fullen	gabbro	3038	610	37
DCL201007A	561615	6705833	Fullen	gabbro	3048	105825	392
DCL201008A	562635	6704609	Fullen	gabbro	3071	121019	368
DCL201010A	570996	6706050	Fullen	gabbro	3087	196275	2518
DSR201001A	565092	6703322	Fullen	gabbro	2999	2346	44
DSR201001B	565092	6703322	Fullen	gabbro	2934	95951	270
DSR201007A	564606	6705058	Fullen	gabbro	2902	38383	208
DSR201009A	563898	6705467	Fullen	gabbro	2990	1194	24
DSR201012A	562912	6706645	Fullen	gabbro	2949	798	27
DSR201013A	562778	6706975	Fullen	gabbro	3042	57141	797
DSR201014A	561976	6708164	Fullen	gabbro	3012	40794	274
DSR201015A	569341	6708278	Fullen	leucogabbro	2805	729	69
DSR201018A	569555	6708126	Fullen	gabbro	2984	11645	178
DSR201021A	569973	6707795	Fullen	gabbro	2966	86675	652
DSR201022A	570040	6707680	Fullen	gabbro	3059	2234	89
DSR201022B	570040	6707680	Fullen	rhyolite	2619	48	17
DSR201023A	570146	6707525	Fullen	rhyolite	2636	247	19
DSR201024A	569949	6707442	Fullen	rhyolite	2701	161	45
DSR201025A	571812	6706600	Fullen	gabbro	2886	12235	9351
DSR201026A	572040	6706492	Fullen	granite	2630	207	45
DSR201027A	572298	6706240	Fullen	gabbro	2990	30775	998
DCL201011A	573892	6713678	Skållberget	gabbro	3117	189161	162
DCL201012A	568024	6712495	Karlsborg	ultramafic	2758	189058	9394

Airborne geophysical measurements and gravity data

As part of this study regional maps describing the residual gravity field (fig. 23) and residual magnetic field (fig. 24) were generated. To generate the regional magnetic field map shown in this report (fig. 24), pre-existing airborne magnetic measurements collected in 1976, 1977, 1982, and 1989 were used. These data were collected with a nominal flight height and line separation of 30 and 200 m, respectively. These data were reduced-to-pole, merged and the regional trend was subtracted. Furthermore, connections and lineaments were interpreted from the regional residual magnetic map in the area around the Flinten intrusion which are also shown in figure 24. The regional residual gravity map (fig. 23) was generated by subtracting the regional trend from the Bouguer anomaly data and includes all available gravity measurements within SGU's database (including new measurements made in 2019).

It is clear from the regional residual magnetic map (fig. 24) that both the Flinten and Fullen intrusions give rise to clear magnetic anomalies. In addition, some of the other mafic and ultramafic intrusions to the northeast of the Fullen intrusion also give relatively strong magnetic anomalies. This is consistent with the petrophysical analysis which shows that the magnetic susceptibilities of these mafic intrusive rocks are typically significantly higher than the other surrounding rock types. Within the Fullen and Flinten intrusions one can observe a series of continuous linear anomalies, which are interpreted to be associated with magmatic layering. These will be discussed in subsequent sections in more detail. It can be observed that the interpreted lineaments and connections lie predominantly in a west-northwest to east-southeast orientation.

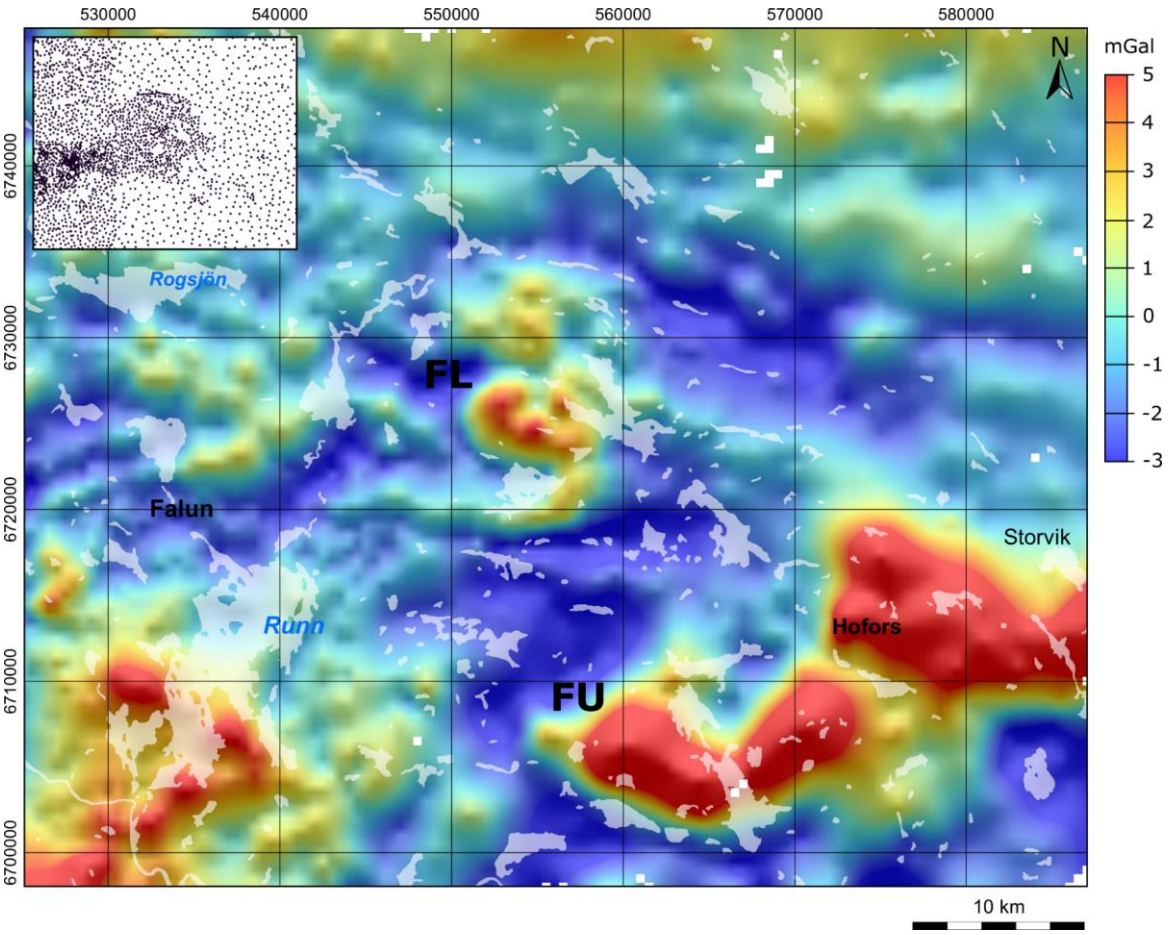

Figure 23. Regional map showing the residual gravity field. The annotations FL and FU denote the location of the Flinten and Fullen intrusions, respectively. The inset map shows the location of the gravity measurements used to generate the map. Note that the spacing between data points is far lower for the Flinten intrusion than the Fullen intrusion.

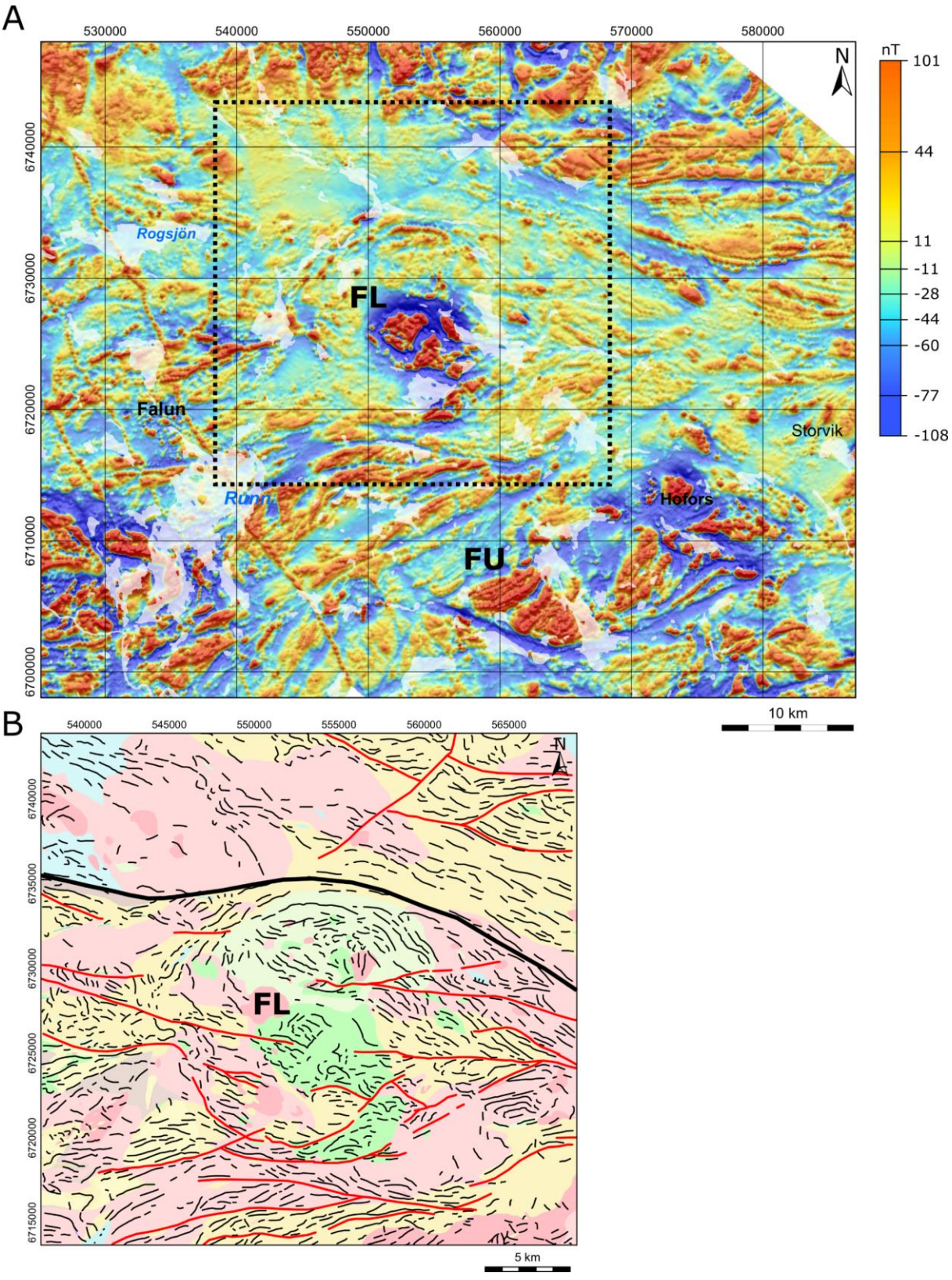

Figure 24. A. Regional residual magnetic field map. The annotations FL and FU denote the location of the Flinten and Fullen intrusions, respectively. The dashed black rectangle denotes the area of the map shown in B. **B.** Map showing interpretation of lineaments (red lines) and connections (black lines) from the regional residual magnetic field data around the Flinten intrusion. The thick black line shows the location of the Gävle-Rättvikzonen, a regional brittle to ductile shear zone. See figure 12 for the legend for the bedrock geology map.

This is consistent with previous studies, which interpret the Flinten area to lie on the edge of a tectonic zone characterized by high strain rates formed under amphibolite-facies conditions (Stephens et al. 2009). The location of a regional brittle to ductile shear zone (Gävle-Rättvikzonen) mapped to the north of the Flinten intrusion is shown in figure 24. The interpreted connections around the Flinten intrusion and extrusive mafic rocks to the north, form a lens-like geometry. This is especially noticeable to the east of the intrusion. This geometry suggests that the extrusive and intrusive mafic rocks within and around the Flinten intrusion, form a more competent zone. Hence it can be interpreted that these mafic rocks are less deformed than the surrounding felsic rocks. The deflection of the otherwise relatively straight Gävle-Rättvikzonen around the zone with mafic rocks, also somewhat supports this interpretation. On the regional residual gravity map (fig. 23) clear anomalies can be observed at both the Flinten and Fullen intrusions. The gravity anomaly in the area of the Fullen intrusion is larger when compared to the Flinten intrusion, suggesting that larger volumes of mafic rocks are present at this location (i.e. greater thicknesses and the presence of additional mafic units which lie below the surficial felsic rocks). The Gävle-Rättvikzonen can be observed to some extent in the gravity data, as a zone of low residual gravity running west-northwest to east-southeast, to the northeast of the Flinten intrusion.

The Flinten intrusion

In this section detailed maps describing the airborne geophysical data and gravity data from the Flinten intrusion are presented and discussed. Figure 25 shows a map of the residual magnetic field from the Flinten intrusion calculated using aeromagnetic data acquired in 2019 (with a nominal line azimuth, line spacing and flight height of 130º, 200 m and 60 m, respectively). Here it can be observed that strong magnetic anomalies occur in association with the intrusion. Within the northern part of the intrusion there are three distinct areas where strong positive residual field values can be observed. In the southern part of the intrusion, the amplitudes of the anomalies are typically lower, compared to the northern part. Measurements of the strike and dip of the magmatic layering, measured during this project and in previous studies, are annotated on the map. In general, the orientation of the magnetic anomalies correlates well with the measurements of magmatic layering.

It is established that variations in magnetic properties can occur in association with magmatic layering, which forms due to differentiation within mafic and ultra-mafic magma chambers (Ferré et al. 2009). Within this study the assumption is made, that on a broad scale, the anomalies in the magnetic field are associated with the magmatic layering in this intrusion. Hence, an interpretation of the layering has been made based on the airborne magnetic data and outcrop observations, which can be seen in figure 25. In addition to this, the intrusion has been divided up into several regions based on their characteristics in the magnetic data and the interpreted layering (labelled F1A, F1B, F1C, F2A and F2B in figure 25). The northern three regions of the intrusion (F1A, F1B and F1C) contain the strongest positive anomalies within the structure. In these regions the central part appears to be more strongly magnetised and to exhibit layering in the anomaly pattern. Conversely, the edges of these regions appear to be relatively weakly magnetised. A possible explanation for this pattern is that the inner parts of these regions crystallised later than the outer parts. Hence, they include a greater amount of magnetite, due to iron enrichment of the magma over time (Ferré et al. 2009). In contrast to the northern regions, the southern two regions (F2A and F2B) do not have a highly magnetised centre and instead exhibit weaker anomalies, interpreted to be associated with layering, over their entire area. There appears to be a discontinuity in layering direction between F1B and F2A in both the magnetic data and outcrop data.

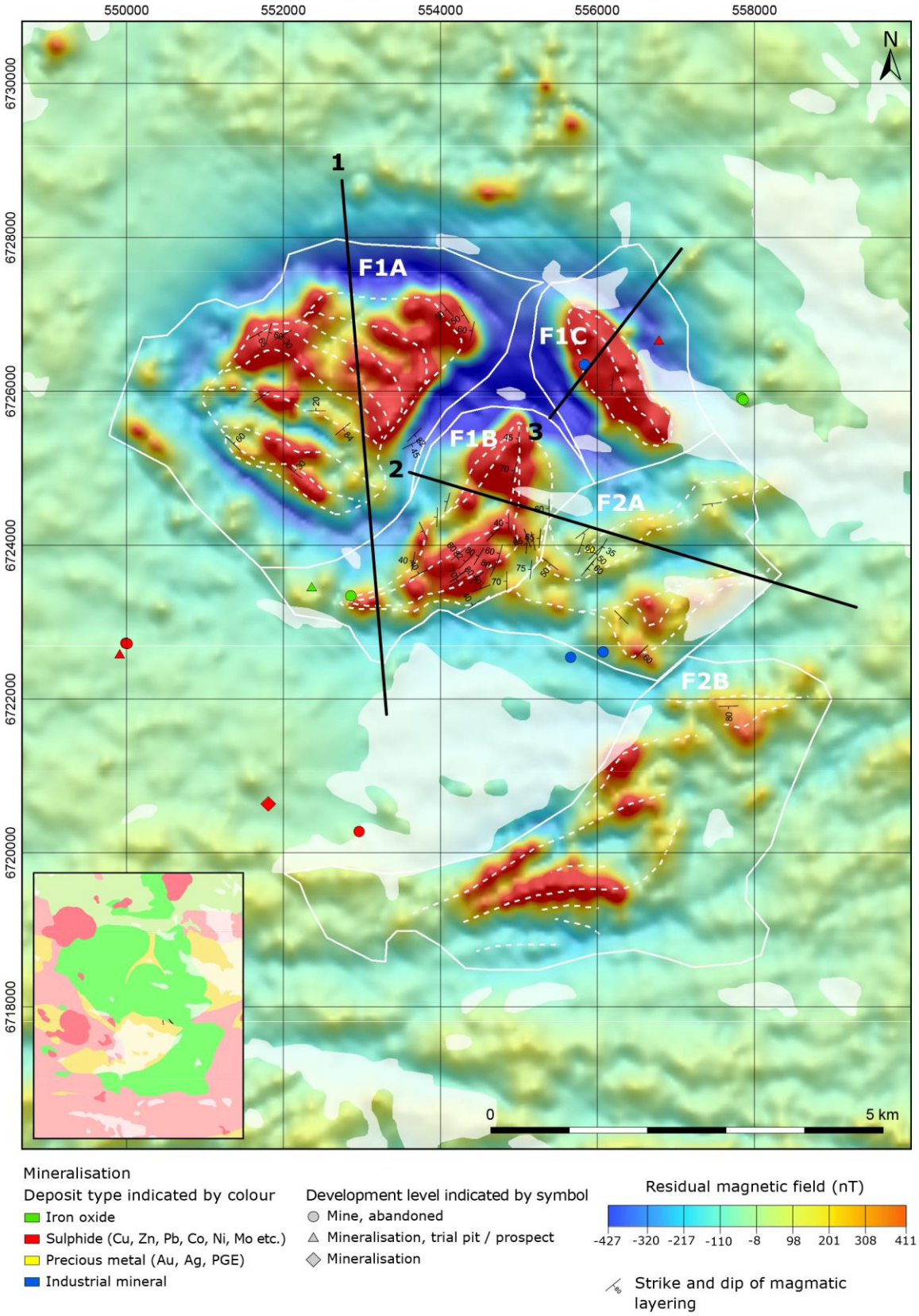

Figure 25. Map showing the residual magnetic field over the Flinten intrusion. Profiles where 2D geophysical modelling has been performed are shown as black lines. Dashed white lines show the interpreted direction of magmatic layering in the intrusion. Solid white lines describe different parts (regions) of the intrusion, discussed in the text. The small inset map in the lower left corner shows the bedrock geology for the area (see figure 12 for the legend).

A possible interpretation of these regions is that F1A, F1B and F1C represent three distinct intrusions which are approximately coeval and hence, have similar geophysical characteristics. F2A and F2B, based on their characteristics, could be also coeval, but would have formed at a different time to F1A, F1B and F1C.

Figure 26 shows a map of apparent resistivity over the Flinten intrusion, generated from airborne VLF measurements (dual transmitters) collected in 2019. Several anomalies with low resistivity exist in the data, within the area of the intrusion. On comparison with the position of infrastructure (such as roads, railroads, and power lines) a number of these features with low resistivity can be disregarded as non-geological. A significant anomaly, which appears to be geological runs southwest and northeast from the position marked with an X in figure 26. This anomaly was the focus of previous investigations and ultimately the target for the Sparvguld borehole (Granar & Henkel 1981, Hammergren 1982). Hence, it can be interpreted to be due to the presence of a water bearing brittle deformation zone. This anomaly appears to separate the F1A region of the intrusion from the F1B and F1C regions. Within the F1A region of the intrusion there appears to be several subtle anomalies with low resistivities, which lie subparallel to the direction of the magmatic layering (interpreted from the residual magnetic data) (shown with Y and Z in figure 26). These could be interesting targets for further investigation as they could indicate the presence of more conductive layers within the intrusion. However, it is possible that they correspond to deformation zones or areas of surficial sediment with a high water-content. Several areas of relatively high resistivity are located within the F1A, F1C and F2B regions of the intrusion. These can be interpreted as areas which are relatively unaffected by brittle deformation.

A map of the residual gravity field is shown in figure 27. This map was generated by subtracting the regional trend from the available Bouguer anomaly data for the area. Data from the new measurements collected in 2019 are included, hence, the average spacing between data points was approximately 500 m. The intrusion is clearly associated with relatively high residual gravity field values. Within the area of the intrusion there appears to be several distinct peak values in the residual field. These peak values correspond, to some degree, with the regions of the intrusion interpreted from the magnetic data (fig. 25). For example, F1C and F2B appears as distinct peaks in the residual gravity values, separated from the other regions by lower values. F1A, F1B and F2A are also, to a lesser extent distinguishable in the gravity data as individual peaks. In between regions F1A and F1C lies an area with relatively low residual gravity values. In this study, this area (which has previously been mapped as gabbro) is interpreted to consist primarily of felsic metavolcanic rocks. This is consistent with several outcrop observations, as well as the data from the Sparvguld borehole (Hammergren 1982). In other parts of the intrusion, where the residual gravity data is relatively low (for example in between F1C and F2A), the intrusion is interpreted to be relatively thin and to consist potentially of less dense rock types (for example diorite-gabbro or leucogabbro). Figure 6B provides an example of these less dense rock types, diorite to gabbro, occurring at the edge of the region F1A. If F1A is considered to represent a separate intrusion (coeval with F1B and F1C), these diorite-gabbro rocks could represent less dense rock types which crystallized relatively early at the edge of the magma chamber.

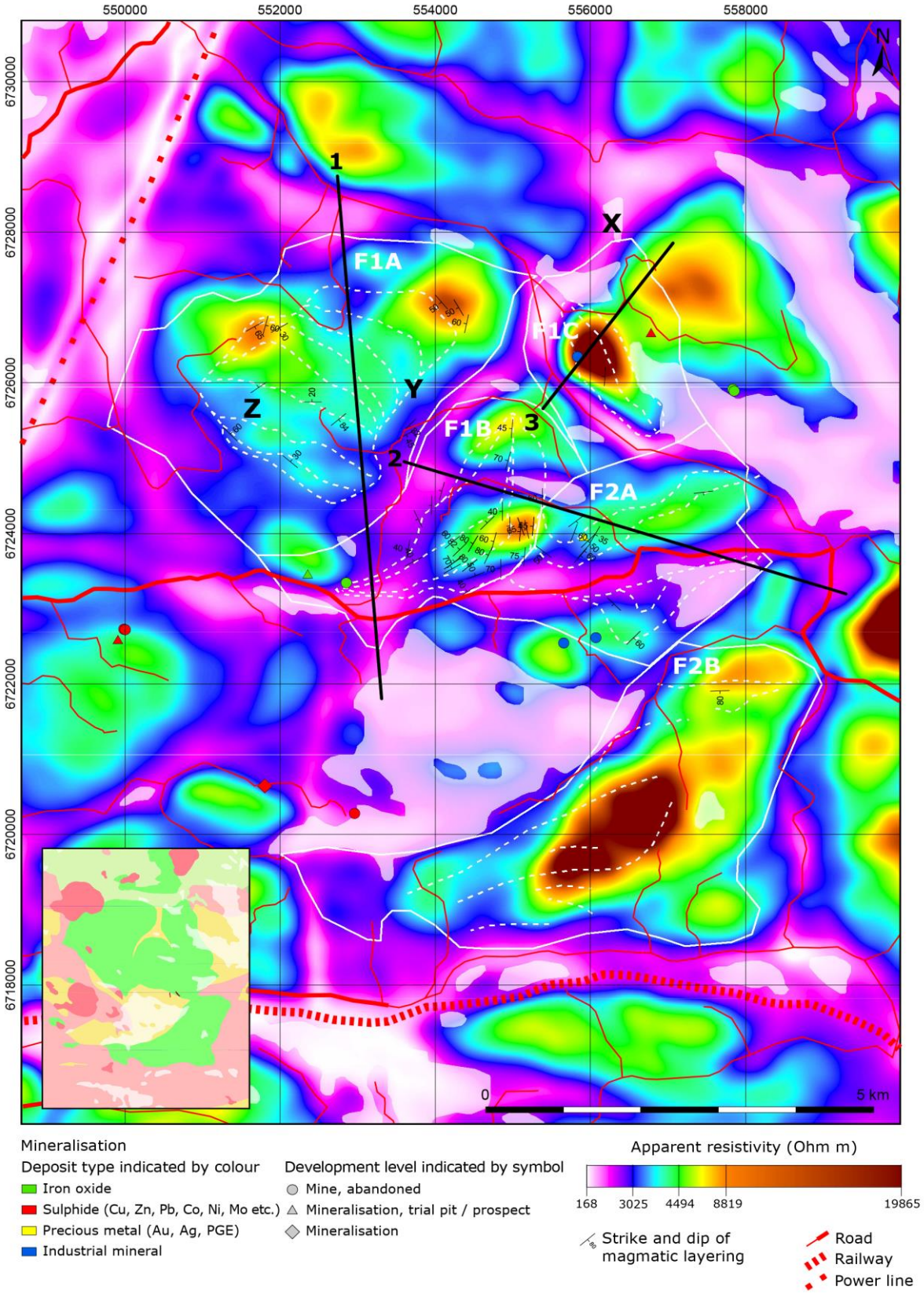

Figure 26. Map of the apparent resistivity of the Flinten intrusion. Profiles where 2D geophysical modelling has been performed are shown as black lines. Dashed white lines show the interpreted direction of magmatic layering in the intrusion. Solid white lines describe different parts (regions) of the intrusion, discussed in the text. The small inset map in the lower left corner shows the bedrock geology for the area (see figure 12 for the legend). X marks the large resistivity anomaly drilled by the Sparvguld borehole. Y and Z mark small low resistivity anomalies, which lie subparallel to the layering direction.

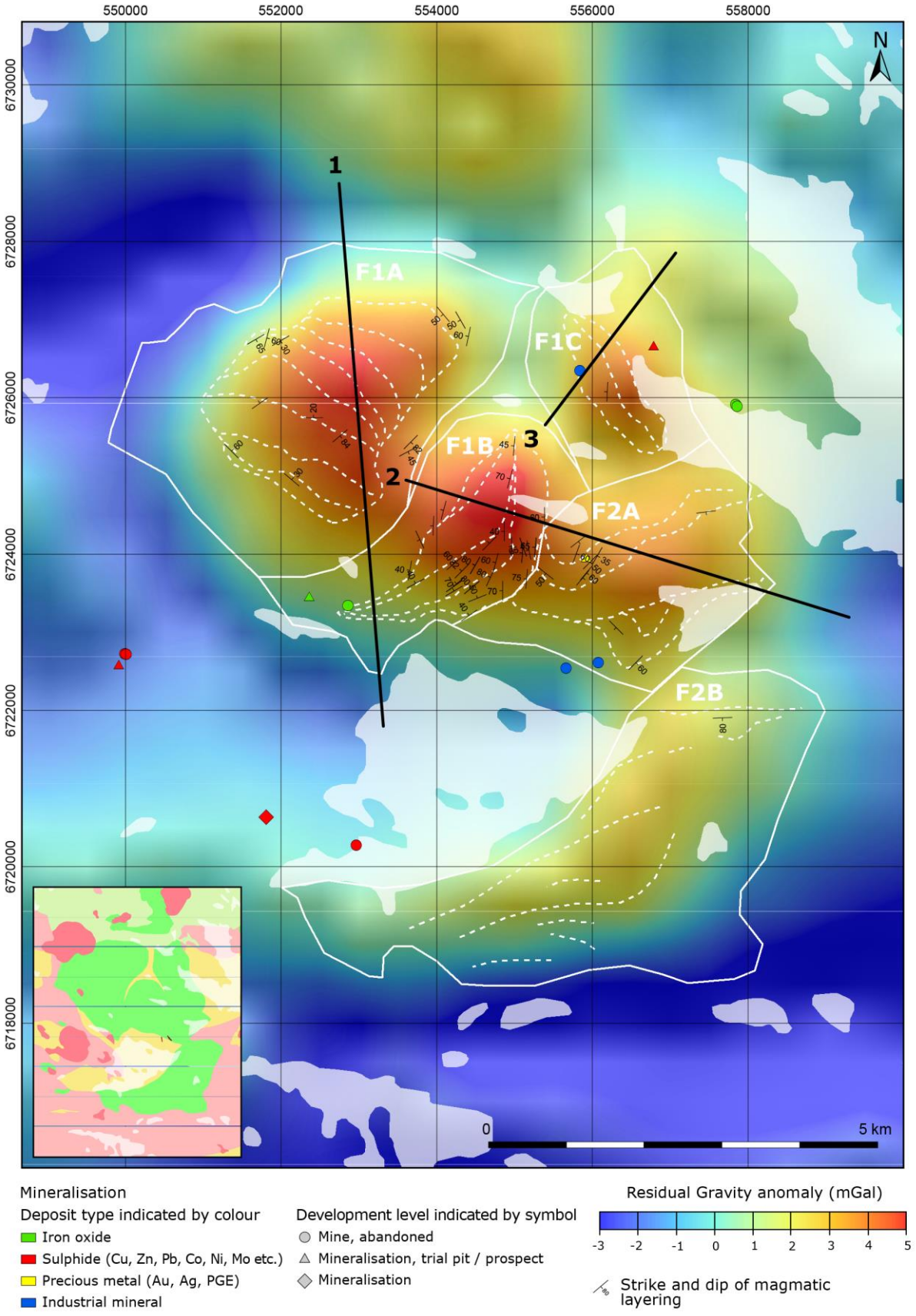

Figure 27. Map showing the residual gravity field at the Flinten intrusion. Profiles where 2D geophysical modelling has been performed are shown as black lines. Dashed white lines show the interpreted direction of magmatic layering in the intrusion. Solid white lines describe different parts (regions) of the intrusion, discussed in the text. The small inset map in the lower left corner shows the bedrock geology for the area (see figure 12 for the legend).

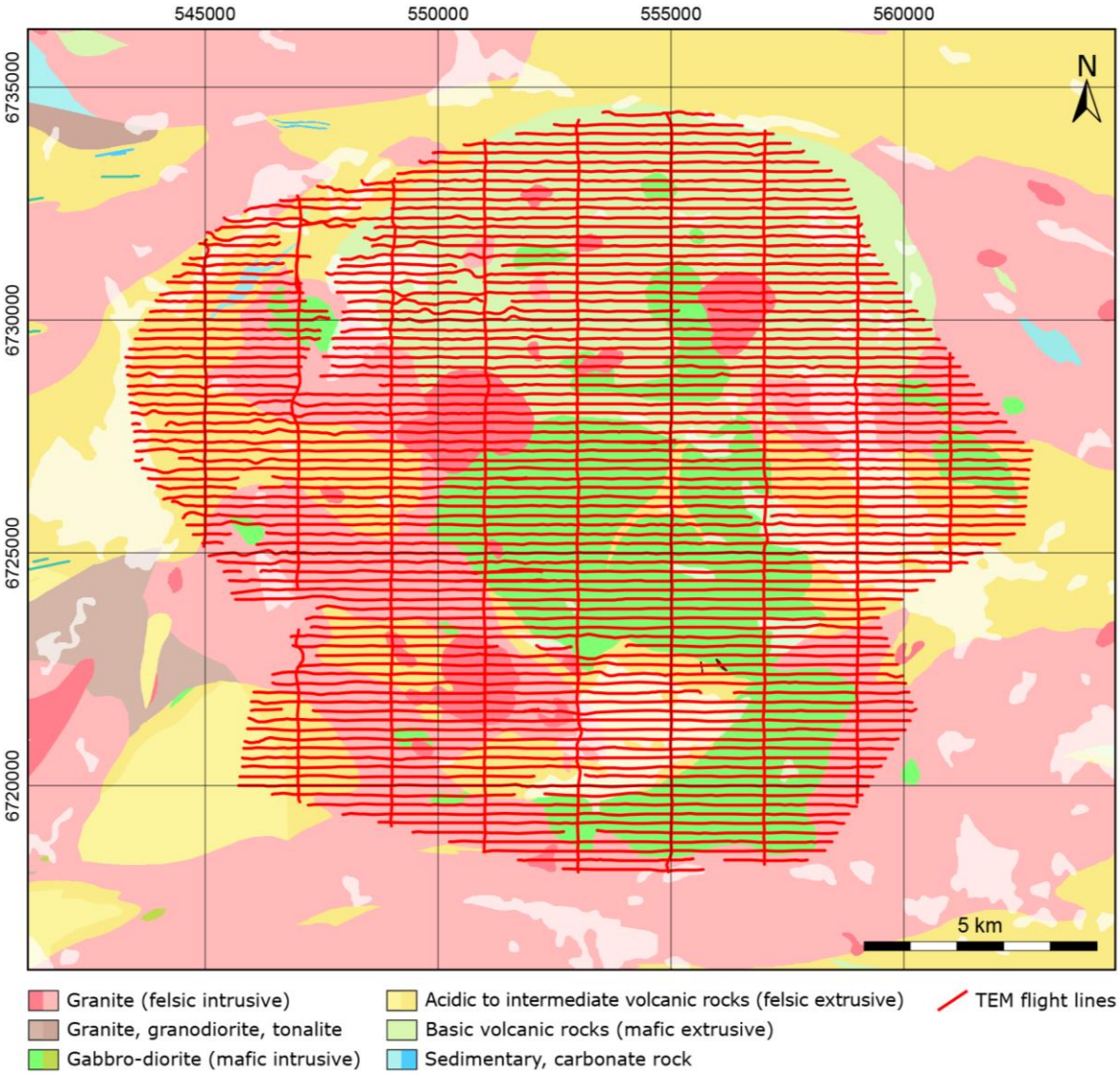

Figure 28. Map showing the location of the flight lines for the ATEM data acquisition in 2019.

Figure 28 shows a map with the location of the flight lines for the ATEM survey, which included the area of the Flinten intrusion. ATEM is an airborne transient electromagnetic method, which is sensitive to the conductive properties of the subsurface. The data were collected in the winter of 2019 and include approximately 1 200 km of flight lines. The average ground clearance during the flight was 60 m. After acquisition, preliminary processing was performed to generate a range of attribute maps. Where possible, the data were inverted to generate resistivity models of the subsurface.

After an inspection of the preliminary results, several low resistive features were highlighted within the subsurface. However, these were not located within the mafic intrusive rocks of the Flinten intrusion. Within the mafic rocks the resistivities were typically too high to perform the inversions and hence, it was not possible to generate resistivity models for most of the Flinten intrusion. It may be possible to obtain better results from the data within the mafic intrusive rocks by re-processing with different parameters, however this was not within the scope of this project. As a result, the ATEM data was not used in this project and will not be discussed further within this report.

The Fullen intrusion

In this section maps generated from airborne geophysical measurements and gravity measurements are presented and discussed for the Fullen intrusion. Note that the airborne geophysical data and gravity data presented here are from the same dataset as presented for the Flinten intrusion (see the previous section for the acquisition parameters). Figure 29 shows a map of the residual magnetic field based on airborne data collected in 2019. Within the data, the Fullen intrusion, as well as the other smaller mafic and ultramafic intrusions, are associated with clear positive anomalies. This is consistent with the petrophysics data which shows that the mafic and ultramafic rock types in this area have significantly higher average susceptibilities than the surrounding, predominantly felsic rocks.

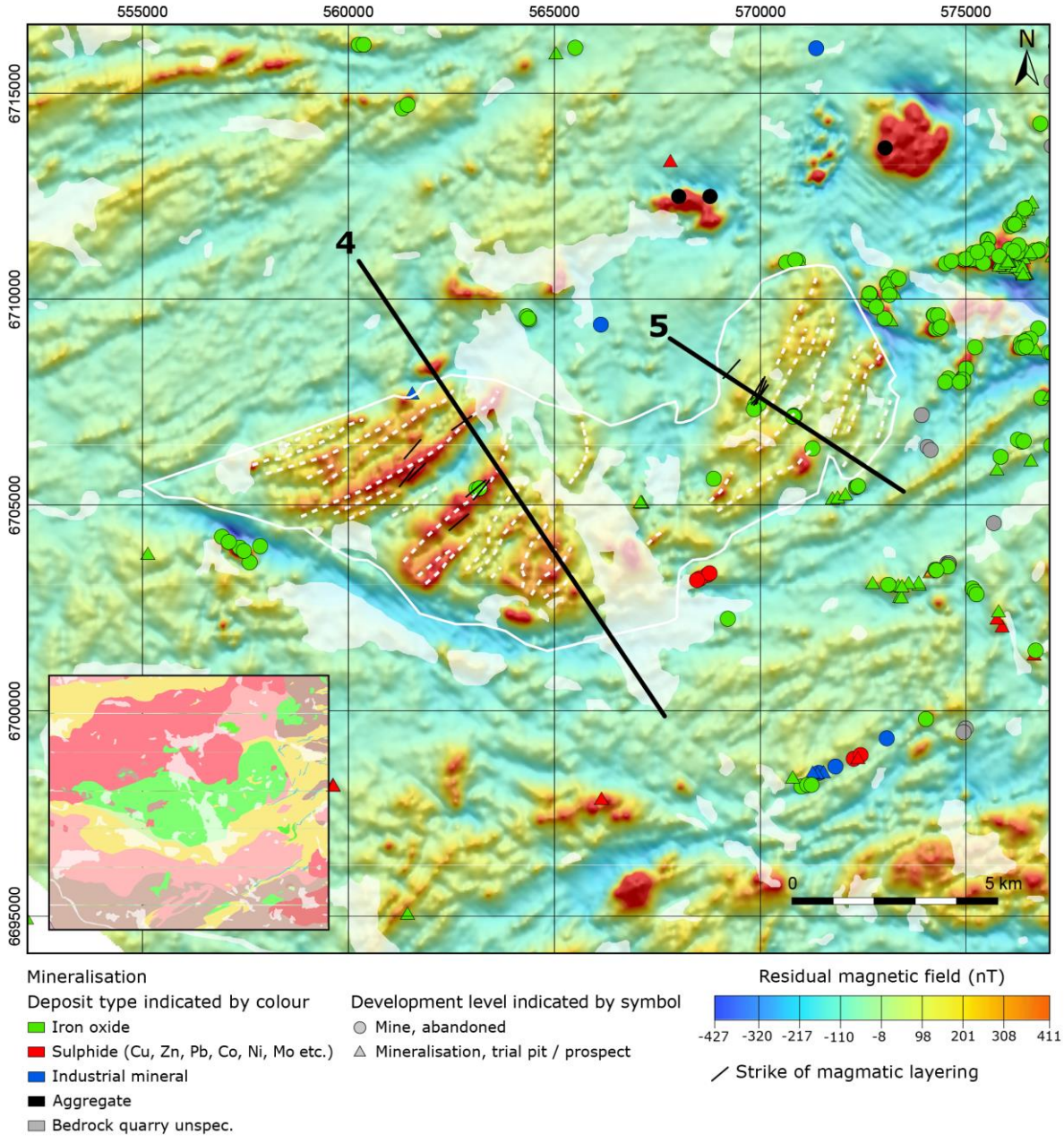

Figure 29. Map showing the residual magnetic field over the Fullen intrusion. Profiles where 2D geophysical modelling has been performed are shown as black lines. Dashed white lines show the interpreted direction of magmatic layering in the intrusion. The solid white line describes the edge of the intrusion. The small inset map in the lower left corner shows the bedrock geology for the area (see figure 12 for the legend).

Within the Fullen intrusion are a series of positive magnetic anomalies which have a general south-west to northeast strike. These anomalies are strongest and most well developed on the western side of the structure. Measurements of the strike of the magmatic layering observed at outcrop during this project are annotated on the map (fig. 29). Here it can be observed that these magnetic anomalies correlate well with the direction of magmatic layering. Hence, at the Fullen intrusion, it is assumed that these magnetic anomalies are indicative of the layering within the intrusion and represent layers which contain greater quantities of magnetic minerals (Ferré et al. 2009).

Figure 30 shows a map of the apparent resistivity over the Fullen intrusion, derived from VLF measurements (dual transmitters) conducted in 2019. Many of the regions of low resistivity shown on the map can be attributed to infrastructure (shown as red lines). However, several low resistive features are likely due to geological factors. To the north of the western part of the Fullen intrusion lies a linear region of low resistivity (marked with an X in figure 30). This is interpreted as a zone with brittle deformation, which contains water. About 1 km south of the position marked with the X in figure 30 a subtle low resistivity anomaly can be observed which lies subparallel to the interpreted magmatic layering. This could indicate a part of the intrusion with lower resistivity values or a small deformation zone. In the southern part of the intrusion, another zone with relatively low resistivity values which lies subparallel to the magmatic layering exits (marked with a Y in figure 30). This could be indicative of a greater level of deformation in this part of the structure or a greater degree of water saturation in the soil layer. However, there is some potential that it is due to lower resistivity values within the intrusion itself. Another low resistivity zone is marked with a Z in figure 30. This is interpreted to be a deformation zone, which juxtaposes the mafic rocks of the Fullen intrusion against a younger granite unit.

Figure 31 shows a map of the residual gravity over the Fullen intrusion. No new gravity measurements were collected in this area as part of the project. Hence, the gravity measurements in this area remain relatively sparse (approximately 1.5 to 2.5 km between measurements). The Fullen intrusion and majority of the smaller mafic and ultramafic intrusions are associated with strong positive residual gravity anomalies. An exception to this is the Karlsborg mine, which is marked with a X in figure 31. The relatively weak gravity anomaly could be due to the small size of the intrusion, but it is also likely to be due to the low-density values of the serpentinised ultramafic rocks at this location. Relative to the Flinten intrusion, the residual anomaly at the Fullen intrusion is significantly larger, which indicates a greater volume of mafic rocks are present at this location. The solid white line delineates the mapped extent of the Fullen intrusion in figure 31. However, it can be observed that the positive gravity anomaly extends beyond the limits of the polygon in several places. Notably to the northwest and to the southeast of the intrusion, close to the northern end of modelling profile 4 and southern end of modelling profile 5, respectively. In these areas the mafic rocks are interpreted to extend below the surficial felsic rocks which are mapped.

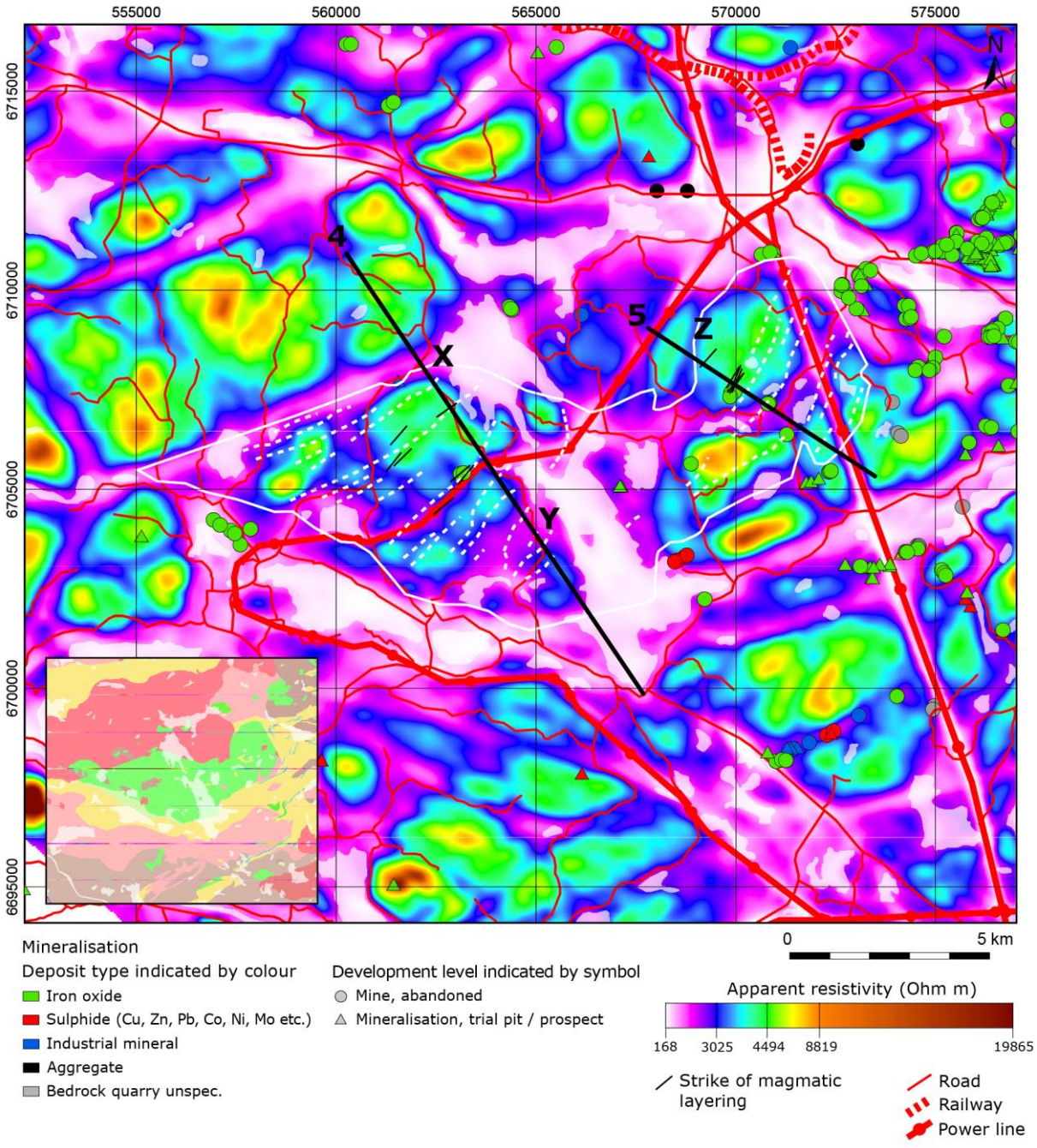

Figure 30. Map of the apparent resistivity of the Fullen intrusion. Profiles where 2D geophysical modelling has been performed are shown as black lines. Dashed white lines show the interpreted direction of magmatic layering in the intrusion. The solid white line describes the area of the intrusion. The small inset map in the lower left corner shows the bedrock geology for the area (see figure 12 for the legend).

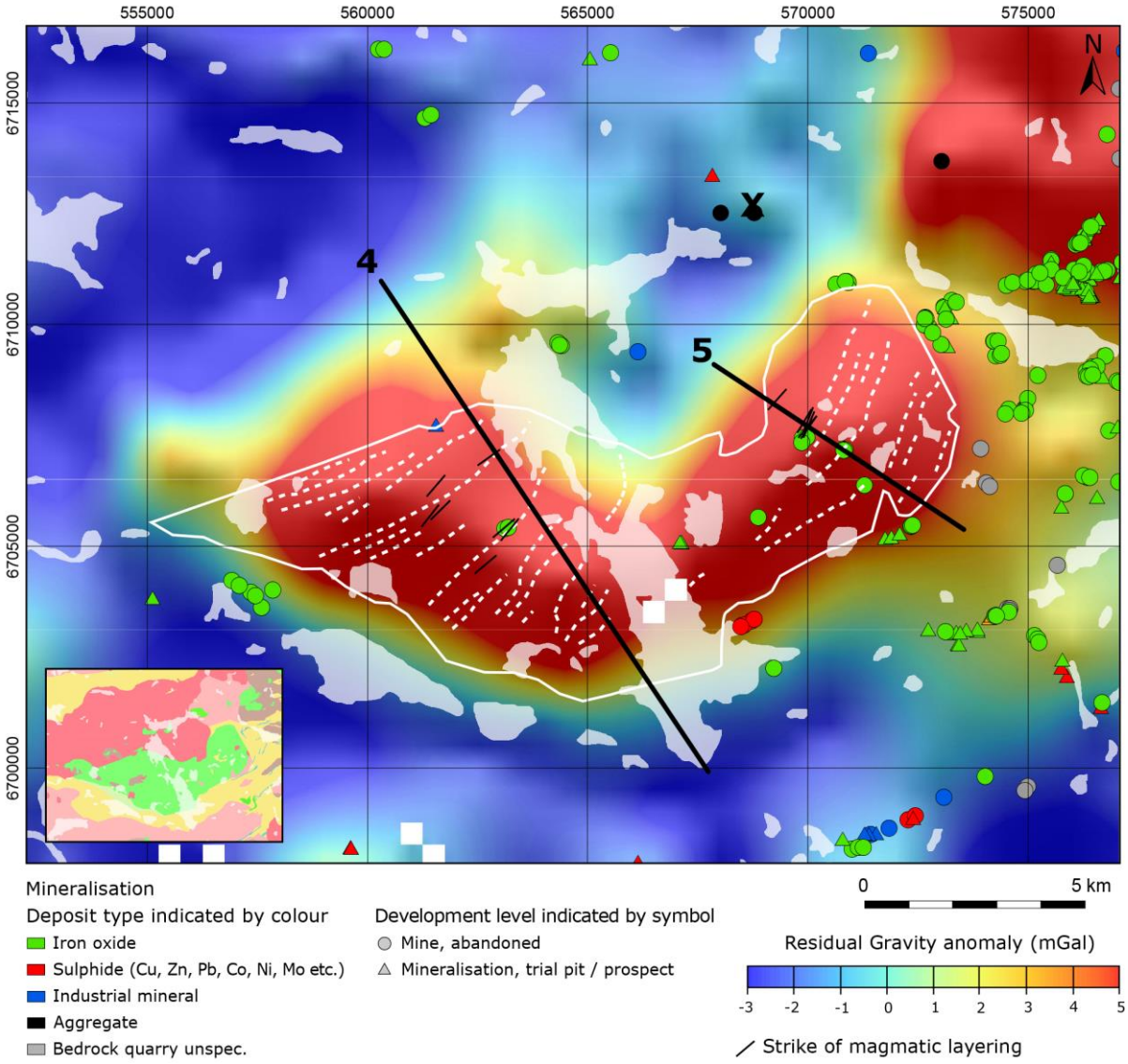

Figure 31. Map showing the residual gravity field at the Fullen intrusion. Profiles where 2D geophysical modelling has been performed are shown as black lines. Dashed white lines show the interpreted direction of magmatic layering in the intrusion. The solid white line describes the area of the intrusion. The small inset map in the lower left corner shows the bedrock geology for the area (see figure 12 for the legend).

Ground based measurement

During the summer of 2019 and 2020 several types of ground geophysical measurements were collected at the Flinten and Fullen intrusions. See figure 12 for the location and type of measurements collected. At both the Flinten and Fullen intrusions ground magnetic and VLF measurements were collected along five regional profiles (fig. 12) for the purpose of providing data for 2D geophysical modelling. Furthermore, maps (2D grids) of the magnetic field were generated over two focus areas (one at each intrusion) by measuring many profiles in parallel. To collect the magnetic data a GEM GSMV-19 instrument was used. Measurements were collected every 1 second whilst walking along the profiles. The data were corrected for diurnal variations using a drift calculated from a minimum of two base station measurements per profile. In the case of the focus area (2D magnetic measurements) at the Flinten intrusion, base station data from the Fiby magnetic observatory were used to correct for the diurnal variation. To collect the VLF data both WADI and GEM GSMV-19 instruments were used. VLF measurements along profiles were taken with a spacing of approximately 20 m. The frequencies which were measured during the VLF profiles were chosen based on the suspected orientation of the subsurface conductors and orientation of the profiles. To provide additional data along the regional profiles and within the two focus areas, petrophysics samples and measurements of natural gamma radiation and magnetic susceptibility were collected.

The magnetic and VLF data collected along the regional profiles are presented later in the report together with the 2D modelling results (see section *Geophysical modelling*). In the following sections the two focus areas, where magnetic measurements were performed over an area are discussed and presented.

Detailed ground magnetic measurements at the Flinten intrusion

Figure 32 shows a map of the magnetic field measured over an area (approximately 1 000 × 1 000 m) within the Flinten intrusion. There were two primary objectives when collecting these measurements. Firstly, the occurrence of precious metals has been documented previously at this location, albeit within boulders detached from the bedrock. Therefore, measurements were performed in this area to better understand the structure of the intrusion at this location. Secondly, magnetic measurements were collected here to gain a better understanding of the relationship between the magnetic anomalies and magmatic layering direction observed at outcrop. An additional practical reason for selecting this area was that the topography was relatively flat, when compared to other parts of the intrusion, which allowed for more efficient data acquisition.

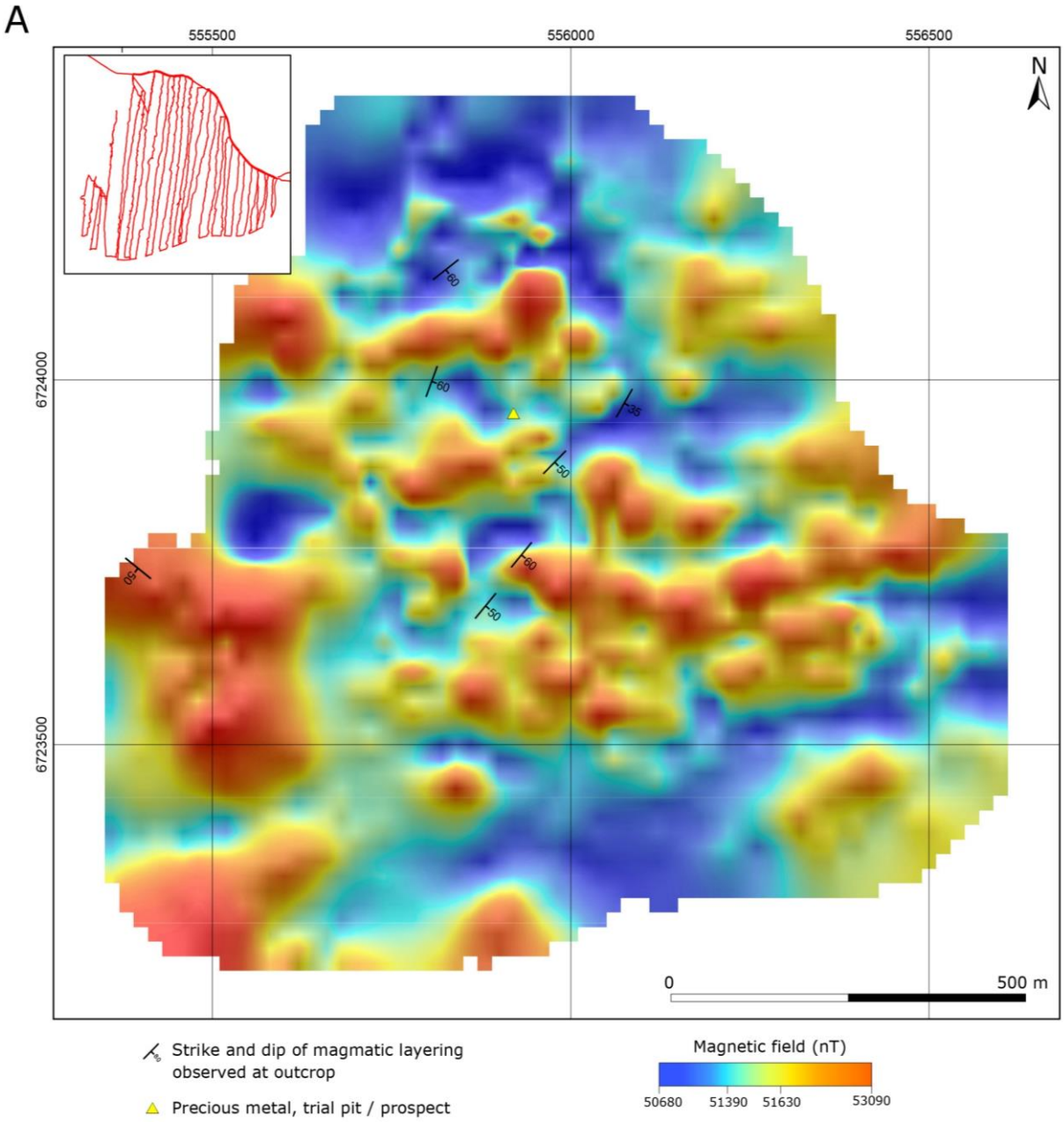

Figure 32. Measurements and interpretation of a focus area within the Flinten intrusion. The location of the focus area is indicated with a star in figure 12. **A.** Map showing the magnetic field measurements collected over the area. The inset map in the upper left-hand corner shows the locations of the measurements.

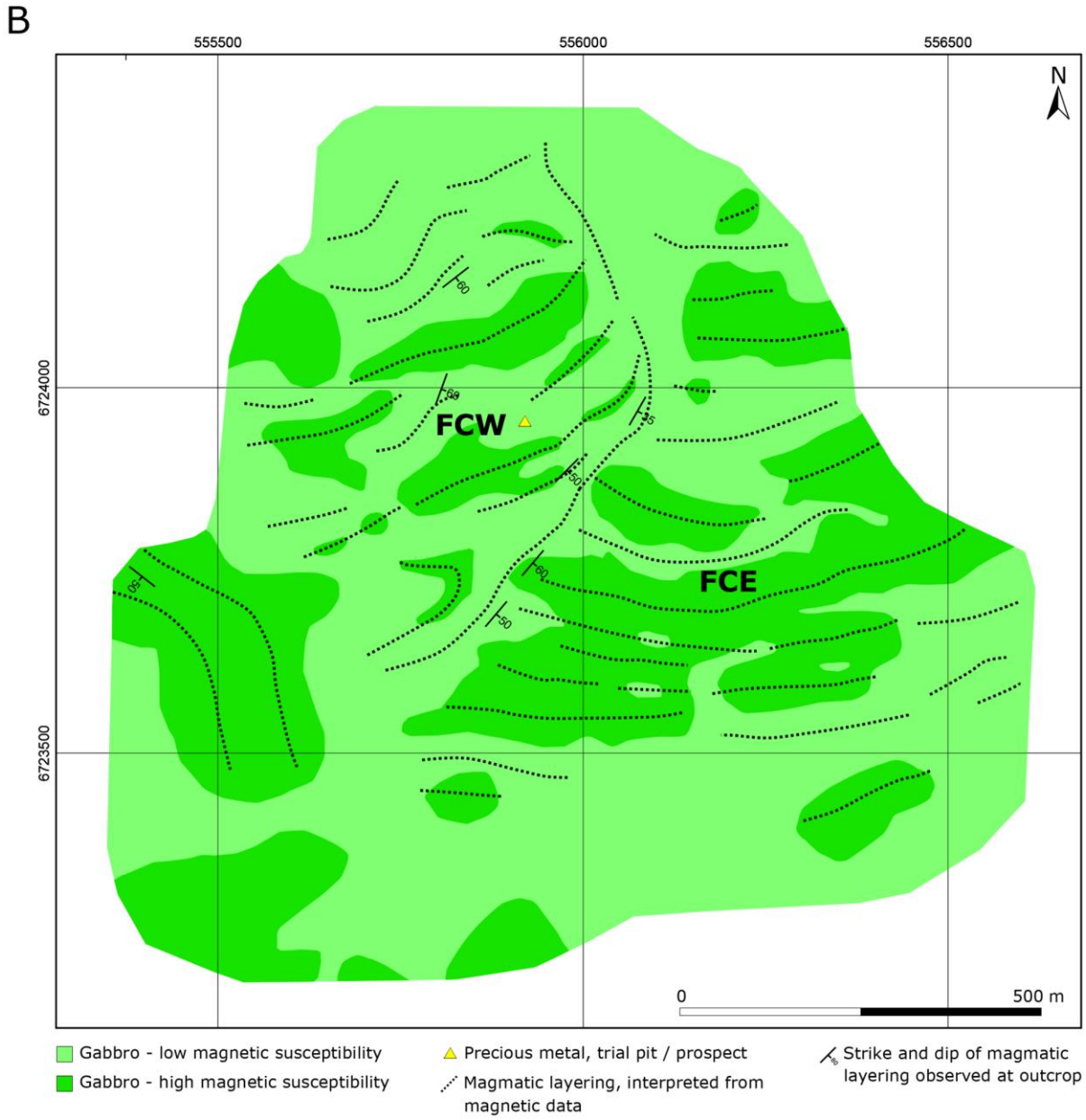

Figure 32 continued. B. Shows an interpretation of the magnetic field measurements.

The magnetic data collected in this area show a somewhat complex pattern. There appears to be two zones, one in the northwest and one in the southeast, which exhibit anomalies with an approximately east-northeast to west-southwest orientation (labelled as FCW and FCE in figure 32B, respectively). Between these two areas there appears to a discontinuity in the anomaly pattern. In general, the observations of magmatic layering do not clearly align with the positive magnetic anomalies in the data. This could be due to several factors: (1) the presence of strong magnetic anomalies can introduce error into the strike measurements and (2) that the majority of layering measurements are located in the discontinuity between the two regions with more consistent magnetic anomaly patterns. Due to the lack of outcrops, it was not possible to make outcrop observations of magmatic layering in the southeastern part of the map, which exhibits perhaps the most consistent magnetic anomalies.

A possible interpretation of the bedrock geology and layering within the intrusion is proposed in figure 32B. Here, consistent layering is interpreted in the two regions (FCW and FCE). The measurements of the strike of the layering in the centre of the map are interpreted to be indicative of the edge of the FCW region, where the layering is discordant with the layering in the FCE region. The results from this area provide a valuable insight into the relationship between the magnetic measurements and the layering at a smaller scale. Hence, although the anomalies interpreted in the aeromagnetic data may correspond well to the large-scale layering direction across the intrusion, on a smaller scale the layering can be far more complex.

Detailed ground magnetic measurements at the Fullen intrusion

Figure 33 shows magnetic measurements collected over an approximately 200 × 200 m area located along modelling profile 5, within the Fullen intrusion. The main objective with these measurements was to gain a better understanding of the relationship between layering in the intrusion and the magnetic measurements on a small scale. This region was chosen due to a series of notable magnetic anomalies and the presence of a relatively extensive area with outcrops, where observations could be made.

In figure 33 a series of linear magnetic anomalies can be observed which exhibit a southwest to northeast orientation. Annotated on the map are the locations of magnetic susceptibility measurements taken from outcrops within the study area. It can be observed that in general the high susceptibility measurements correlate with the regions where positive magnetic anomalies are present. Measurements of the direction of magmatic layering from outcrops are also annotated on the map. These correlate well with the direction of the magnetic anomalies. However, it should be noted that, as a compass was used to measure the orientation, there is likely some error in these measurements due to the relatively strong magnetic anomalies in the vicinity.

An interpretation of the magnetic map is shown in figure 34. Here it has been assumed that the magnetic anomalies are associated with layers of the intrusion (i.e. due to variation in the amount of magnetic minerals present in the different layers). It appears from the data that the layers are not always parallel to each other. Where, in some cases, layers appear to diverge or pinch-out, giving rise to a lens-like geometry. Small orthophotos were generated for several outcrops within the study area using photographs taken with a Mavic 2 pro camera drone. Two of these orthophotos, as well as their location, are shown in figure 34. The layering in these two outcrops can clearly be observed and its direction correlates well with the magnetic data. The outcrop shown at location B in figure 34 is the same as documented in observation DSR201022, discussed earlier in the report (fig. 9C). On this image the unconformity between the xenolith of rhyolite and layers in the gabbro can clearly be observed.

The results from this focus area in the Fullen intrusion show a clear relationship between the magnetic properties and the magmatic layering. The results also correlate well with the layering direction which can be interpreted from the airborne magnetic data (fig. 29). Hence, based on this example, it is reasonable to use the airborne magnetic data to interpret the layering within the intrusion on a large scale. However, as observed in the focus area from the Flinten intrusion, it is also likely to be the case that the layering can be more complex than observed from airborne data in some areas.

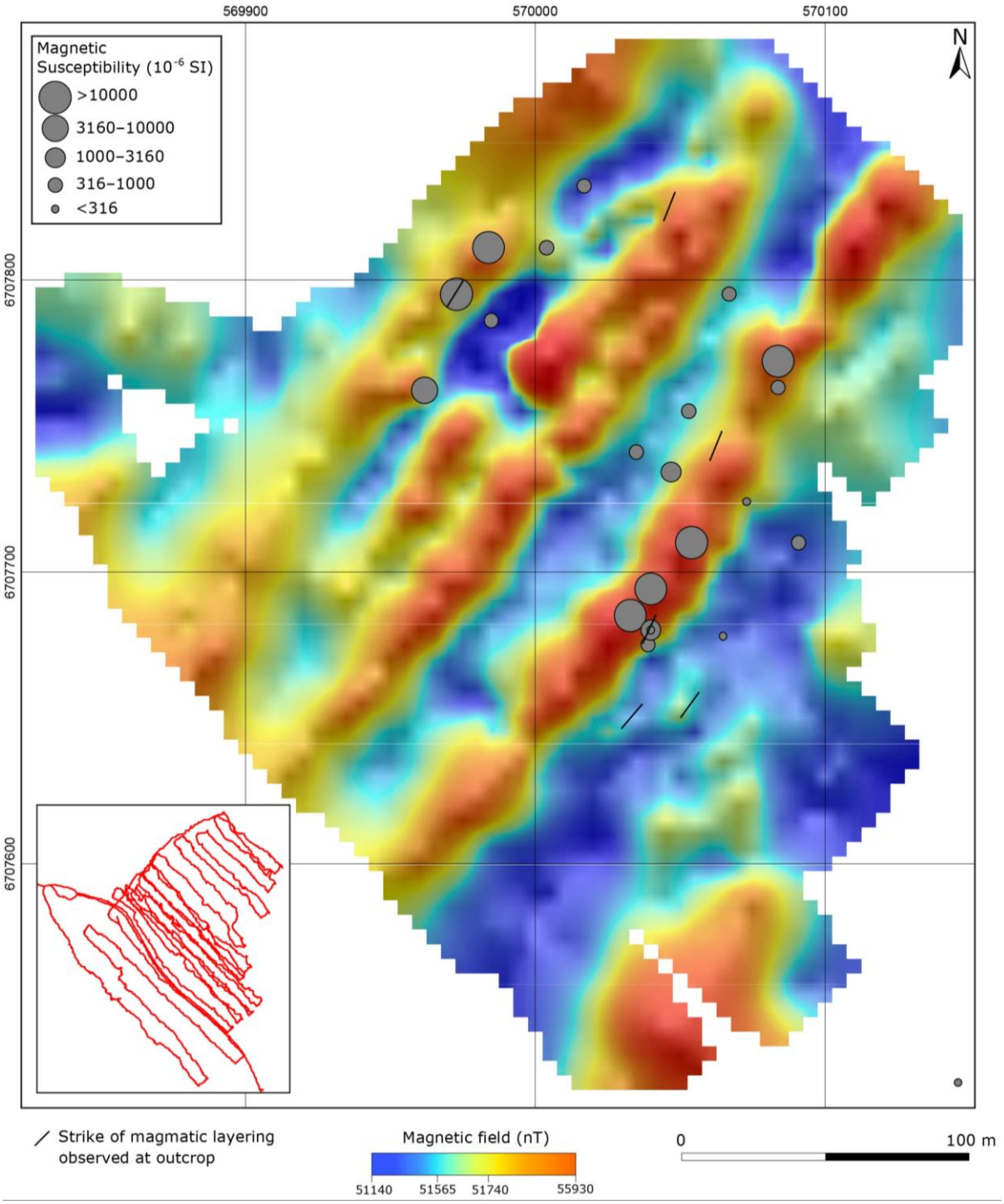

Figure 33. A map showing the magnetic field measurements collected over a focus area within the Fullen intrusion. The inset map in the lower left-hand corner shows the locations of the measurements. Magnetic susceptibility measurements from outcrops within the survey area are indicated with grey circles. The location of the focus area is indicated with a star in figure 12.

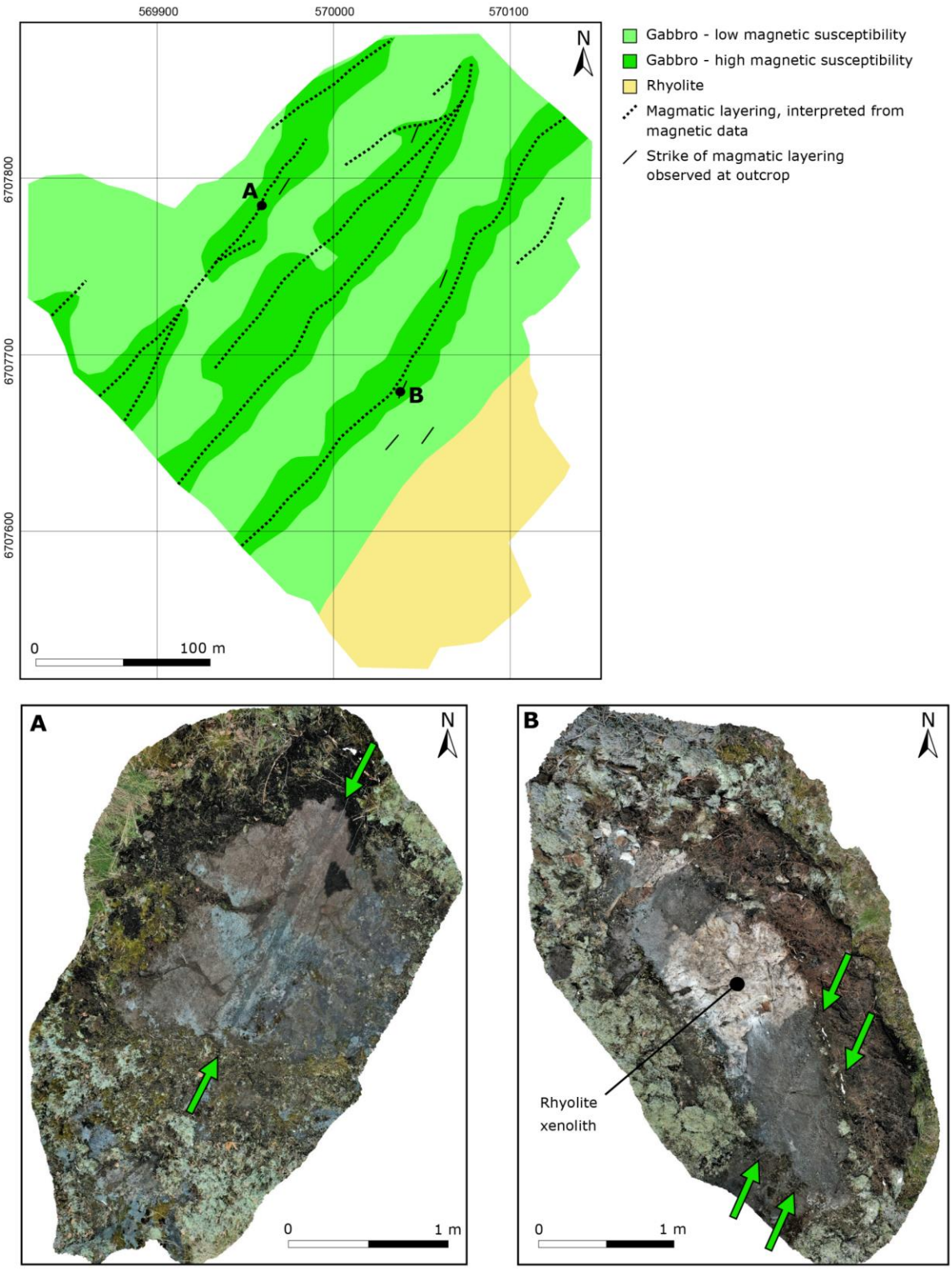

Figure 34. A map showing the interpretation of the magnetic field data from the Fullen focus area. **A.** and **B.** show the location of two orthophotos on the map where magmatic layering can be observed. The orthophotos are displayed at the bottom of the figure. The location of the focus area is indicated with a star in figure 12. The green arrows in the orthophotos highlight magmatic layering in the outcrops.

Geophysical modelling

During the project five regional profiles were modelled in 2D from the Flinten and Fullen intrusions (fig. 12) with the objective of investigating the large-scale geometry of the intrusions and their internal layering. Both airborne and ground-based measurements of the magnetic field were used in the modelling, as well as gravity measurements. In addition, resistivity models were generated from ground based VLF measurements for parts of the profiles. Finally, a 3D model was generated for the Flinten intrusion based on the airborne magnetic and gravity data. In the following sections the methodology and modelling results are described and presented.

Method for 2D modelling

The following workflow was used to generate the regional 2D models for both Flinten and Fullen intrusions:

1. The ground-based measurements along with outcrop observations and structural measurements were projected onto a straight modelling profile.
2. The ground-based geophysical measurements were filtered to remove noise and re-sampled to give a regular sampling interval.
3. Airborne magnetic data and gravity data were extracted from the gridded data to provide data along the modelling profiles.
4. The data were imported into Potent (modelling software) and the large scale density model was constructed manually.
5. The large scale density model was imported into Matlab where a script was used to build more detailed density and magnetic susceptibility models, taking into account the surface geology and available structural measurements.
6. The detailed susceptibility models were then imported into Potent, where they were used as a starting model for inversion with both the airborne and ground-based magnetic measurements.
7. The final models were then quality controlled against the outcrop observations and petrophysical data along the profile. The models were also checked to ensure that they have a similar distribution of physical properties, in general, to those observed in the petrophysical data.

To process the VLF data, the following workflow was used:

1. The VLF data were projected onto a straight modelling profile
2. some simple filtering was performed on the data to remove noise
3. the data were then inverted in Matlab to obtain a resistivity model.

Based on the petrophysical analysis, remnant magnetisation is often equal to, or greater than, the induced magnetisation within the intrusive mafic rocks in the Flinten and Fullen intrusions. Hence, efforts have been made to include remnant magnetisation within these 2D models utilizing a statistical approach. Remnant magnetisation was added to the model using the trend between remnant magnetisation (J) and magnetic susceptibility, shown in figures 17 and 22 for the Flinten and Fullen intrusions, respectively. In this process a certain degree of random variation was included to account for the spread observed in the petrophysical data. In both intrusions the orientation of the remanent magnetisation was assumed to be the same as the Earth's magnetic field.

It is important to emphasize several limitations of these 2D models. Firstly, these models are only 2-dimensional and hence, are calculated with the assumption that the model does not change perpendicular to the profile. As a result, they are a simplification of the true geological situation. Furthermore, these modelling results are non-unique and are only one of many possible models which can match the data. As data are only available from the surface (or sometimes only at altitude) uncertainty in these models increases with depth.

During the inversion process the data fit with the ground-based magnetic data has been prioritized over the airborne data, due to its higher resolution. In some cases, most notably for the large anomalies, the fit with the airborne data can be quite poor while the fit with the ground data is good. This is attributed to the fact that the inversion obtains a susceptibility value for a given body in the model assuming that that body continues a specific distance perpendicular to the profile (e.g. 1 000 m). In each model the perpendicular extension is constant for all the bodies being modelled. For a given body, the combination of susceptibility and perpendicular extent, which matches the ground-based data, may lead to an anomaly which is too large on the airborne data. In such cases it is likely that the true extent of the body perpendicular to the profile, which is giving rise to a strong anomaly, may be less than specified in the model. Hence, this is, to some extent a limitation of modelling in 2-dimensions.

2D modelling results from Flinten

The following section presents the 2D modelling results from the Flinten intrusion. All of the models from the Flinten area are assumed to extend 1 300 m perpendicular to the profile in both directions.

Figure 35 shows the susceptibility and density models for geophysical modelling profile 1 (see fig. 12 for profile location). The measured data (airborne and ground-based magnetic measurements as well as gravity measurements) are shown, together with the modelled responses. Figure 36 shows the same model as in figure 35 but colour-coded with the interpreted rock type.

The main feature in the gravity data along profile 1 is a large positive anomaly, which is interpreted to be associated with the Flinten intrusion. A constant density of 3 000 kg/m^3 was used to model the intrusive mafic rocks. An exception to this is a region which is interpreted to contain less dense leucogabbro rocks located at approximately 2 500 m along the profile. These rocks are interpreted to lie between the F1A and F1B regions, which were interpreted based on aeromagnetic data (fig. 25). This zone also coincides with the deformation zone which can be observed in the resistivity data (fig. 26). The intrusion is modelled to reach a maximum thickness of about 1 500 m along this profile, gradually reducing in thickness towards the edges of the intrusion. To match the gravity data several subsurface mafic units are required at the southern end of the profile.

Based on outcrop observations, the magmatic layering in the F1A region appears to be concentric and to dip towards the centre of the region (fig. 25). Layering has been introduced into the model by splitting the model up into many concentric bodies (fig. 35). To capture the small-scale variations in the magnetic data, a variable body thickness is used, where thin bodies are used in areas where a strong magnetic anomaly is present. These bodies dip at approximately 40º towards the centre of the F1A region (approximately 4 250 m along the profile). Some degree of symmetry in the ground magnetic measurements (centred at 4 250 m along the profile) can be interpreted within the F1A region, which supports modelling this region as a concentric, bowl-like structure. The magnetic susceptibility model shows a significant amount of variation between layers within the intrusion. However, it can be observed that higher susceptibilities tend to occur in the centre of the F1A region. This is consistent with observations from the airborne magnetic data. Within the F1B region the higher susceptibility values tend to occur towards the southern extent of the mafic intrusive rocks.

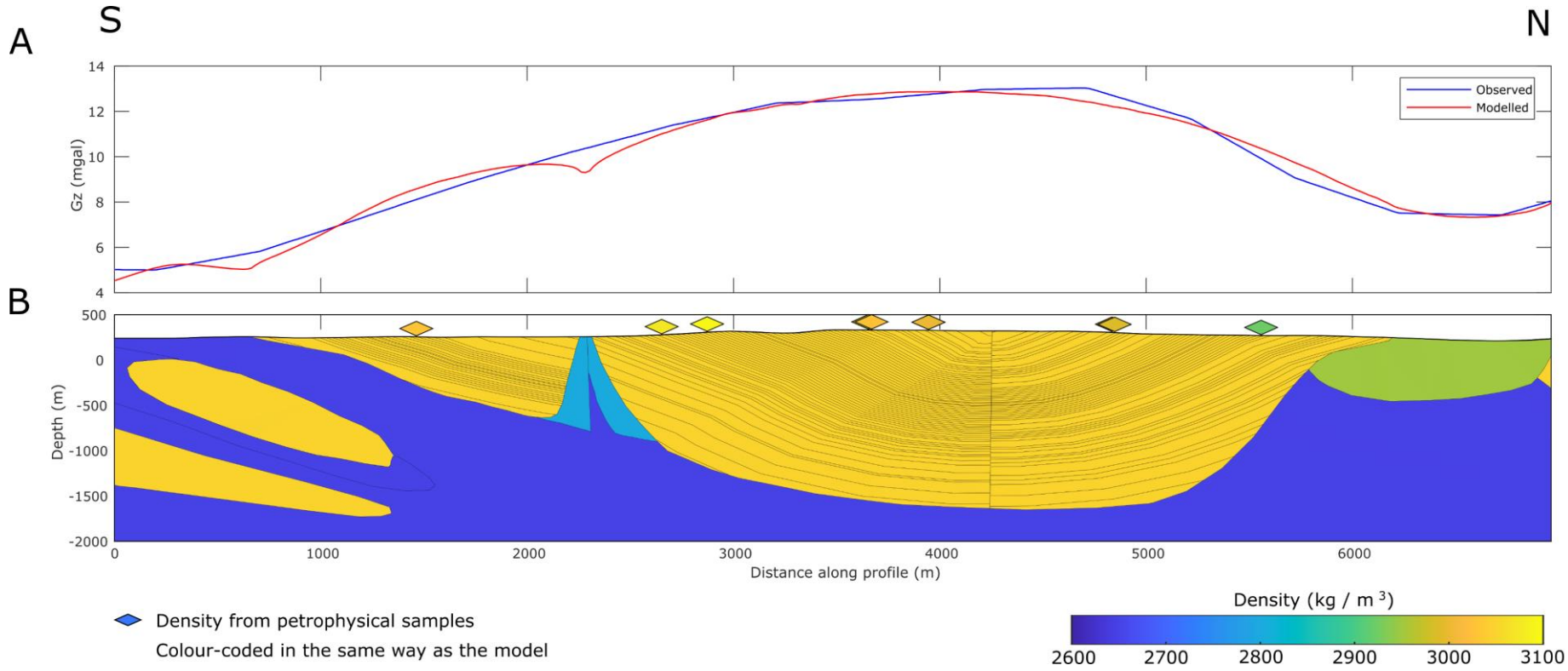

Figure 35. Models for geophysical modelling profile 1. See figure 12 for profile position. **A.** Gravity data, both observed and calculated from model. **B.** Density model as well as density values from petrophysical samples.

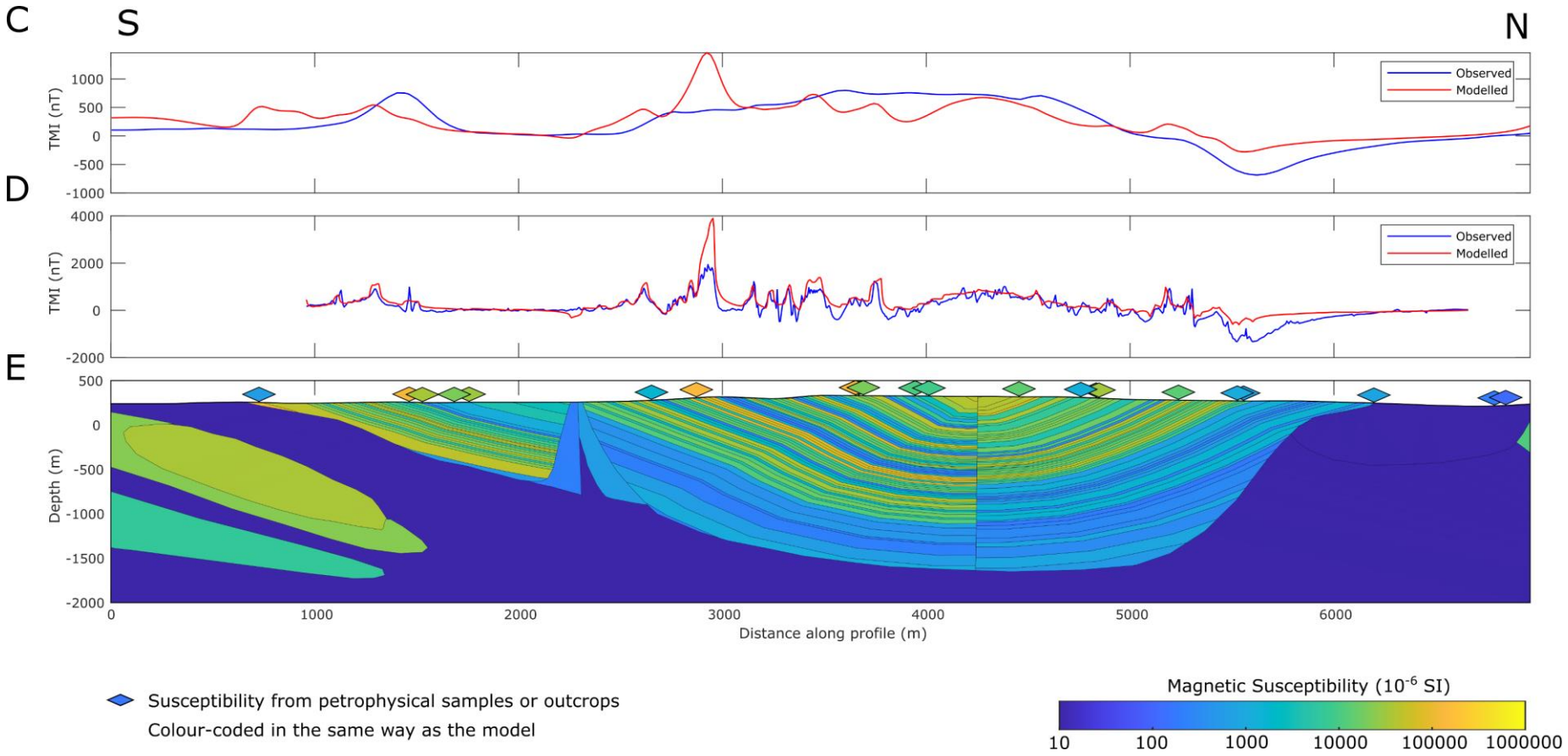

Figure 35 continued. Models for geophysical modelling profile 1. See figure 12 for profile position. **C.** Airborne magnetic data, both observed and calculated from model. **D.** Ground-based magnetic data, both observed and calculated from model. **E.** Magnetic susceptibility model, as well as susceptibility values from petrophysical samples and outcrop measurements.

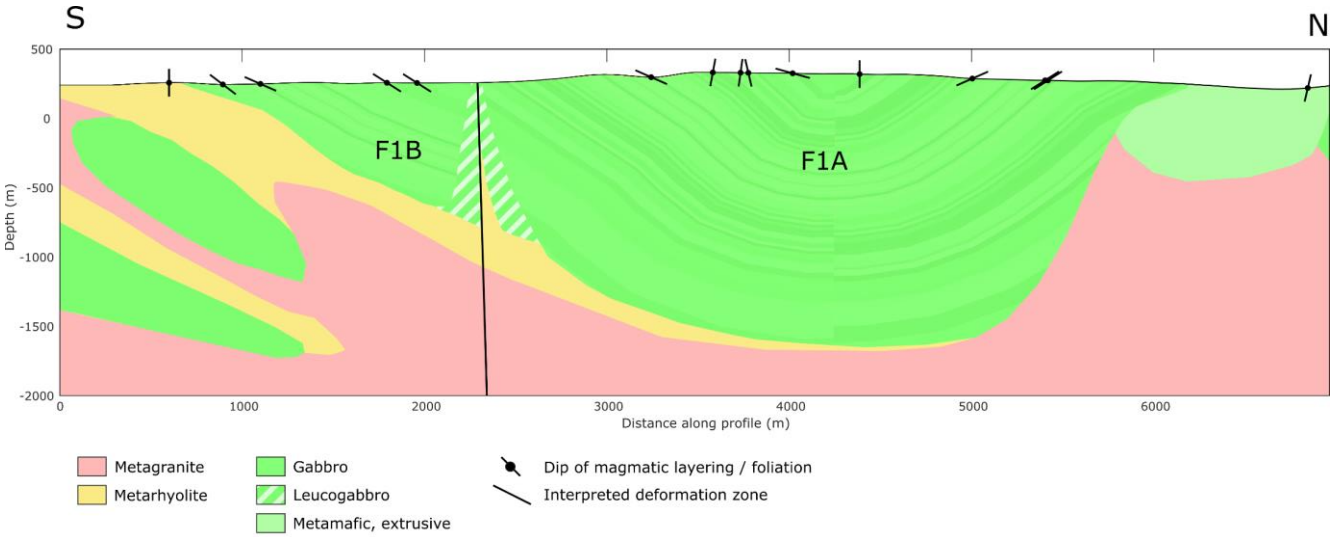

Figure 36. Model for geophysical modelling profile 1, colour-coded by interpreted rock type. The dip of foliation or layering from outcrop observations is shown on the profile.

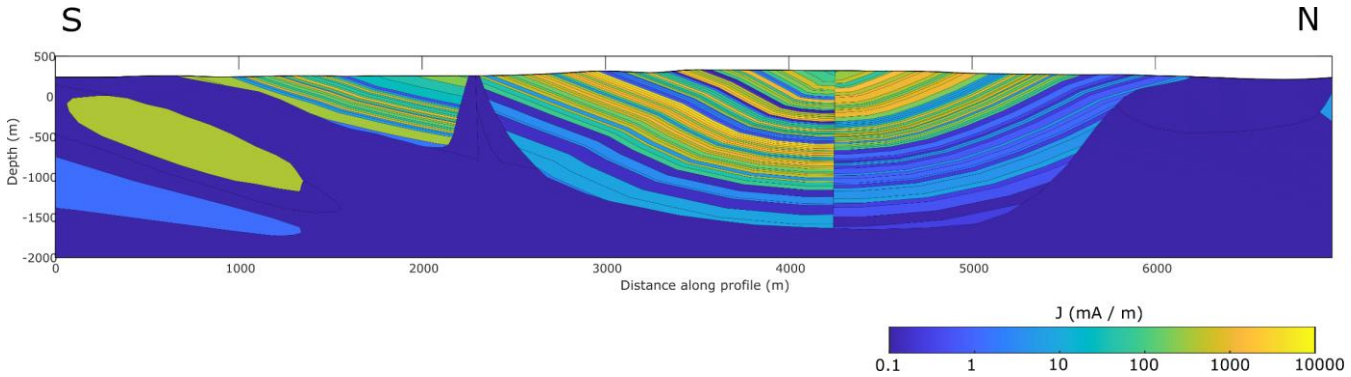

Figure 37. Model for geophysical modelling profile 1, colour-coded by remnant magnetisation (J).

Details will now be discussed regarding the modelling of remanent magnetisation and quality control procedure (i.e. statistical analysis of the model properties) for the model from profile 1. These steps have been performed and included in the modelling process for all subsequent profiles (i.e. profiles 2, 3, 4 and 5). However, these aspects will not be discussed in this report for the subsequent profiles. Figure 37 shows the remnant magnetisation (J) assigned to the different bodies in the model. Here the strongest remnant magnetisation is modelled to occur in the centre of the F1A region and in the southern part of the F1B region, which is generally coincident with areas of high magnetic susceptibility.

Figure 38 shows statistics generated from the model generated for profile 1 for mafic intrusive rocks. To generate these statistics the property values of each body in the model were extracted and collated. Note that these results are biased since not all bodies in the model have the same cross-sectional area. Hence, high magnetic susceptibility values will be overrepresented in these statistics as many thin bodies are used to model areas with strong magnetic anomalies. However, these statistics still provide a broad form of quality control for the property values within the model. With regards to remanent magnetisation in the model, approximately 30 to 40 percent of the Q values are above 1 and values for remnant magnetisation lie between 0.1 and 10 000 mA/m. These values match well with the distributions in the petrophysical data (fig. 17). With regards to the magnetic susceptibility, the values in the model have a bimodal distribution and lie between 100 × 10^{-6} SI and 100 000 × 10^{-6} SI, which also matches well with the petrophysical data (fig. 14).

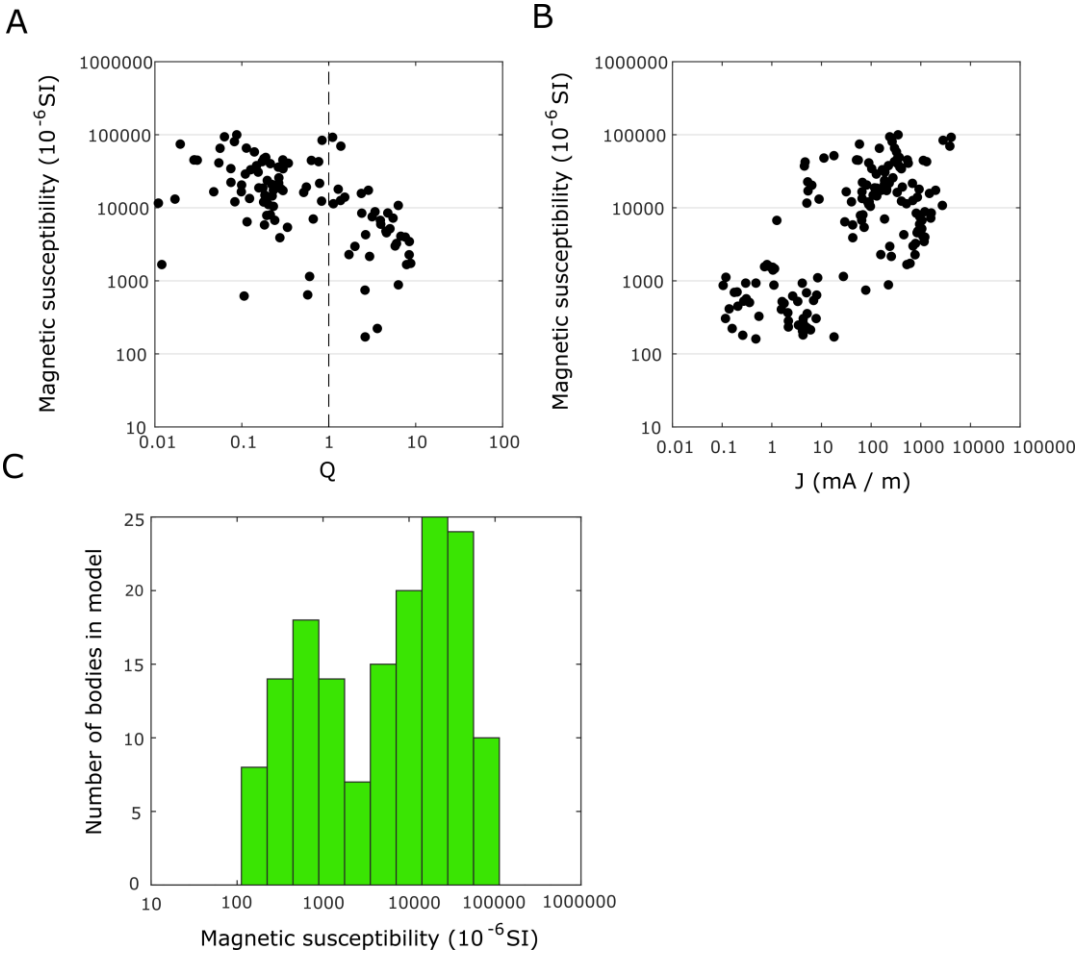

Figure 38. Statistics for mafic intrusive rocks within the model generated for profile 1. **A.** Cross plot of magnetic susceptibility and Q. **B.** Cross plot of magnetic susceptibility and remnant magnetisation. **C.** Histogram of magnetic susceptibility.

Figure 39 shows the density and susceptibility models for geophysical modelling profile 2, along with the modelled and measured data. Figure 40 shows the same model colour-coded by interpreted rock type. The gravity data exhibits a general trend of decreasing values from west to east along the profile. However, two local maxima can be observed at approximately 1 500 m and 3 500 m along the profile. The first is interpreted to correspond to region F1B and the second to region F2A interpreted from airborne magnetic data (See figures 25 and 40 for a description of these regions). The local drop in the gravity measurements in-between regions F1B and F2A is modelled to be due to the absence of relatively dense gabbro (3 000 kg/m^3) and the presence of less dense leucogabbro rocks (2 800 kg/m^3). In the petrophysical data, the anomalously low-density value at about 1 500 m along the profile, is due to the presence of an approximately 50 m wide pegmatite (containing quartz, feldspar, and mica). The mafic intrusive rocks are modelled to reach a maximum depth of approximately 2 250 and 1 000 m below regions F1B and F2A, respectively.

Based on observations of magmatic layering from outcrop, there appears to be a clear shift in dip direction between the F1B and F2A regions (at about 2 000 m along the profile). Attempts have been made to capture this variation in the dip of the layering along the modelling profile. There appears to be significant variation in the susceptibility values of the different bodies in the model. However, in general, higher susceptibility values occur to the west of the profile, within region F1B. A zone with anomalously low magnetic susceptibility is modelled at approximately 1 500 m along the profile. This is interpreted to correspond to the presence of the pegmatite discussed earlier (fig. 40).

Figure 41 shows the physical properties of the model together with the observed and modelled data for geophysical modelling profile 3. Figure 42 shows the same model, colour-coded by interpreted rock type. Profile 3 runs southwest to northeast through the north-eastern part of the Flinten intrusion. The profile intersects the F1C region (based on the interpretation of the aeromagnetic data shown in figure 25). Along the profile the gravity data shows a clear positive anomaly with a peak value at about 1 100 m along the profile. This maximum value is interpreted to correspond to the thickest sequence of intrusive mafic rocks. In addition to the greater thickness of intrusive mafic rocks, the density of the uppermost gabbro layers has also been increased to 3 100 kg/m^3 to match the observed gravity data. This could be interpreted as the presence of dense gabbro rocks with relatively low proportions of feldspar. A gradual decrease in the thickness of the intrusive mafic rocks is modelled away from the maximum thickness at 1 100 m along the profile. To the southwest the profile crosses the boundary between F1C and F1B, here the intrusive mafic rocks are interpreted to be relatively thin and less dense leucogabbro rocks are interpreted to be present. The relatively high gravity values at the north-eastern end of the profile, require the continuation of mafic intrusive rocks below the surficial felsic and extrusive mafic rocks in the model.

No structural measurements of the layering are available along this profile. However, it is assumed that layering is present and that the layers dip towards thickest point of the intrusion (at 1 100 m). Hence, along the profile, the intrusion is modelled with a bowl-like geometry, similar to the geometry of the F1A region along profile 1. Within the susceptibility model, the highest values are modelled in the centre of the profile (between 750 m and 1 500 m along the profile). As discussed previously this can be interpreted as layers within the intrusion which crystalized later during the cooling process and hence, contain a greater proportion of iron and associated magnetic minerals (Ferré et al. 2009).

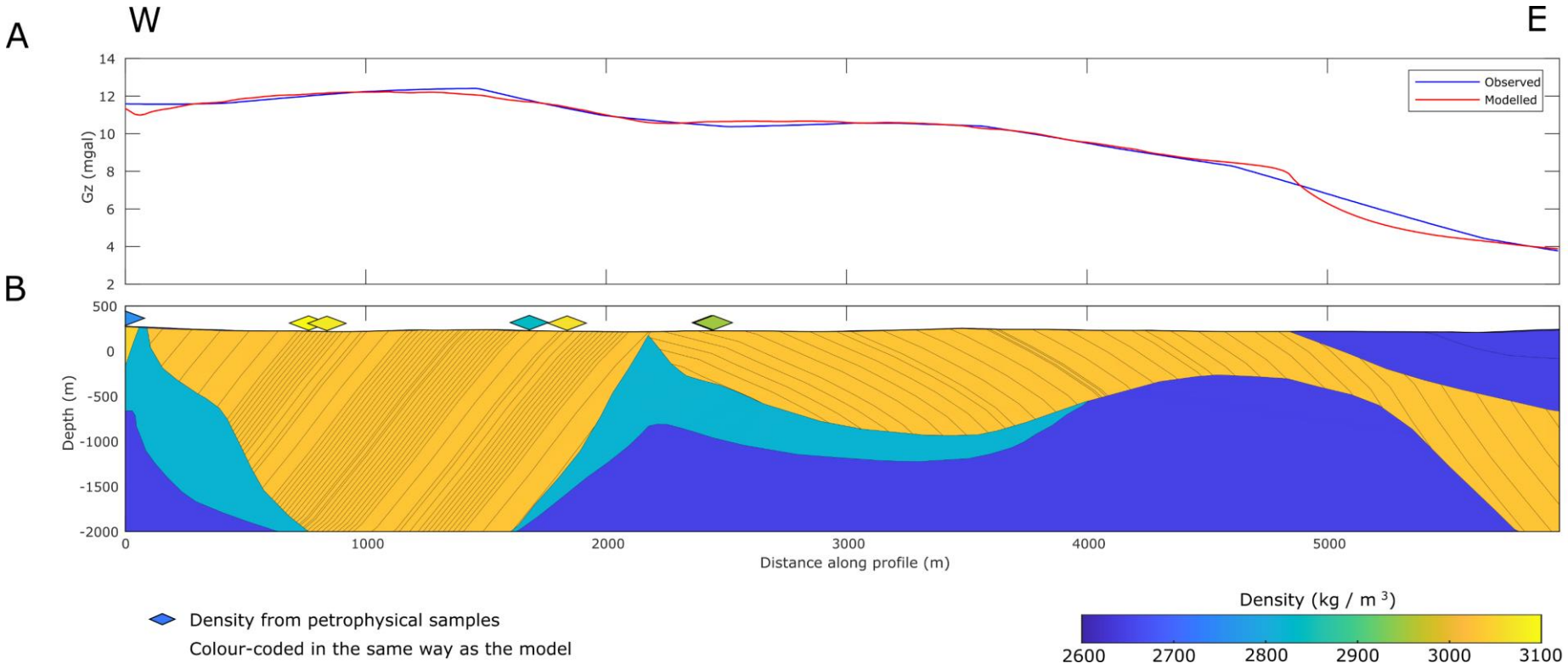

Figure 39. Models for geophysical modelling profile 2. See figure 12 for profile position. **A.** Gravity data, both observed and calculated from model. **B.** Density model as well as density values from petrophysical samples.

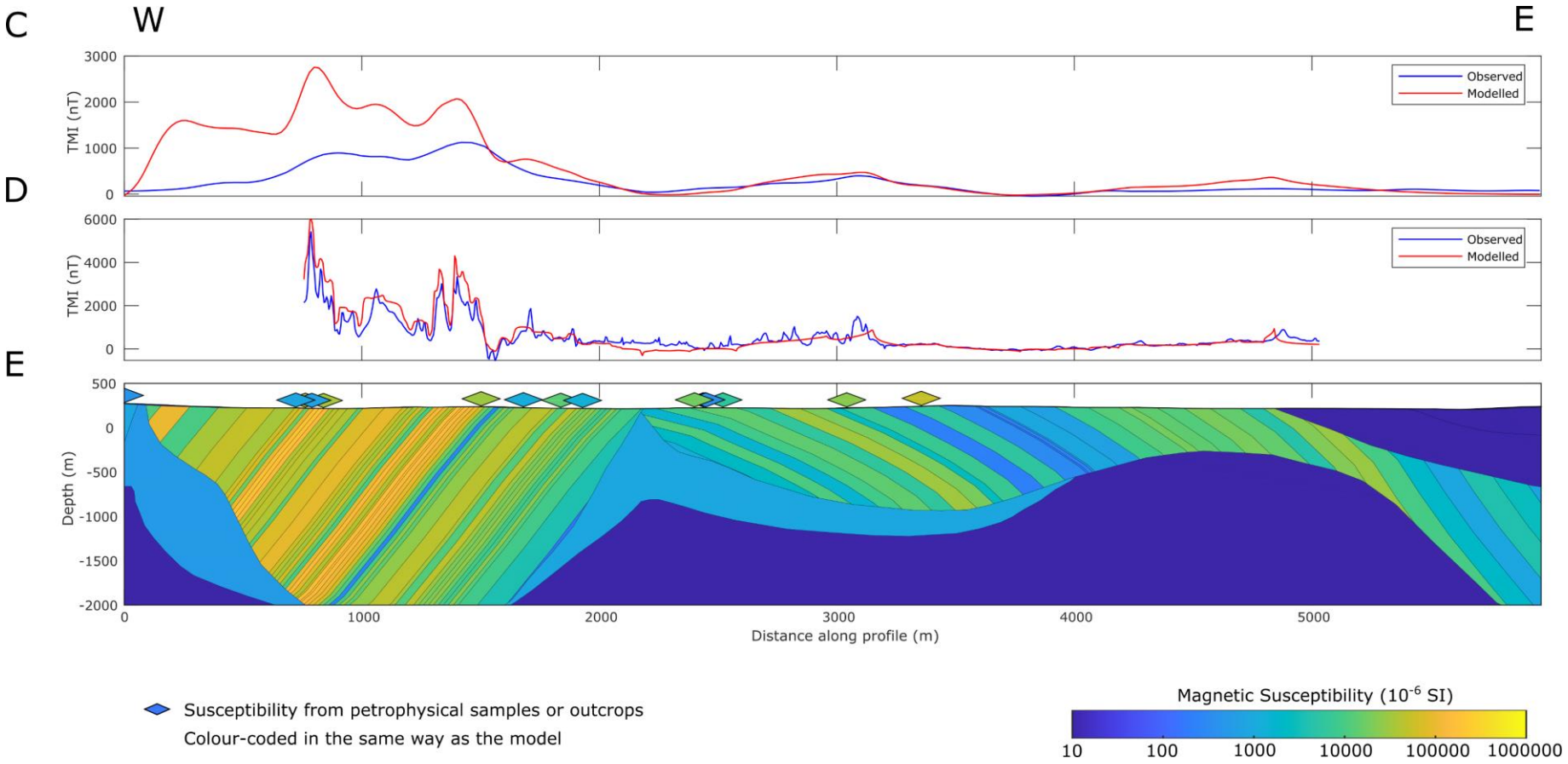

Figure 39 continued. Models for geophysical modelling profile 2. See figure 12 for profile position. **C.** Airborne magnetic data, both observed and calculated from model. **D.** Ground-based magnetic data, both observed and calculated from model. **E.** Magnetic susceptibility model, as well as susceptibility values from petrophysical samples and outcrop measurements.

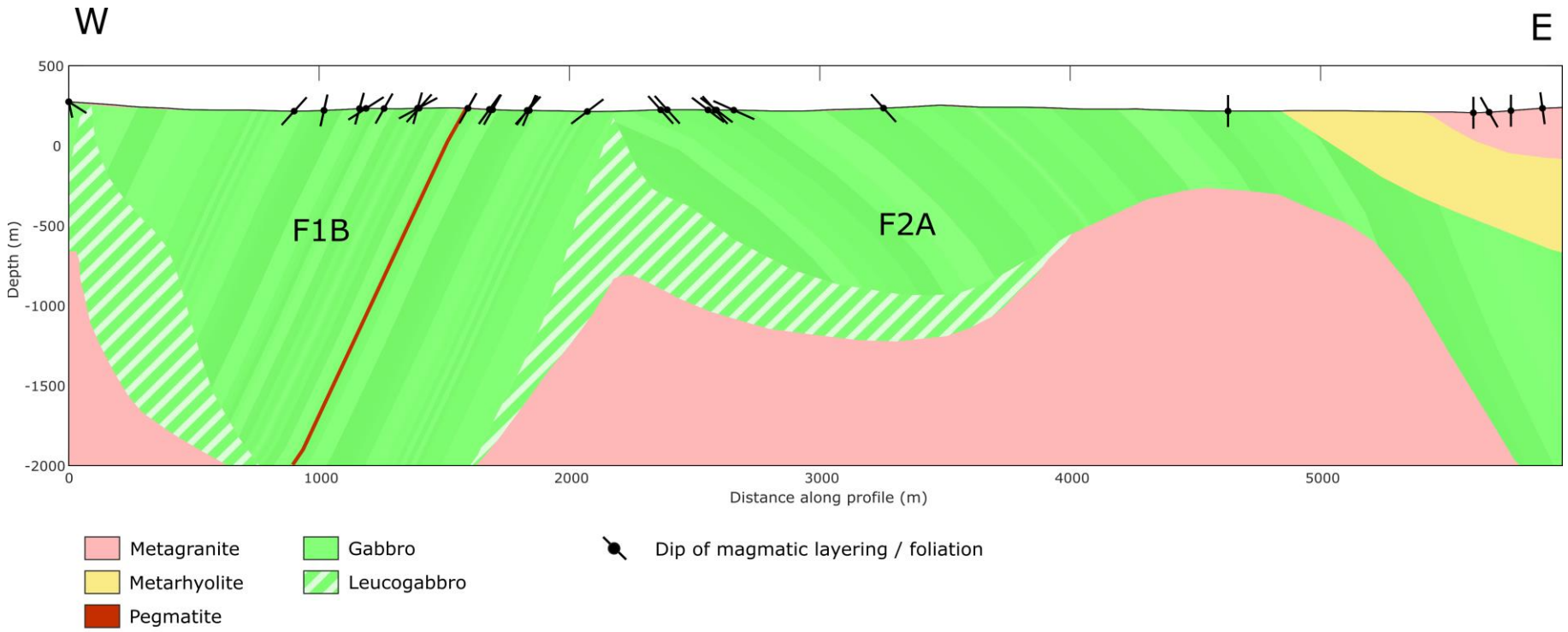

Figure 40. Model for geophysical modelling profile 2, colour-coded by interpreted rock type. The dip of foliation or layering from outcrop observations is shown on the profile.

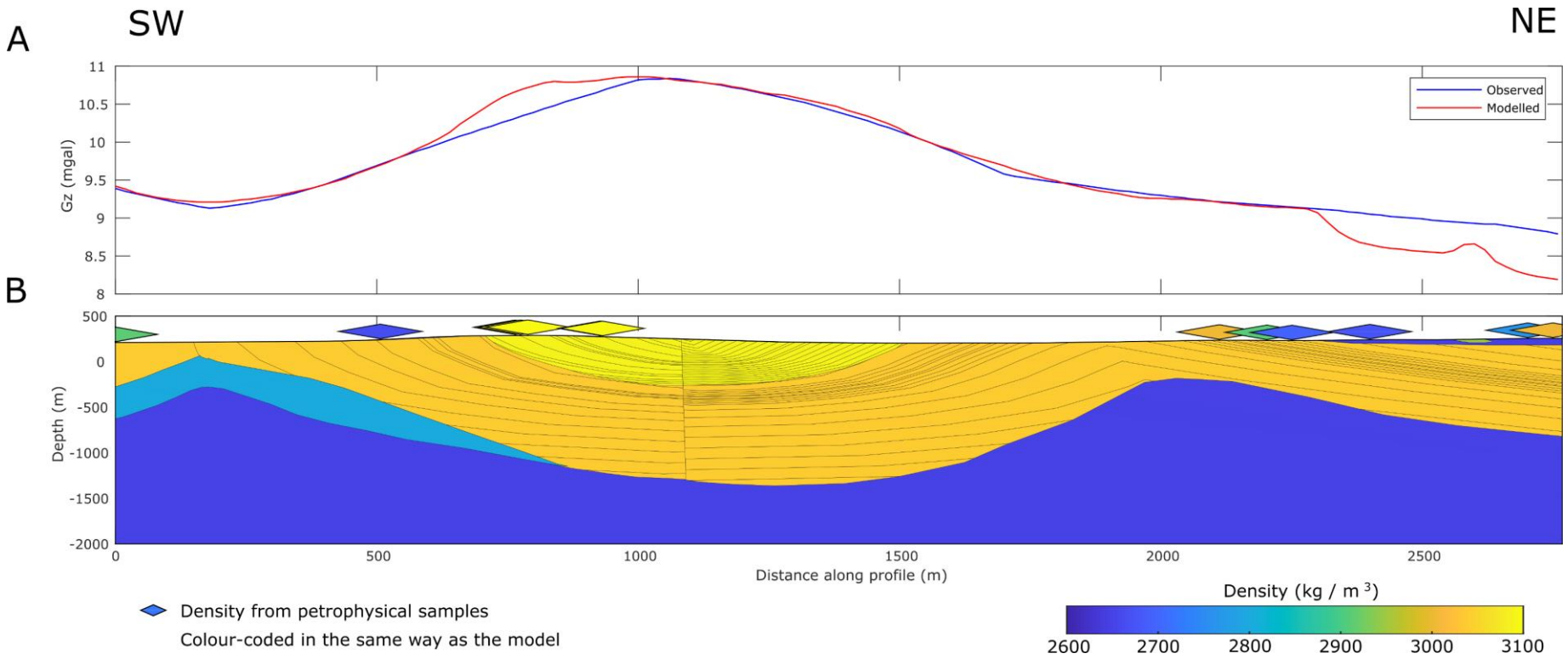

Figure 41. Models for geophysical modelling profile 3. See figure 12 for profile position. **A.** Gravity data, both observed and calculated from model. **B.** Density model as well as density values from petrophysical samples.

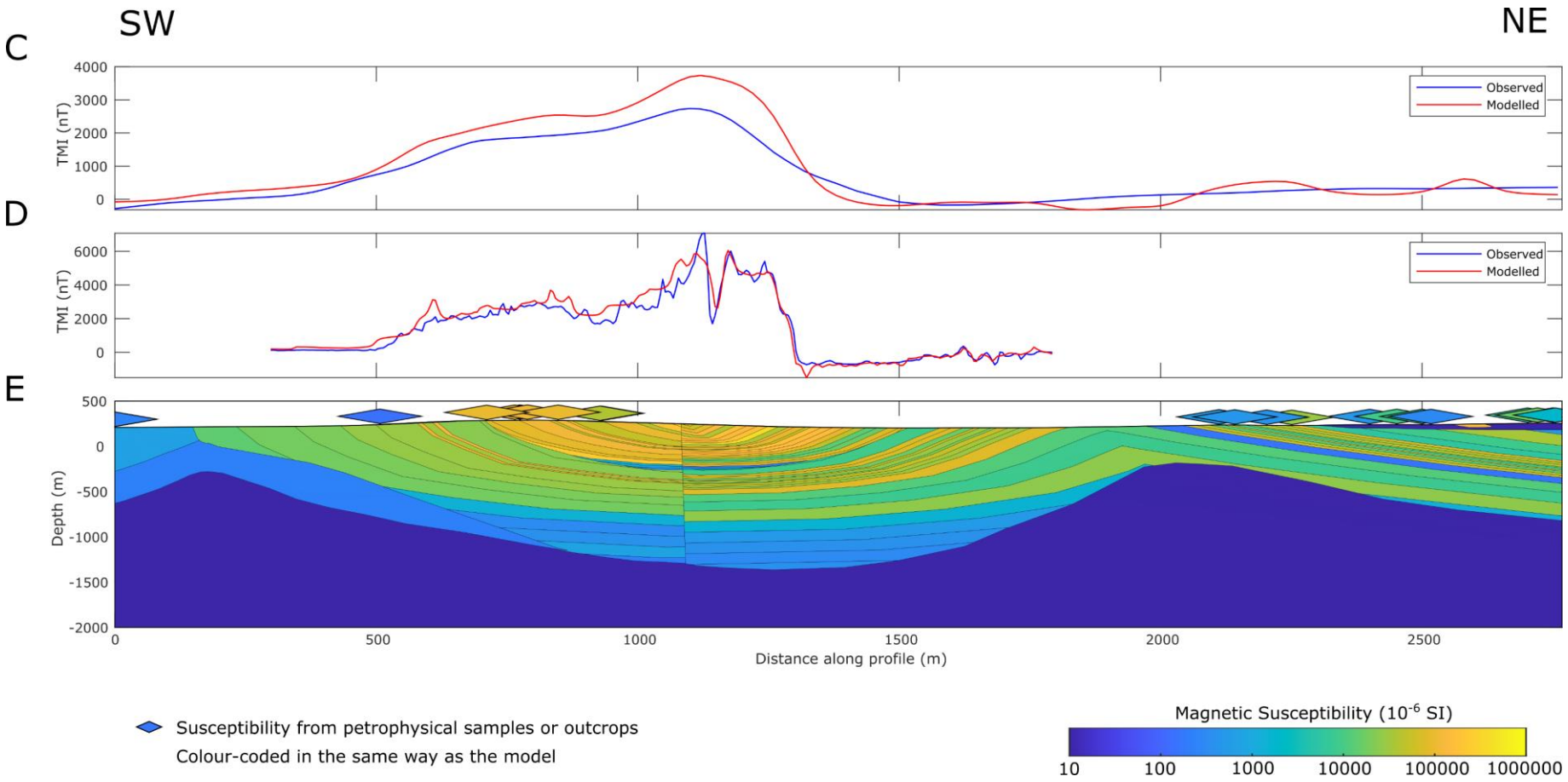

Figure 41 continued. Models for geophysical modelling profile 3. See figure 12 for profile position. **C.** Airborne magnetic data, both observed and calculated from model. **D.** Ground-based magnetic data, both observed and calculated from model. **E.** Magnetic susceptibility model, as well as susceptibility values from petrophysical samples and outcrop measurements.

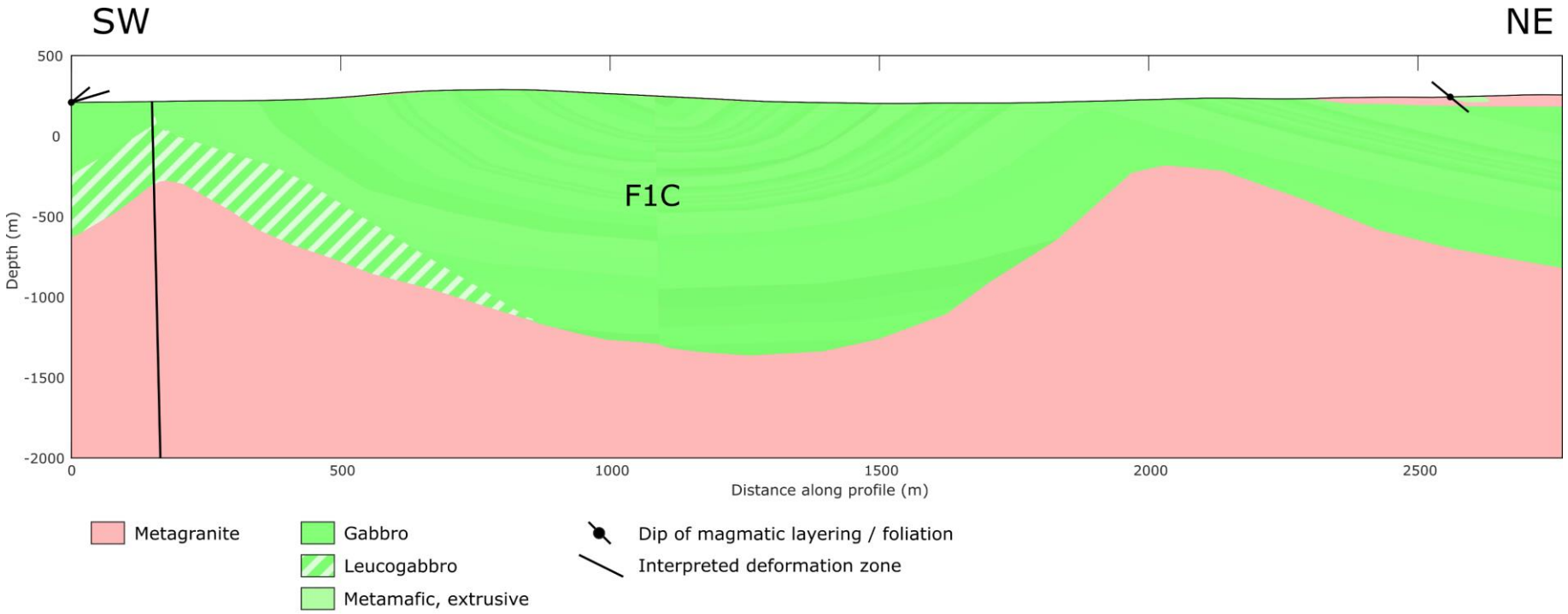

Figure 42. Model for geophysical modelling profile 3, colour-coded by interpreted rock type. The dip of foliation or layering from outcrop observations is shown on the profile. Note that only a very small body of mafic extrusive rocks are modelled at the north eastern end of the profile.

2D modelling results from Fullen

The following section presents the 2D modelling results from the Fullen intrusion. All of the models from the Fullen area are assumed to extend 2 000 m perpendicular to the profile in both directions.

Figure 43 shows the measured data and corresponding modelled data along profile 4, located in the western part of the Fullen intrusion (fig. 12). Density and susceptibility values in the model are also shown in the figure. VLF data and a resistivity model generated using these data along profile 4 are shown in figure 44. Finally, the combined density and susceptibility model is shown, colour-coded by interpreted rock type in figure 45.

Within the model, a constant density of 3 000 kg/m^3 was used for the intrusive mafic rocks, while a density of 2 950 kg/m^3 was used for the extrusive mafic rocks. The felsic extrusive and intrusive rocks were assumed to have a density of 2 650 kg/m^3. The gravity data along profile 4 consists of a single, large positive anomaly, with a peak value at approximately 8 000 m along the profile. The thickness of the intrusion was modelled to be greatest at this position, reaching a depth of about 2 000 m. South of this position, the thickness of the intrusion is modelled to decrease to about 250 m at its southernmost extent. In the northern part of the profile, the intrusion is modelled to reduce in thickness to about 1 000 m. The contact between mafic and felsic intrusive rocks is mapped at about 3 500 m along the profile. At this position, the main body of the intrusion is modelled to be downthrown across a deformation zone (labelled with an X in fig. 30). To match the gravity anomaly at the far northern end of the profile, it was necessary to include mafic bodies below the surficial felsic rocks.

The largest positive anomaly in the magnetic data lies at the northern end of the profile, within the small mafic unit immediately to the north of the deformation zone. The relatively high magnetic susceptibility values within this small unit, when compared to the rest of the Fullen intrusion, could indicate that it is not part of the main intrusion. Instead, it could be more like the smaller intrusions which occur to the north and northeast of the Fullen intrusion, which tend to give rise to large magnetic anomalies (for example the ultramafic intrusion where the Karlsborg mine is situated). Less observations of magmatic layering are available from the Fullen intrusion than the Flinten intrusion (fig. 29). Within these measurements the dip is typically steep (70–80 degrees) with a strike of approximately 45 or 225 degrees. From the limited information available the prevailing dip direction in the model was assumed to be to the southeast. Within the main part of the Fullen intrusion, the susceptibilities in the model typically lie between 1 000 × 10^{-6} SI and 10 000 × 10^{-6} SI and have a complex pattern. The zones with the highest susceptibilities appear to occur at approximately 5 000, 6 500 and 9 000 m along the profile.

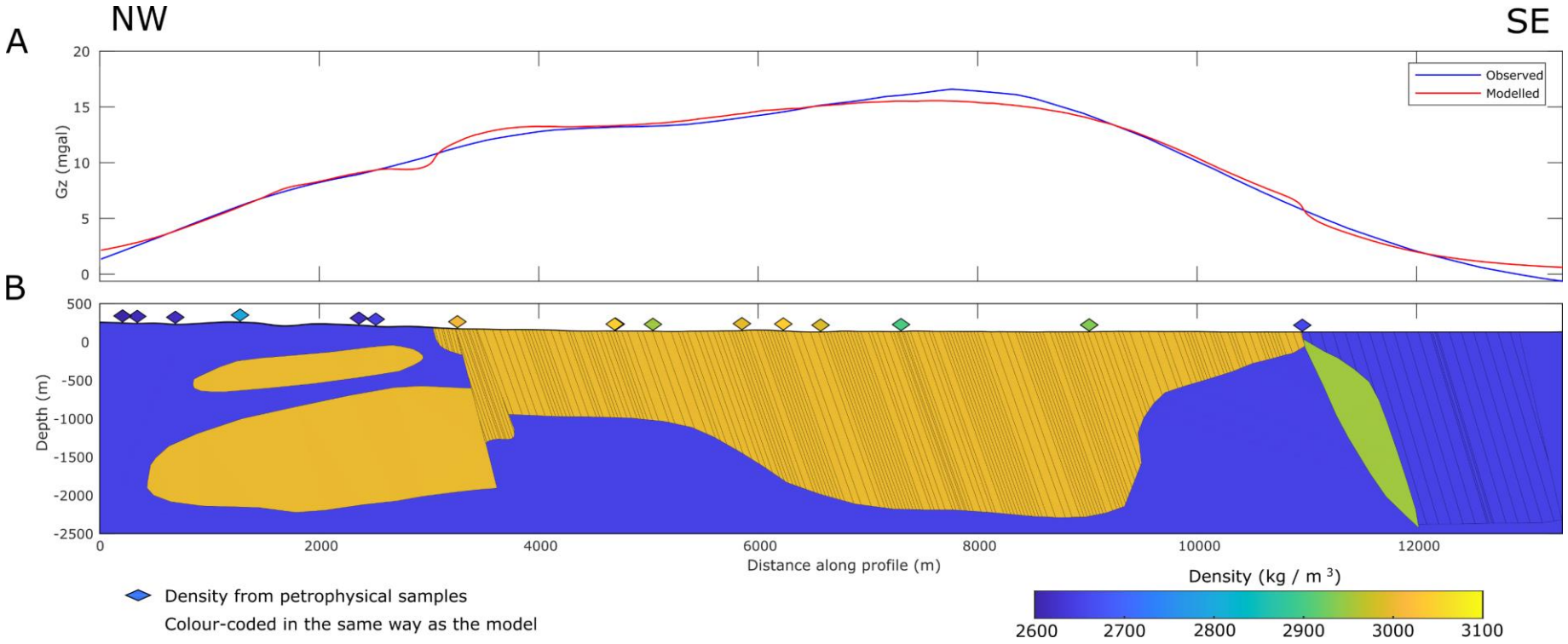

Figure 43. Models for geophysical modelling profile 4. See figure 12 for profile position. **A.** Gravity data, both observed and calculated from model. **B.** Density model as well as density values from petrophysical samples.

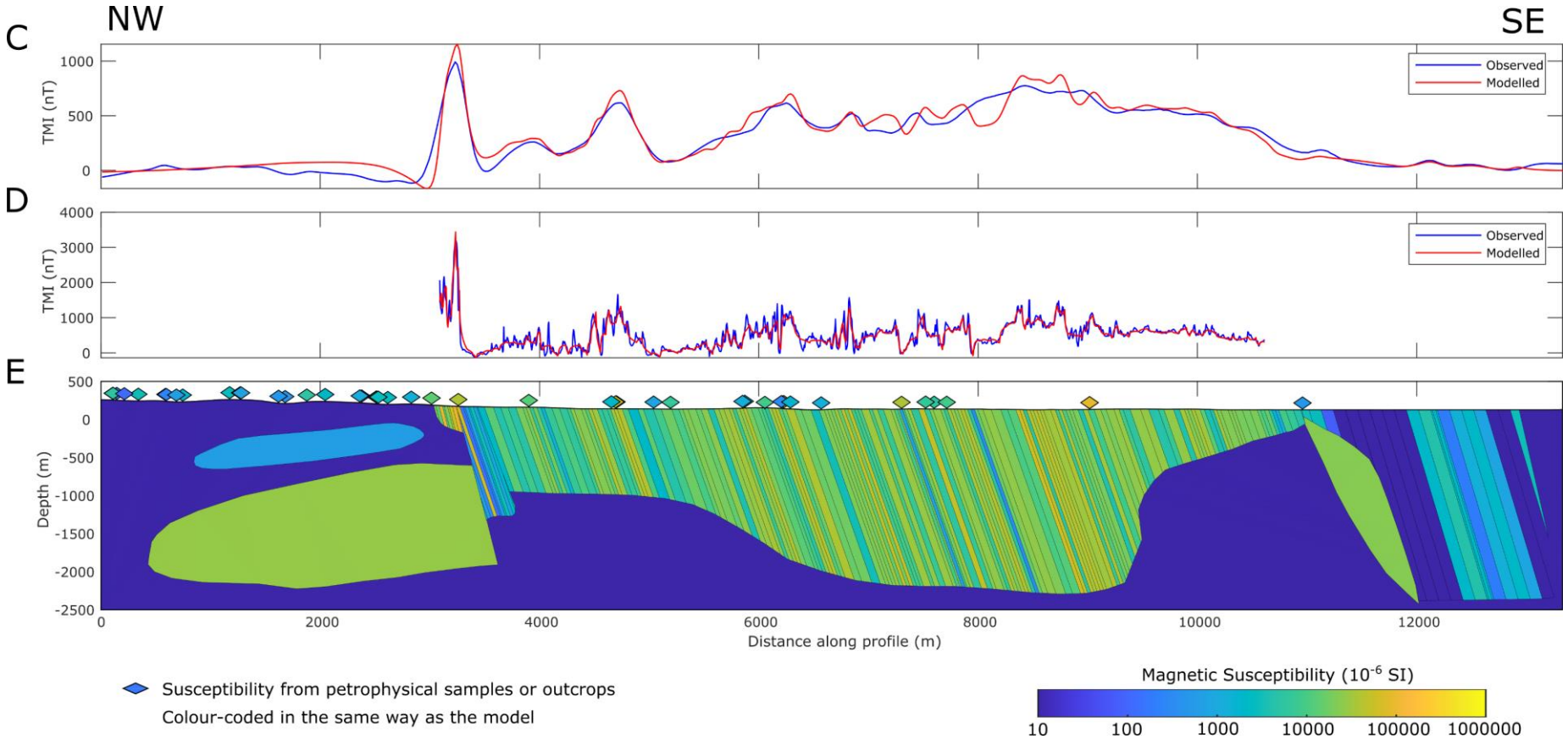

Figure 43 continued. Models for geophysical modelling profile 4. See figure 12 for profile position. **C.** Airborne magnetic data, both observed and calculated from model. **D.** Ground-based magnetic data, both observed and calculated from model. **E.** Magnetic susceptibility model, as well as susceptibility values from petrophysical samples and outcrop measurements.

VLF measurements were collected at the same time as the ground based magnetic measurements along profile 4. Figure 44 shows the observed and modelled data as well as a resistivity model obtained from inversion. A section of the data between about 5 800 and 7 500 m was removed due to the presence of power lines. The most notable feature in the model is a region with low resistivities which occurs at about 3 200 m along the profile. This is interpreted to be due to the deformation zone which lies at the northernmost part of the intrusion (shown with an X in figure 30). At about 4 500 m along the profile a feature with lower resistivities and gentle dip to the southeast is observed. This could indicate deformation but could also indicate a region of the intrusion which is more conductive. This anomaly appears to correlate with a subtle low resistive feature in the airborne resistivity data (fig. 30), which lies approximately parallel to the magmatic layering. An additional zone with low resistivities is present in the model at approximately 8 000 m along the profile. Here the low resistivities appear to be present at a depth of about 200 m. This feature also correlates with the low resistivity zone labelled with a Y in figure 30.

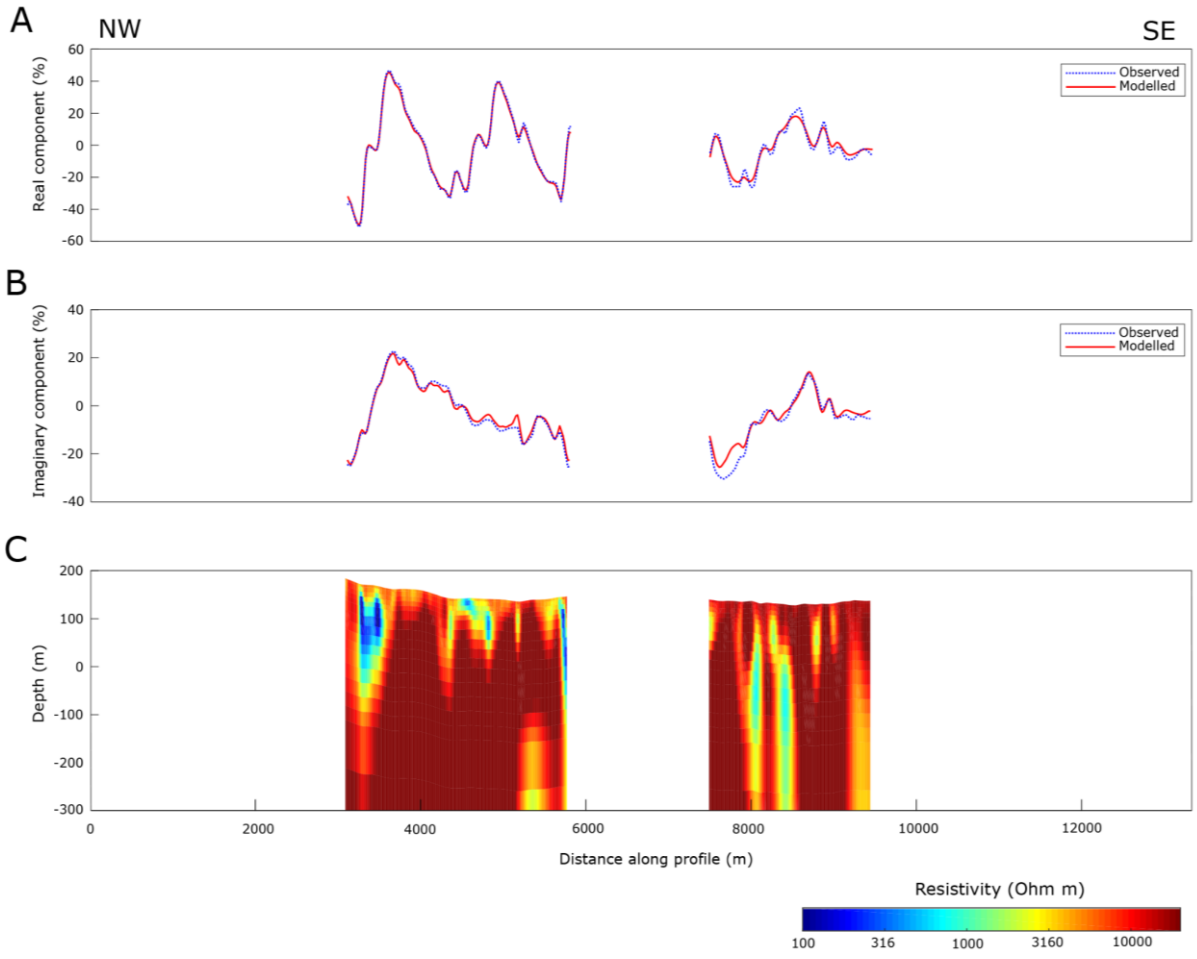

Figure 44. VLF data (22.2 kHz) and resistivity model for geophysical modelling profile 4. **A.** Both measured and modelled data for real component. **B.** Both measured and modelled data for the imaginary component. **C.** Resistivity model.

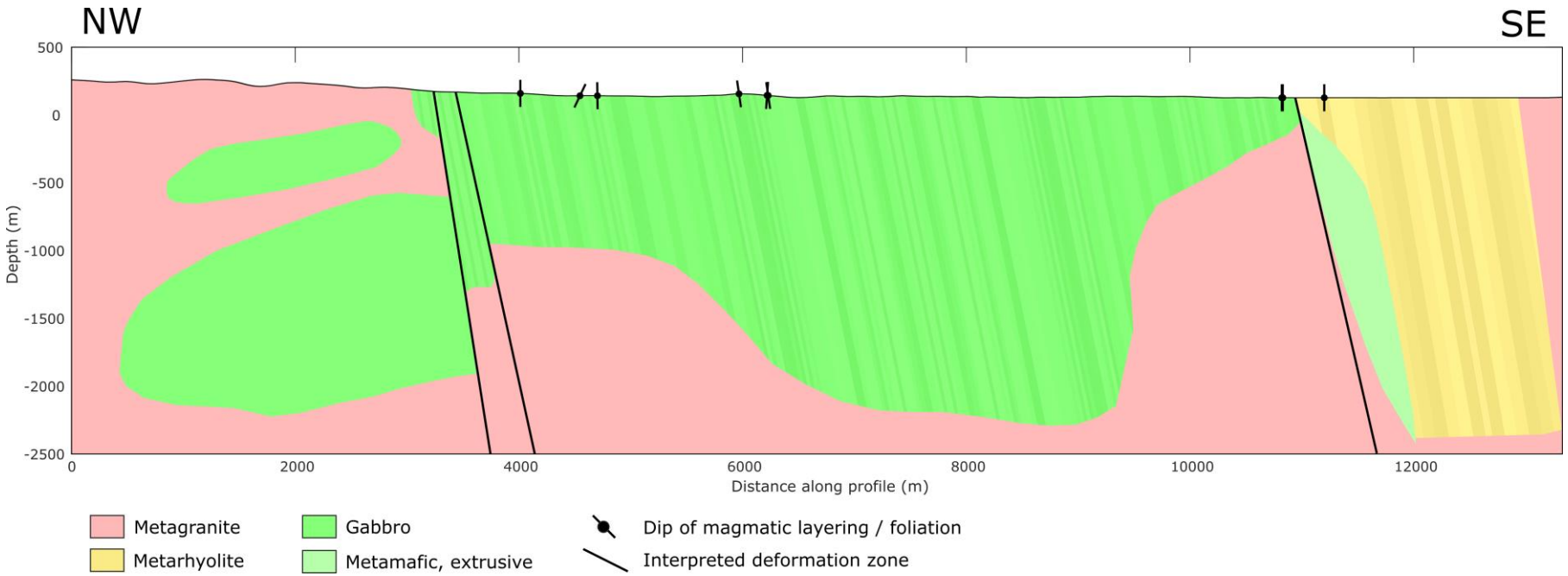

Figure 45. Model for geophysical modelling profile 4, colour-coded by interpreted rock type. The dip of foliation or layering from outcrop observations is shown on the profile.

Figure 46 shows the density and susceptibility models for geophysical modelling profile 5, together with the observed and modelled data. Figure 47 shows approximately 2 km of VLF data collected along the northern side of profile 5. Finally, figure 48 shows the model from figure 46, colour-coded by interpreted lithology.

The gravity data along profile 5 is characterized by a large positive gravity anomaly. The peak gravity value occurs at 3 000 m along the profile, where the intrusion is modelled to be thickest and to reach a depth of approximately 1 800 m. The thickness of the intrusion is modelled to gradually decrease to the south and north of the profile. To the north of the profile a deformation zone is interpreted to have downthrown part of the intrusion below the surficial granitic rocks. The presence of this deformation zone is suggested by the resistivity map generated from airborne measurements (labelled with a Z in figure 30). Along this profile several regions containing felsic extrusive rocks have been mapped and observed at outcrops. These are interpreted to be xenoliths within the mafic intrusion. There is limited information about the geometry and contact of these felsic rocks with the surrounding mafic rocks. However, from observations of a small xenolith of rhyolite (observation DSR201022, shown in figures 9C and 34), it can be assumed that they have irregular geometry and may not necessarily be orientated parallel to the layering direction. A series of small bodies containing felsic extrusive rocks have been incorporated into the density and susceptibility models, to match the observed geology on the surface. These bodies have a relatively low-density (2 650 kg/m^3) when compared to the surrounding mafic rocks (3 000 kg/m^3).

A similar overall dip direction for the magmatic layering in the intrusion was assumed for profile 5, as profile 4, during the modelling process (i.e. a steep dip to the southeast). The ground magnetic data show a complex pattern of positive anomalies within the intrusion, which are interpreted to be associated with layers with greater amounts of magnetic minerals. Several anomalies, however, are likely to be associated with mineralisation, which is documented to be present within some of the felsic xenoliths along the profile. For example, the anomalies at 2 750, 3 100 and 3 500 m along the profile are interpreted to be due to mineralisation within felsic xenoliths. No felsic rocks have been mapped (or were observed during this project) at the large magnetic anomaly located 2 000 m along the profile. In this model this has been interpreted to be due to mineralisation within a felsic xenolith (this is based on both the magnetic and VLF results). However, it is possible that this could represent a layer rich in magnetic minerals within the intrusion.

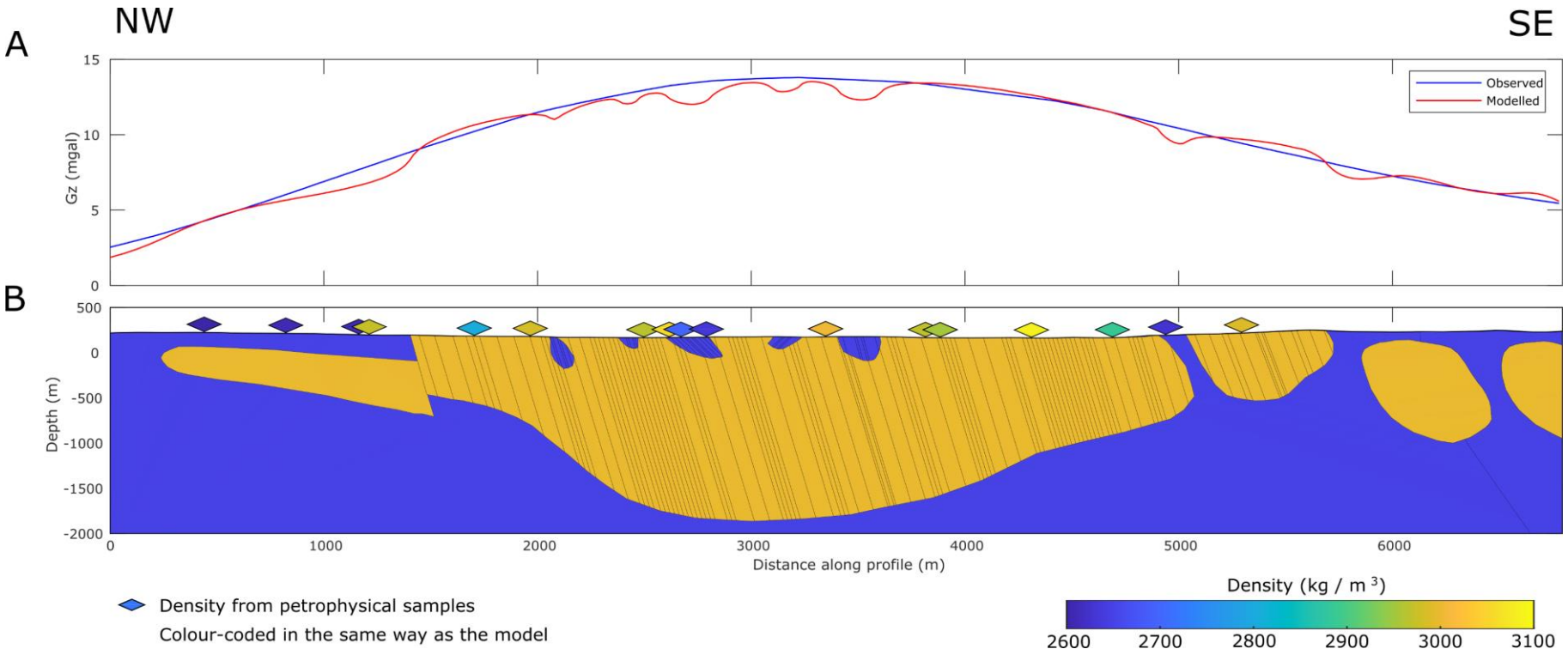

Figure 46. Models for geophysical modelling profile 5. See figure 12 for profile position. **A.** Gravity data, both observed and calculated from model. **B.** Density model as well as density values from petrophysical samples.

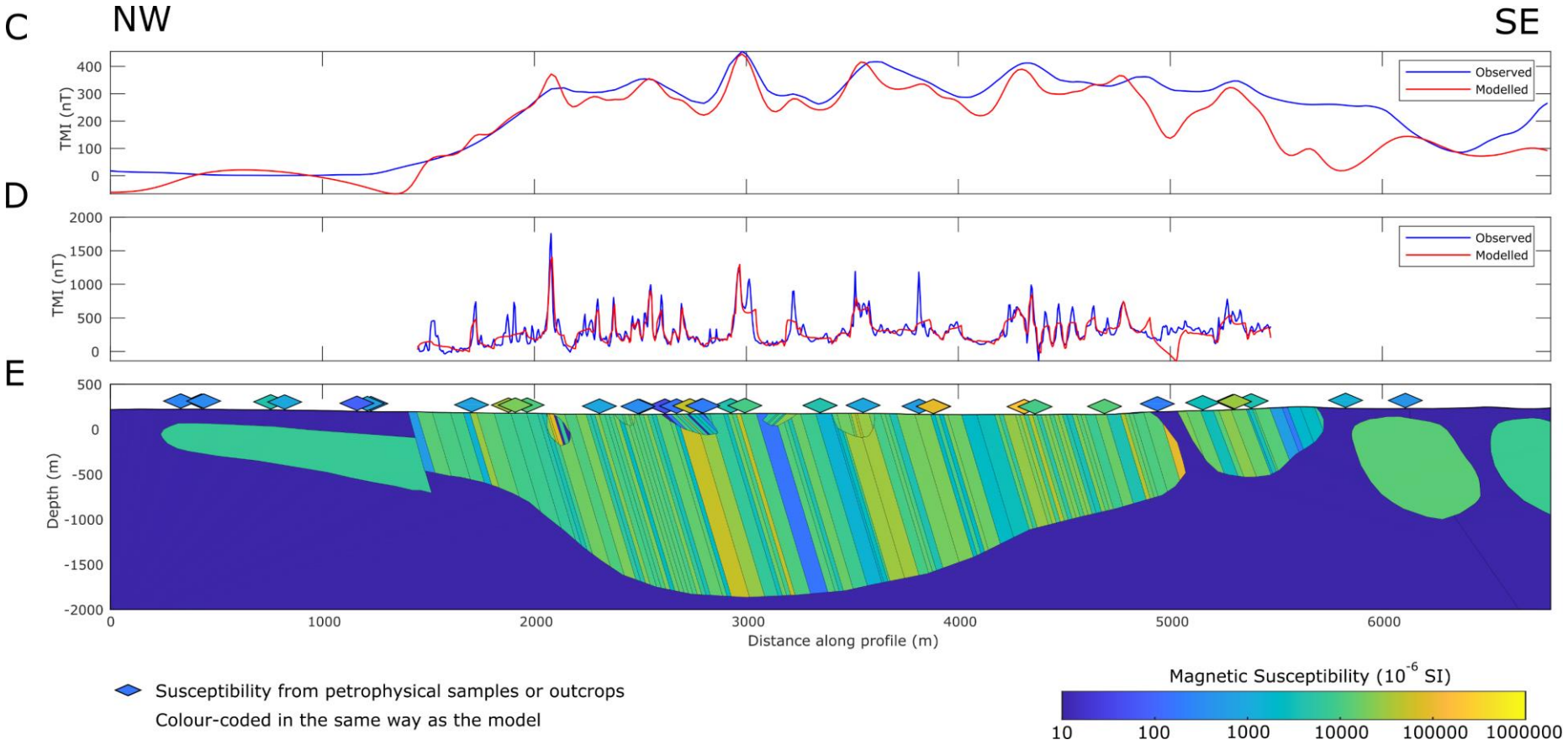

Figure 46 continued. Models for geophysical modelling profile 5. See figure 12 for profile position. **C.** Airborne magnetic data, both observed and calculated from model. **D.** Ground-based magnetic data, both observed and calculated from model. **E.** Magnetic susceptibility model, as well as susceptibility values from petrophysical samples and outcrop measurements.

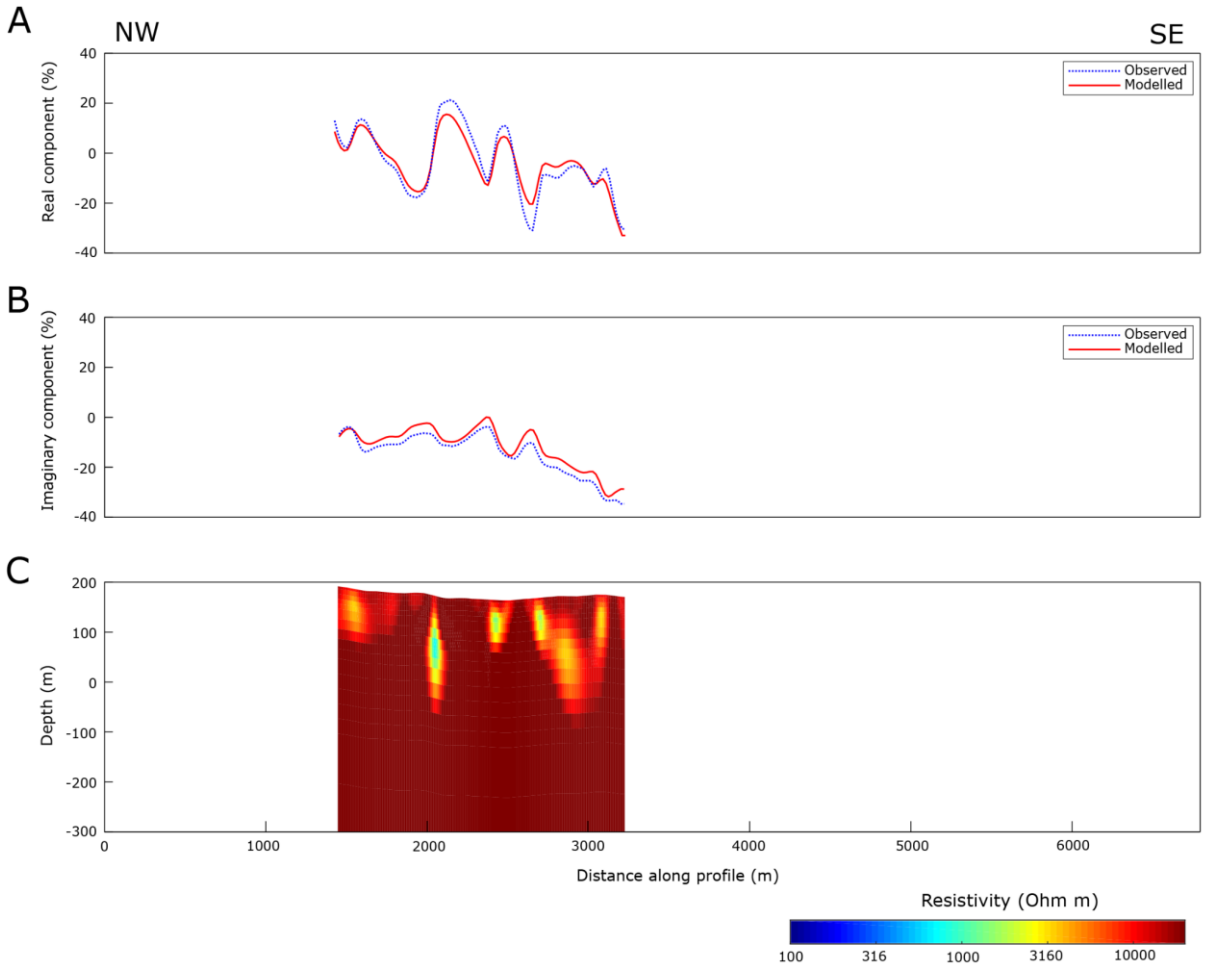

Figure 47. VLF data (23.4 kHz) and resistivity model for geophysical modelling profile 5. **A.** Both measured and modelled data for real component. **B.** Both measured and modelled data for the imaginary component. **C.** Resistivity model.

Due to the presence of infrastructure such as power lines and built-up areas it was only possible to collect VLF data along a relatively small section of profile 5. The observed and modelled data, as well as the inversion result for the VLF data (23.4 kHz) along the profile are shown in figure 47. Several notable low-resistive features can be observed in the model. The anomalies at 2 400, 2 700 and 3 100 m along the profile correspond to regions where felsic rocks have been mapped. Hence, they are attributed to mineralisation within these felsic xenoliths. The anomaly located at approximately 2 000 m along the profile is interpreted to also be due to mineralisation within a near surface felsic xenolith (fig. 48). However, the possibility remains that this could represent some form of mineralisation within the mafic intrusion.

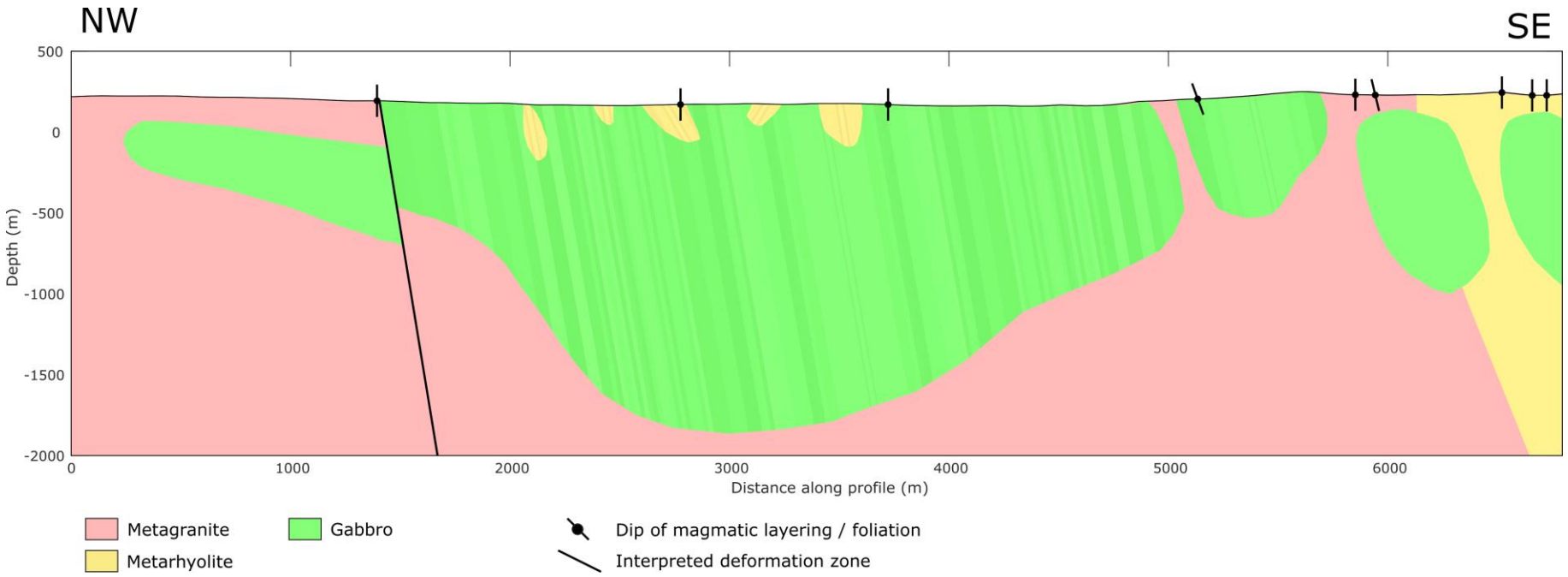

Figure 48. Model for geophysical modelling profile 5, colour-coded by interpreted rock type. The dip of foliation or layering from outcrop observations is shown on the profile.

Method and 3D modelling results from Flinten

During the project, efforts were made to generate a 3D density and susceptibility model of the Flinten intrusion. The objectives of this work were firstly, to gain a better understanding of the geometry of the structure in 3D and secondly, to check if the geometries captured in the 2D models were reasonable when modelling in 3D.

The following method was used to generate the model:

1. The gravity and magnetic field data were first imported into Geosoft VOXI software and a smooth inversion was performed to generate density and susceptibility models.
2. A combination of Matlab and Geoscene3D software were then used to generate a geological model of the intrusion. In this process the surface geology was considered. Efforts were made to include a series of layers within the geological model which had a high susceptibility. These layers were assumed to have the same geometry as those mapped with dashed white lines in figure 25. The strike and dip observations of magmatic layering were used to guide the geometry of the layers where possible. In addition, the smooth inversion results were used to help construct the geological model. Magnetic susceptibility and density values were then assigned to the different parts of the geological model.
3. In the case of the density model, forward modelling was performed to obtain modelled gravity data.
4. In the case of the susceptibility model, the geological model was used to perform a constrained inversion using the airborne magnetic measurements. In this inversion high magnetic susceptibility values were only allowed to occur in the layers which had been defined as high susceptibility (i.e. close to the dashed white lines in figure 25).
5. The susceptibility model obtained from the constrained inversion in step 4 was forward modelled to obtain modelled magnetic field data.

It should be noted that due to practical constraints, remanent magnetisation was not included in the 3D model. Furthermore, in this model mafic bodies were only modelled directly below where mafic rocks are mapped at the surface. This results in a poor match between the observed and modelled gravity data at the edges of the model. To improve this, additional mafic bodies would need to be included in the model below the surficial felsic rocks.

Figure 49 shows some images of the 3D density and magnetic susceptibility model for the Flinten intrusion. Maps showing the observed and modelled data for both models are shown in figure 50. Within the density model a constant density of 3 000 kg/m^3 is assumed for the mafic intrusive rocks. To generate the model the intrusion was divided into five regions (described in figure 25). At the edge of these regions the thickness of mafic rocks was typically assumed to be relatively low. The maximum thickness of each of the regions can be compared in figure 49C. The northern regions F1A, F1B and F1C have maximum thicknesses of 2 200, 2 400 and 2 100 m, respectively, while the southern regions F2A and F2B have maximum thicknesses of 1 850 and 1 000 m, respectively. These thicknesses are somewhat larger than observed on the 2D models, this is partially because the 2D profiles do not necessarily intersect the thickest part of the structure. However, it also likely reflects uncertainty in the modelling procedure as well as differences between 2D and 3D calculations. A reasonable match is obtained between the observed and modelled gravity data (shown in figure 50) within the central area. The fit could be improved in the surrounding area with the inclusion of additional mafic units below the surface.

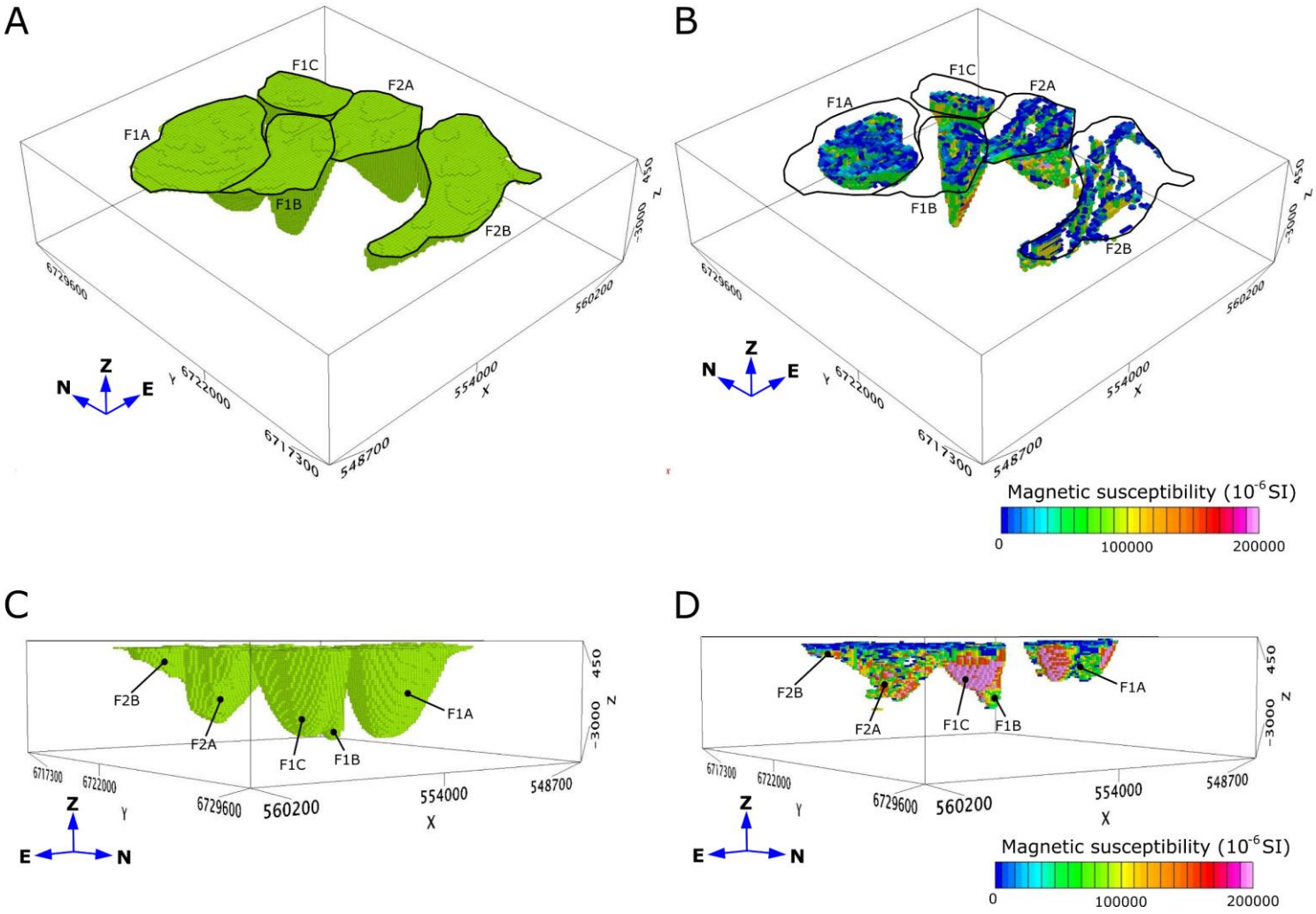

Figure 49. 3D density and magnetic susceptibility model for the Flinten intrusion. **A.** Density model viewed from the southwest. **B.** Magnetic susceptibility viewed from the southwest. Note only cells with susceptibility values above 1000 × 10^{-6} SI are shown. **C.** Density model viewed from the northeast. **D.** Magnetic susceptibility model viewed from the northeast. Note only cells with susceptibility values above 1000 × 10^{-6} SI are shown. The five regions of the intrusion interpreted from aeromagnetic measurements are annotated on the model.

Figure 49 shows the magnetic susceptibility model, where only cells with values above $1\ 000 \times 10^{-6}$ SI are displayed. Here it can be observed that high susceptibility values are only included along layers corresponding the high magnetic anomalies in the aeromagnetic data (fig. 25). In the case of the F1A, F1C and to some extent the F1B region, this constrains the high susceptibility values to the centre of the region. Within the model the layers with high magnetic susceptibility do not always extend to the base of the intrusion. In the case of regions F1A and F1C, the highly magnetised layers only extend to a depth of approximately 800 and 900 m, respectively. The match between the data modelled from the magnetic susceptibility model and the observed data is relatively good (fig. 50). This infers that most of the magnetic response is due to a limited number of key layers, with high magnetic susceptibilities.

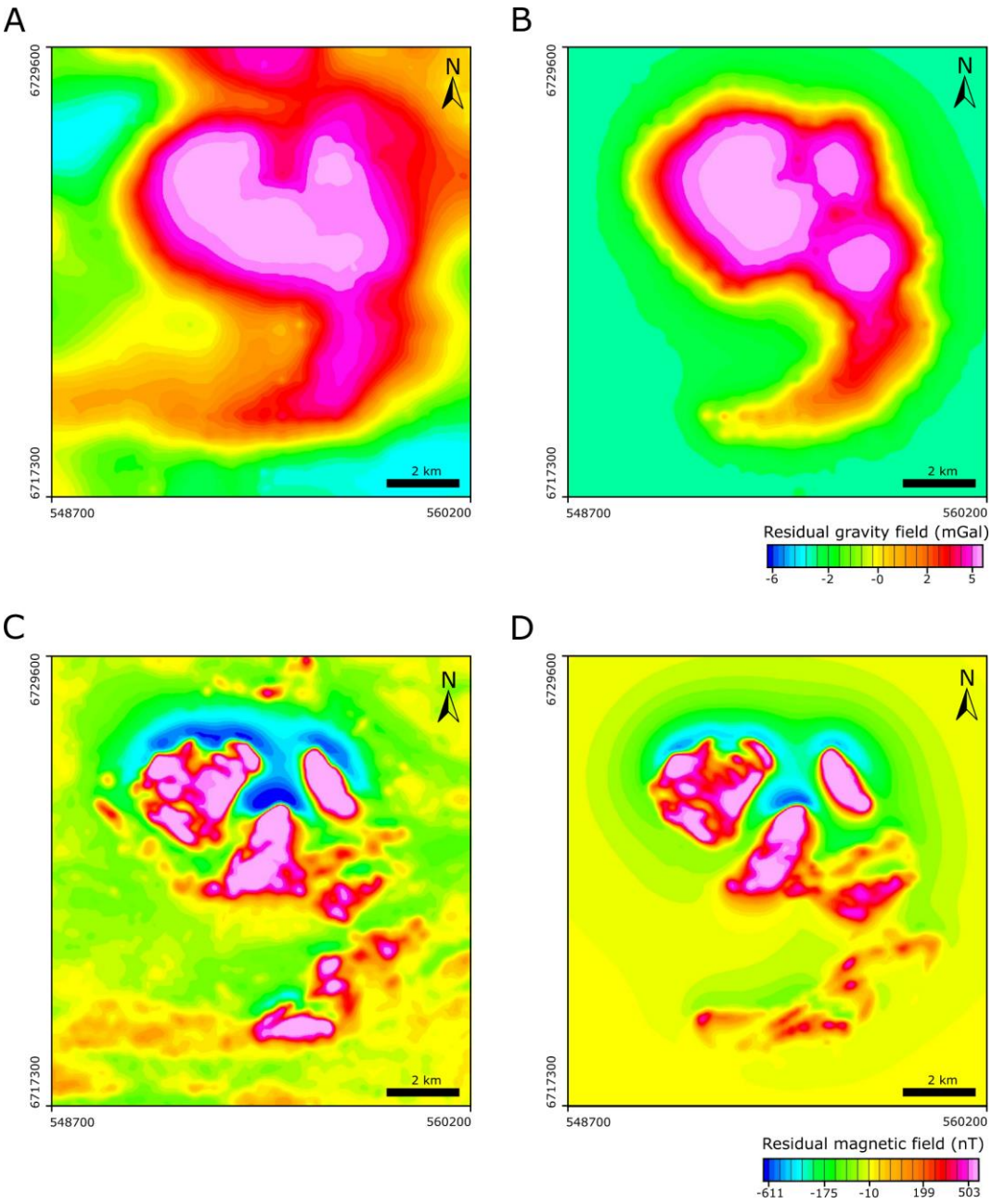

Figure 50. Data fit for 3D density and magnetic susceptibility models of the Flinten intrusion. **A.** Measured residual gravity data. **B.** Modelled residual gravity data. **C.** Measured residual magnetic field. **D.** Modelled residual magnetic field.

Discussion and summary of geophysical work

During the project, significant amounts of new geophysical and petrophysical data have been collected from the Flinten and Fullen intrusions, improving both the quality and quantity of information available for others, who may go on to investigate these areas in the future.

Based on the petrophysical analysis of the mafic intrusive rocks within this study it is apparent that the density and magnetic susceptibility values can vary significantly between different types of mafic rocks present within the intrusion. Relatively low densities of approximately 2 800 kg/m^3 are observed for feldspar-rich rocks such as troctolite or serpentinised ultramafic rocks, while densities of up to about 3 300 kg/m^3 can be reached for some gabbro-ultramafic rocks. Magnetic susceptibilities can vary between about 1 000 × 10^{-6} SI and 100 000 × 10^{-6} SI within the intrusion. This reflects variations in the amount of magnetic minerals within layers of the intrusions, which are interpreted to result from changes in the magma composition over time as the layers were formed (Ferré et al. 2009). Remanent magnetisation is significant for the rocks within both the Fullen and Flinten intrusions, where about 30–40% of petrophysical samples have Q values above 1. From the limited data available, the remanent magnetisation appears to typically be oriented in a similar direction to the present-day magnetic field.

The geometry of the magmatic layering in the Flinten intrusion has been interpreted based on aeromagnetic data and outcrop measurements. Some small low-resistive anomalies can be observed in the VLF based resistivity data, within the area of the intrusion. These appear to lie subparallel to the interpreted layering and hence, could be interesting for further investigation (fig. 26). In this study the intrusion has been interpreted to be split up into five regions, based on the airborne magnetic data, gravity data and outcrop measurements of layering direction (fig. 25). The gravity data suggests that the thickness of the mafic intrusive rocks is lower between these regions. Based on their characteristics in the airborne magnetic data, these regions can be grouped into northern regions (F1A, F1B and F1C) and southern regions (F2A and F2B). A tentative interpretation of these data is that the northern regions represent three separate sub-intrusions which are coeval, occurring at a different time to the southern two regions, which are coeval. Based on the magnetic data, the outer parts of F1A, F1B and F1C can tentatively be interpreted to represent layers which formed early in the life of the magma chamber, containing lower proportions of magnetic minerals (magnetite) and on average, higher proportions of feldspar. The central areas could represent layers which formed later in the life of the magma chamber when the composition was more iron rich. The felsic rocks encountered by the Sparvguld borehole are interpreted to be country rock (rock pre-dating the intrusion) which, were trapped and possibly further deformed between the three sub-intrusions (F1A, F1B and F1C) as they formed.

The 2D and 3D modelling performed during this study has been based on this interpretation of the intrusion. Hence, as it was possible to match the geophysical data, it shows that this interpretation is not unreasonable with regards to the available data.

Figure 51 shows a petrophysical analysis of the Flinten intrusion, grouped by some of the regions and areas discussed in the text above. Here it can be observed that there appears to be some differences in the density and magnetic susceptibility distributions between some areas. For example, the densities in the southern regions appear to be slightly lower than the northern regions. Similarly, the densities of the outer parts of the northern regions appear to be less dense than the central parts. However, before such an interpretation could be substantiated, more data (including petrophysical, mineralogical and geochemical) would need to be collected from the intrusion and analysed.

Using the aeromagnetic data from the Fullen intrusion the large-scale geometry of the magmatic layering has been interpreted (fig. 29). In general, these layers tend to be aligned southwest to northeast and to dip predominantly to the southeast. Results from a small-scale ground based magnetic survey show a good correlation between the magnetic anomalies and the layering direction (figs. 33 and 34). Several low resistivity anomalies have been identified based on airborne and ground-based VLF data, some of which appear to lie subparallel to the magnetic layering (figs. 29, 44 and 47). These anomalies could be interesting for further investigation.

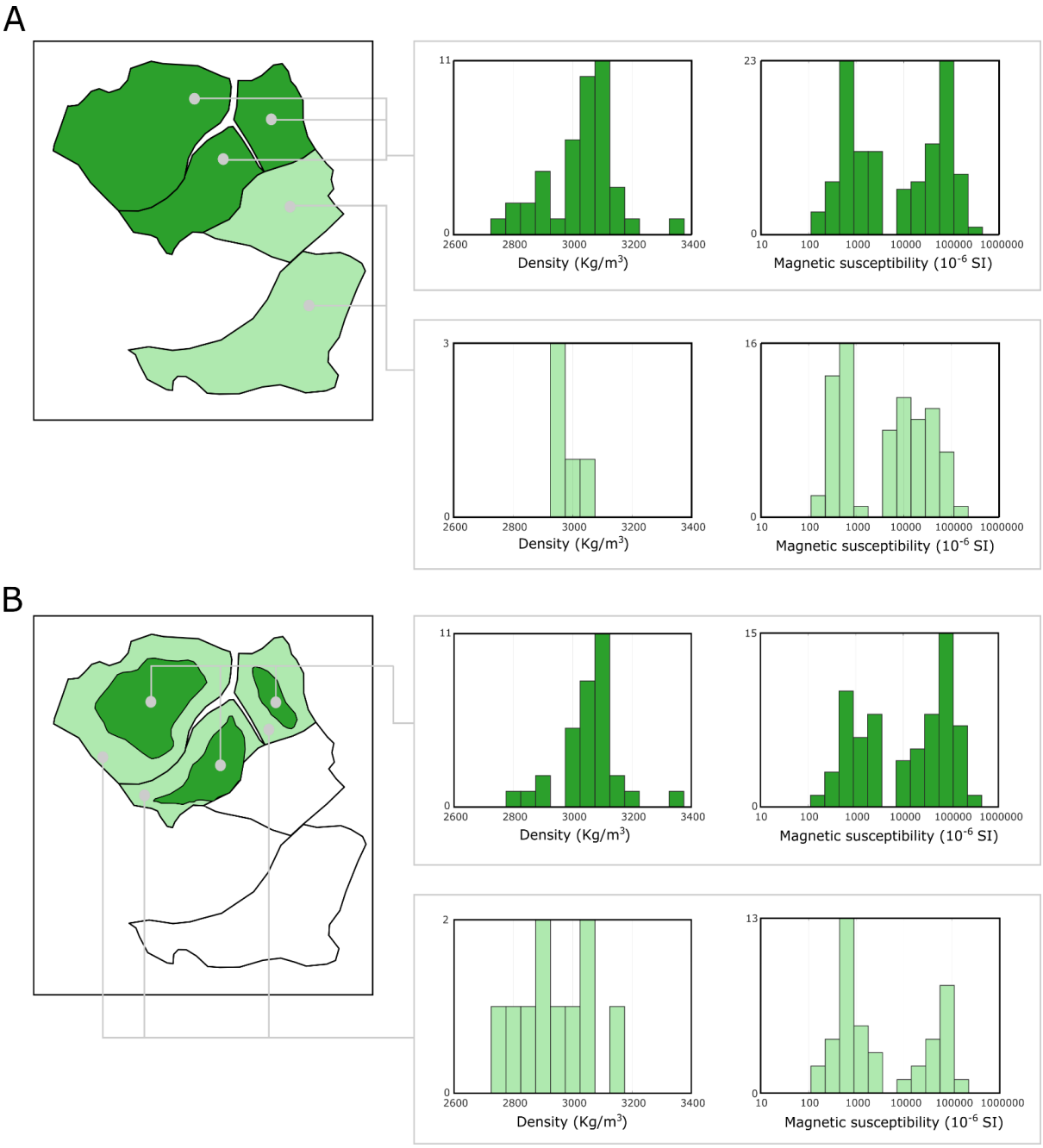

Figure 51. Statistical analysis of density and magnetic susceptibility data grouped by area, for the Flinten intrusion. **A.** Data grouped by northern regions (F1A, F1B and F1C), shown in dark green and southern regions (F2A and F2B), shown in light green. For a description of the regions see figure 25. **B.** Shows data form the northern regions (F1A, F1B and F1C), data is grouped by the central part of these regions (dark green) and the outer part of these regions (light green). The numbers on the y-axis of the different histograms denote the number of samples.

LITHOGEOCHEMISTRY

The similarities and differences between the different mineralised gabbro intrusions, with respect to their lithogeochemical signatures will be discussed in this section. However, it is important to note that presently, it is unknown whether there is a link between the age of the intrusions and their geochemistry. Radiometric age determination has only been performed on the gabbro at Kuså, which resulted in an age of 1.80 billion years, contradicting previous interpretations that it was of an older generation (Ripa et al. 2017). During previous regional mapping and sampling campaigns within the Bergslagen region by SGU, the basic intrusions have been considered to be of an older generation, interpreted to have formed 1.90–1.87 billion years ago. This also applies to the Flinten, Fullen-Hofors, Brunnsjöberget, and Gaddebo mines. However, the few age determinations of basic intrusions in the Bergslagen region show that at least two generations exist. At Flinten, a metamorphic age determination with the $^{40}Ar/^{39}Ar$ method was performed on amphibole in a deformed gabbroid. It resulted in a plateau age of 1 797 +/-7 Ma, reflecting a minimum age of shearing (Högdahl et al. 2009). Whether this metamorphic age differs completely from the magmatic age of the Flinten intrusion is not discussed in that study.

Method

All reported samples were analysed at ALS Scandinavia AB with the analysis packages CCP-PKG01, ME-MS41, and PGM-ICP23. In connection with these, SGU's standard samples for quality control were also analysed. All data are available at https://apps.sgu.se/kartvisare/kartvisare-bergartskemi.html.

The computer program GCD-kit 4.1 was used for plots and calculations (Janousek et al. 2006).

The Flinten intrusion

Most of the sampled rocks at the Flinten intrusion have ultrabasic to basic compositions and their magnesium number ($mg\# = 100*(MgO/40.3)/((MgO/40.3)+(0.9*(Fe_2O_3/71.8))))$ ranges from early formed rocks at 79 to later formed rocks at 40 (table 4). They are interpreted as cumulates formed from several injections of magma where a supernatant magma fractionated and evolved. Based on the geophysical data, the Flinten intrusion is interpreted to consist of several regions, representing a series of magma pulses (see section *Geophysical work,* specifically figures 25 and 49). However, it should be noted that the number of samples available is not sufficient to investigate if differences in composition exist between these interpreted regions.

The compositions of the Flinten samples are geochemically classified as subalkaline with a tholeiitic affinity in the AFM diagram (fig. 52). In the R1-R2 classification diagram, the samples mainly plot as gabbro and ultramafic rock, with a single sample plotting as alkali gabbro (fig. 52).

In the multi-element diagram and in the REE diagram, the analysis from Vargberget västra (10 light blue) differs from the other samples by generally having much higher concentrations of REE, as well as having a positive anomaly for P and a higher content of Ti (fig. 53). This is most easily explained by the fact that the rock is rich in the mineral apatite and Fe-Ti oxides, and that it is a relatively late-formed derivative of the magmatic fractionation. Of the samples analysed, it has the lowest mg#. Samples 19 and 22 also have low mg# as well as positive Ti anomalies in the multi-element diagram, hence these samples are also interpreted to be late-formed derivatives. Samples 10, 22, and 29 have negative Pb anomalies, whereas the remaining samples all have positive anomalies of varying magnitude (fig. 53). Of these sample 19 has the most distinct positive Pb anomaly. All rocks have distinct negative Zr anomalies.

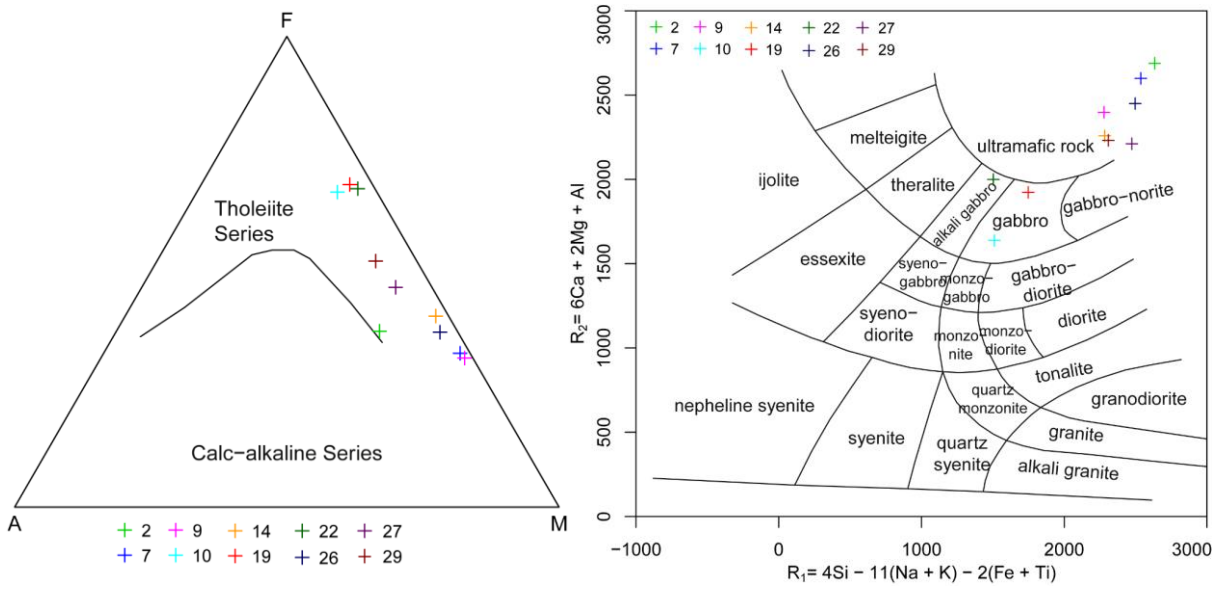

Figure 52. Classification diagrams of gabbroid rocks from the Flinten intrusion. AFM plot (Irvine & Baragar 1971) and R1-R2 plot (De la Roche et al. 1980).

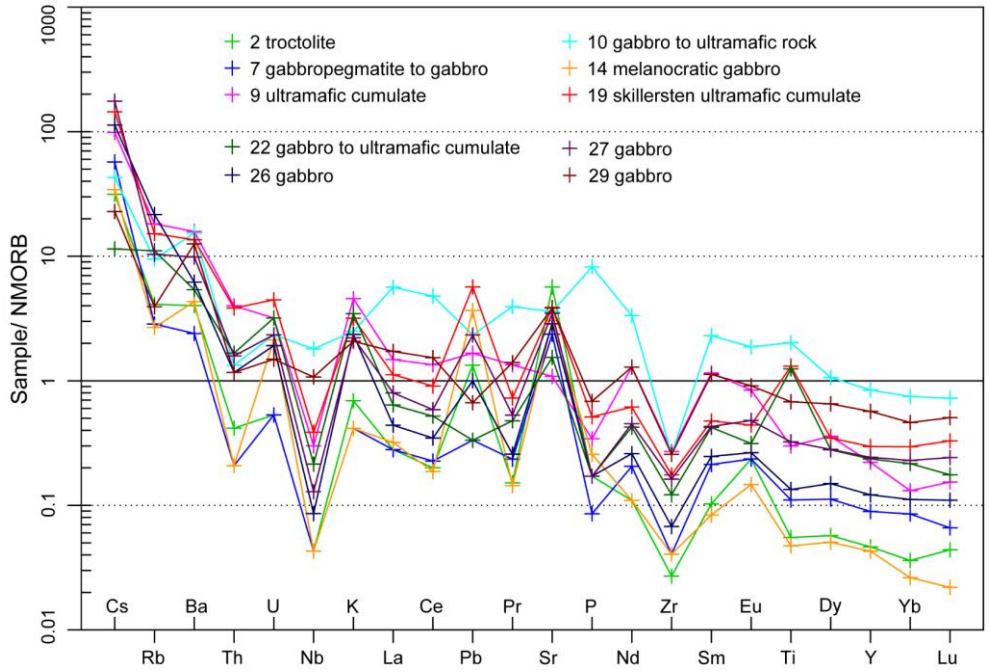

Figure 53. Multi-element diagram of gabbroid rocks from the Flinten intrusion. Normalising values N-MORB from Sun & McDonough (1989).

The analyses from the Flinten intrusion and the sulphide mine at Brunnsjöberget, Hedemora show consistent patterns in both multi-element diagrams and in REE diagrams (figs. 53–54, Claeson et al. 2018, 2019).

It can be noted that the mg # of the rocks where PGEs were detected at both the Flinten intrusion and the sulphide mine at Brunnsjöberget (Claeson et al. 2018, 2019), are significantly higher than from the sulphide mines in the Kuså area and the mines at Gaddebo (tables 4 and 9).

This indicates that there may be a petrogenetic difference in how PGEs have accumulated within the Flinten and Brunnsjöberget intrusions and within the sulphide mines (such as Kuså and Gaddebo). Elevated levels of specific elements, such as As and Sb can indicate that the magma has been contaminated by the incorporation of sulphide-bearing sedimentary rocks. On inspection of the results from Flinten and Brunnsjöberget, this is obviously not the case (tables 4 and 9). However, for the mines in the Kuså area and the mines at Gaddebo this could be a factor contributing to the overall sulphur content of the rocks (table 9).

Normative values for the Flinten intrusion, according to CIPW dry and wet systems, are presented in tables 5 and 6.

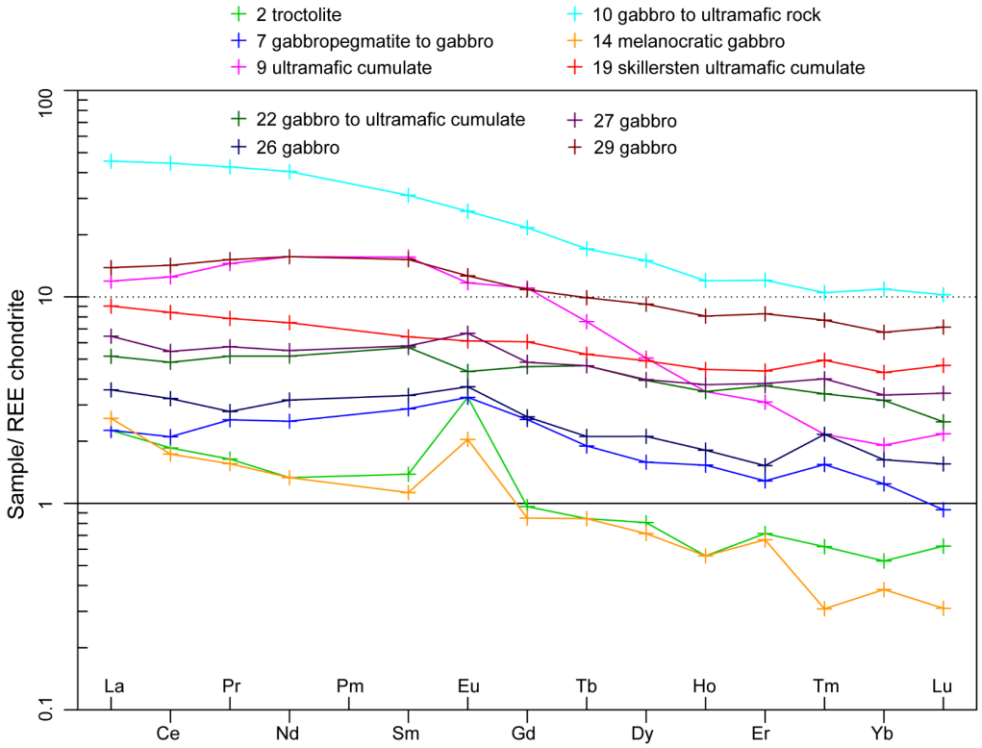

Figure 54. REE diagram of gabbroid rocks from the Flinten intrusion. Normalising values for chondrite from Boynton (1984).

Table 4. Lithogeochemical analyses for samples from the Flinten intrusion.

	2 T	7 PG	9 UM	10 MG	14 MG	19 SK	22 MG	26 G	27 G	29 G
SiO2	45.4	43.7	41.6	41.7	41.8	41.1	37.6	44.9	48	46.5
Al2O3	30.2	14.5	3.56	14.55	19.15	14.1	11.3	15.4	16.95	18.15
Fe2O3	2.67	8.65	12.9	20.5	11.5	21.9	24.8	9.53	10.35	11
CaO	18.15	14.4	10.4	9.34	10.85	11.75	12.15	13.7	13.25	14
MgO	3.11	15.6	24.5	7.12	14.55	7.85	9.63	13.75	9.3	7.61
Na2O	0.87	0.41	0.23	1.82	0.57	0.97	0.79	0.59	1.17	1.28
K2O	0.05	0.03	0.33	0.18	0.03	0.23	0.25	0.17	0.16	0.15
TiO2	0.07	0.14	0.38	2.56	0.06	1.66	1.58	0.17	0.41	0.86
MnO	0.04	0.13	0.17	0.32	0.17	0.23	0.2	0.15	0.2	0.18
P2O5	0.02	0.01	0.04	0.96	0.03	0.06	0.02	0.02	0.02	0.08
Cr	170	870	510	50	60	10	20	170	60	200
Ni	15	159	364	57	210	6	17	98	32	49
Cu	23	32	25	87	400	71	222	77	76	56

Table 4. Continued.

	2 T	7 PG	9 UM	10 MG	14 MG	19 SK	22 MG	26 G	27 G	29 G
Au	<0.001	0.001	0.004	<0.001	0.001	0.001	0.001	<0.001	<0.001	<0.001
Pt	<0.005	<0.005	**0.009**	<0.005	<0.005	<0.005	<0.005	<0.005	<0.005	<0.005
Pd	<0.001	0.001	**0.044**	0.001	0.001	0.001	0.001	0.001	<0.001	0.001
Co	10	60	107	59	94	63	91	71	41	38
Pt:Pd	N.A.	N.A.	1:4.89	N.A.	N.A.	N.A.	N.A.	N.A.	N.A.	N.A.
mg#	69.8	78.1	79.0	40.7	71.5	41.5	43.5	74.1	64.0	57.8
Co#	20.8	23.9	21.6	29.1	13.4	45.0	27.6	28.9	27.5	26.6
Ni#	39.5	83.2	93.6	39.6	34.4	7.8	7.1	56.0	29.6	46.7
Ni/Cu	0.7	5.0	14.6	0.7	0.5	0.1	0.1	1.3	0.4	0.9
S/Se	1 000	667	2 000	4 330	2 530	7 170	4 270	3 000	1 830	1 430
Sb	<0.05	<0.05	<0.05	0.07	0.05	<0.05	0.08	<0.05	<0.05	<0.05
As	0.3	0.1	0.3	0.5	0.4	0.2	0.3	0.3	0.2	<0.1

Co# = 100*Co/(Co+Ni+Cu), Ni# = 100*Ni/(Ni+Cu), mg# = 100* MgO/(FeO+MgO) [mol%]
T = troctolite, PG = pegmatitic gabbro, UM = ultramafic, MG = melanocratic gabbro, SK = ”skillersten” gabbro, G = gabbro.

Table 5. Normative values for the Flinten intrusion according to CIPW.

	2 T	7 PG	9 UM	10 MG	14 MG	19 SK	22 MG	26 G	27 G	29 G
Q	0	0	0	4.466	0	3.151	0	0	3.801	2.893
Or	0.295	0.177	1.95	1.064	0.177	1.359	1.477	1.005	0.946	0.886
Ab	7.362	3.469	1.946	15.4	4.823	8.208	6.685	4.992	9.9	10.831
An	78.351	37.636	7.707	31	49.605	33.44	26.549	38.87	40.525	43.335
Di	8.812	26.213	33.381	0.115	2.973	14.54	21.869	22.087	18.649	17.805
Hy	0.909	8.007	11.219	17.683	16.103	12.815	10.411	14.912	14.522	10.703
Ol	1.929	13.107	24.064	0	13.15	0	2.411	6.378	0	0
Ilm	0	0.231	0.316	0	0	0	0	0	0.167	0.148
Hm	2.67	8.651	12.901	20.502	11.501	21.902	24.802	9.531	10.351	11.001
Tn	0.172	0.046	0.524	6.285	0.147	4.075	3.879	0.417	0.791	1.92
Ap	0.047	0.024	0.095	2.274	0.071	0.142	0.047	0.047	0.047	0.189
Py	0.068	0.037	0.037	0.541	0.288	0.389	0.338	0.254	0.206	0.187
Sum	100.62	97.60	94.14	99.33	98.84	100.02	98.47	98.49	99.90	99.9

T = troctolite, PG = pegmatitic gabbro, UM = ultramafic, MG = melanocratic gabbro, SK = ”skillersten” gabbro, G = gabbro.

Table 6. Normative values for the Flinten intrusion according to CIPW with hornblände.

	2 T	7 PG	9 UM	10 MG	14 MG	19 SK	22 MG	26 G	27 G	29 G
Q	0	0	0	4.175	0	1.866	0	0	1.762	1.312
Ab	5.701	0	0	15.399	2.925	8.207	0	0	9.9	10.83
An	78.348	37.634	7.706	30.999	49.604	33.439	26.548	38.868	40.524	43.334
Wo	1.391	0	0	0	0	1.844	3.665	0	0.222	2.358
Ilm	0	0.231	0.316	0	0	0	0	0	0.167	0.148
Hm	2.67	8.651	12.901	20.502	11.501	21.902	24.802	9.531	10.351	11.001
Ap	0.047	0.024	0.095	2.274	0.071	0.142	0.047	0.047	0.047	0.189
Py	0.068	0.037	0.037	0.541	0.288	0.389	0.338	0.254	0.206	0.187
Bi	0.424	0.254	2.797	1.526	0.254	1.95	2.119	1.441	1.356	1.272
Hbl	11.893	48.458	62.447	12.943	5.909	28.619	35.992	41.772	35.044	28.483
Sum	100.54	95.29	86.3	88.36	70.55	98.36	93.51	91.91	99.58	99.12

T = troctolite, PG = pegmatitic gabbro, UM = ultramafic, MG = melanocratic gabbro, SK = ”skillersten” gabbro, G = gabbro.

The Fullen, Skållberget and Furulund intrusions close to Hofors

Most of the sampled rocks have ultrabasic to basic compositions (table 7). The mg# of rocks from the Fullen intrusion range from early formed rocks at 74 to later formed at 39 (table 7). They are interpreted as cumulates formed from several injections of magma where a supernatant magma fractionated and evolved. However, the number of samples is not enough to further discuss starting compositions that filled up the magma chamber (see figs. 45, 48). The sample from Skållberget has a mg# of 46 and the sample from the Karlsborg mine (Furulund intrusion) has a mg# of 83.

The compositions are geochemically classified as subalkaline with a tholeiitic affinity on the AFM diagram (fig. 55). The samples plot as gabbro, gabbronorite, and ultramafic rocks in the R1-R2 classification diagram (fig. 55).

In the multi-element diagram and in the REE diagram, the analyses from the Fullen intrusion (sample 1–10) have consistent patterns and for the most part only differ according to how evolved the rocks are (figs. 56–57). In the multi-element diagram a weak positive Pb anomaly is present in most samples. Furthermore, in most samples a strong negative Nb and Zr anomaly, while the Ti anomaly is mostly weak or absent (fig. 56). The Fullen samples in the REE diagram display a subtle REE-enrichment, while the curves are relatively flat for the heavy REEs (fig. 57). The ultrabasic cumulate sample 7 is the only one displaying a strong Eu anomaly (which is negative at 0.62), while the remaining samples from Fullen have minor Eu anomalies, with Eu/Eu* values between 0.90 and 1.10 (fig. 57). This would infer that plagioclase fractionation during magma evolution in the chamber was not a major process for the most part.

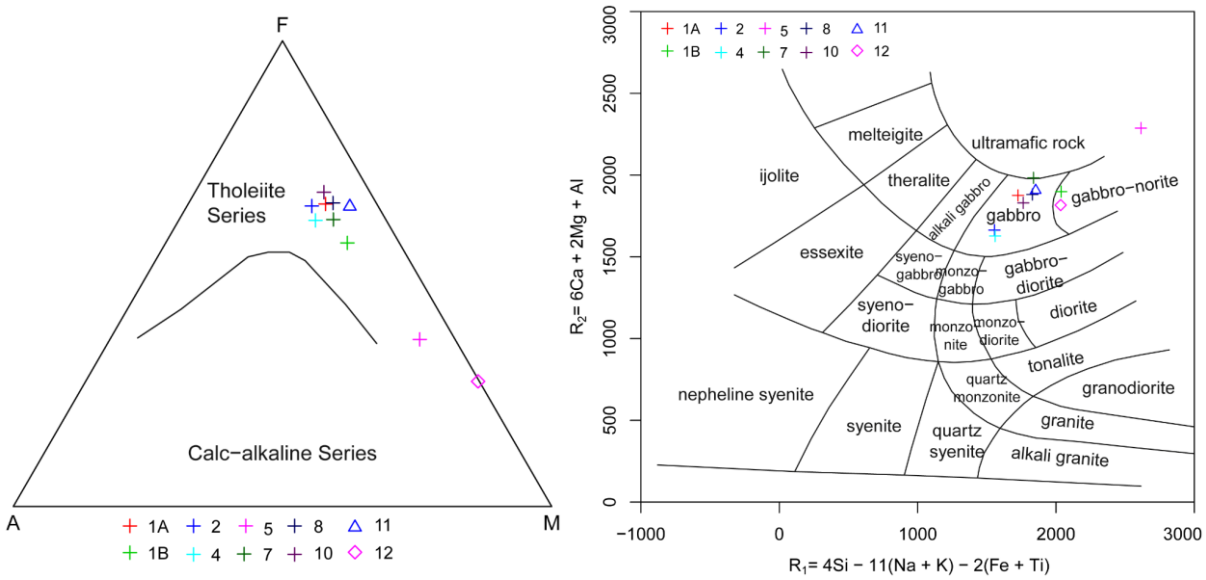

Figure 55. Classification diagrams of gabbroid rocks from the Fullen, Skållberget and Furulund intrusions. AFM plot (Irvine & Baragar 1971) and R1-R2 plot (De la Roche et al. 1980). Sample 11 = Skållberget and 12 = Furulund intrusions.

However, it could also infer that sample 7 displays a negative europium anomaly due to a change in oxidation state of the magma. In this case, prior to the formation of the rocks sampled at location 7, the magma may have contained europium as Eu^{3+} which behaved as the rest of the REEs (i.e. a more oxidized magma). At a later stage, this magma may have been altered into a more reduced magma (containing Eu^{2+} instead) and thus preferentially incorporated in plagioclase and accordingly fractionated from the other REEs that continued as trivalent ions. This also opens the possibility that there are several batches of magma with significantly different characteristics.

The Karlsborg mine sample (within the Furulund intrusion) contains, for the most part, relatively low amounts of the elements shown in the multi-element diagram, with the exception of Cs and Rb, which are enriched (figs. 56–57). Both Cs and Rb are readily moved around by hydrothermal fluids and more than likely increased in concentration within the rock during serpentinisation (e.g. Pirajno 2009). The Skållberget sample has a similar pattern as the Furulund sample. An exception to this is in the amounts of Sr and Ti where strong positive anomalies are seen at Skållberget. Conversely, in the Furulund sample a negative anomaly and a flat (non-anomalous) value are observed for Sr and Ti, respectively (fig. 56). This is due to the Furulund sample being from an early-formed cumulate (mg# 83), which would have initially formed with miniscule amounts of both plagioclase and Ti-bearing oxides, where Sr and Ti respectively would be present. In contrast the Skållberget sample represents a late-formed cumulate (mg# 46) with abundant plagioclase and Ti-bearing oxides.

The Skållberget sample has an almost flat REE pattern with a distinct europium anomaly at Eu/Eu* 1.46, indicating plagioclase fractionation and accumulation (fig. 57). The Furulund sample has a relatively flat REE pattern and low abundances overall (fig. 57). Since there is no known mineral found with prevalence of Tm over the other REE, the positive anomaly at Tm and Yb is most probably an artefact, due to very low levels, which are close to the detection limit.

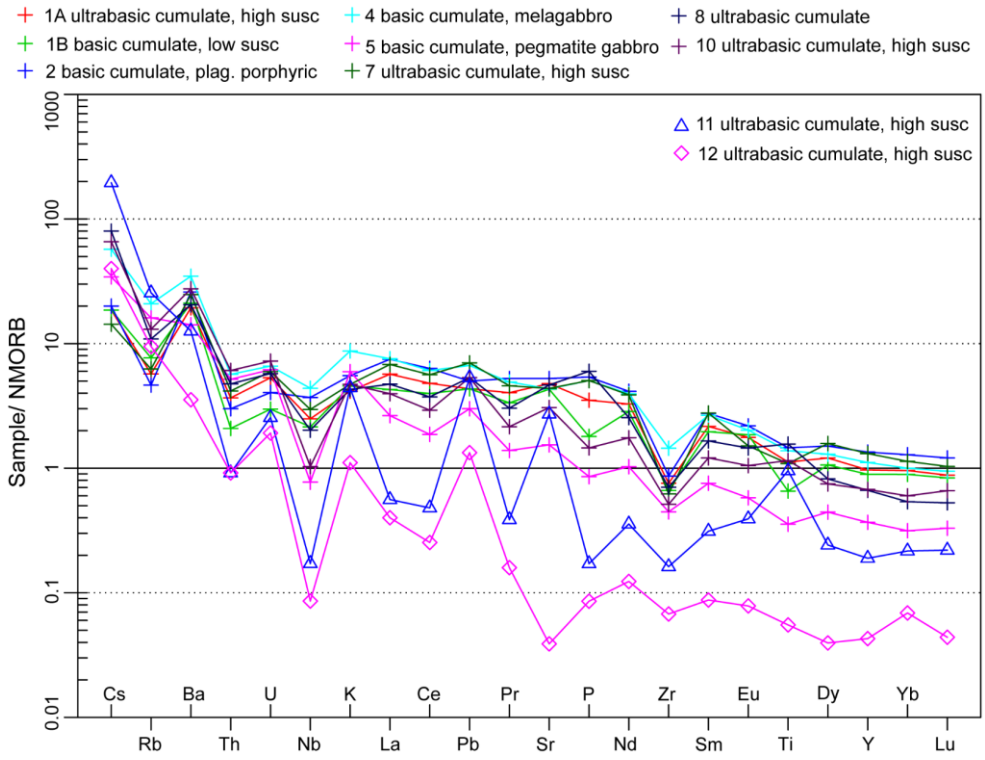

Figure 56. Multi-element diagram of gabbroid rocks from the Fullen, Skållberget and Furulund intrusions. Normalising values N-MORB from Sun & McDonough (1989). Sample 11 = Skållberget and 12 = Furulund intrusions.

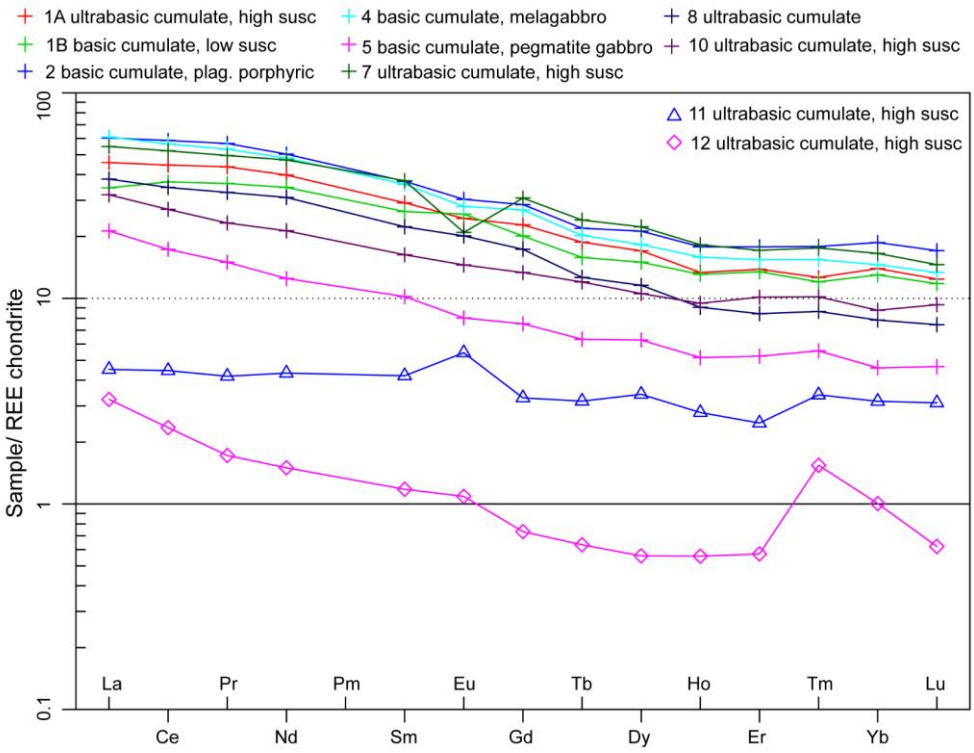

Figure 57. REE diagram of gabbroid rocks from the Fullen, Skållberget and Furulund intrusions. Normalising values for chondrite from Boynton (1984). Sample 11 = Skållberget and 12 = Furulund intrusions.

The hydrothermal alteration of the original rock at Furulund may have changed the content of REEs. However, since this rock originally formed as an ultrabasic cumulate, consisting mostly of olivine and pyroxene (indicated by the Ni and Cr contents) it would likely have had low amounts of REEs initially. The subsequent alteration to a serpentine-bearing rock is not likely to have significantly changed the REE content.

The analyses of gabbroid rocks from the Fullen, Skållberget, and Furulund intrusions were plotted in a ternary diagram to document fractionation and variation of some elements, which are important for interpretation of ore genesis and interesting for exploration of this type of sulphide ore (fig. 58). The data were also plotted in bivariate plots (fig. 59).

An originally cobalt-bearing olivine is a probable source of the high Co and Ni contents in the Karlsborg mine at Furulund, both preferentially partition into olivine and thus are compatible. Furthermore, early formed olivine will have higher contents of Co and Ni than ones crystallised from more evolved magmas (e.g. Ehlers et al. 1992, Herzberg et al. 2016). Another source could be cobalt-bearing pentlandite, $(Fe, Ni)_9S_8$, but since the analysis shows sulphur at only 0.01%, this is probably not the case at Furulund. Unless the sulphur was removed from the cumulate rock during the hydrothermal alteration while Ni and Co remained.

Normative values for the Fullen, Skållberget and Furulund intrusions, according to CIPW dry system, is presented in table 8.

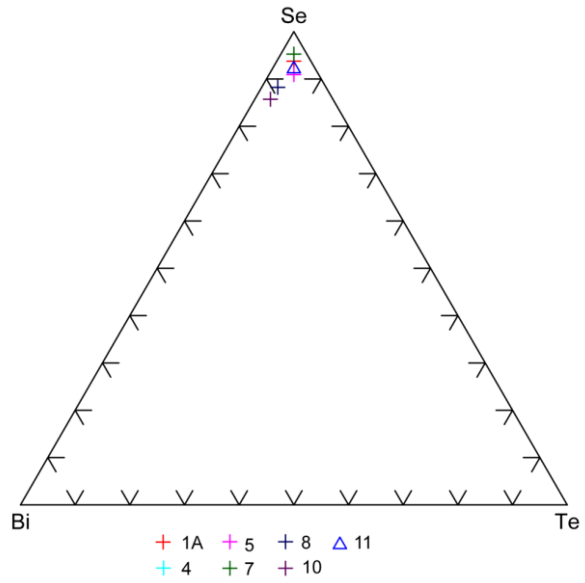

Figure 58. Ternary Bi-Se-Te diagram of gabbroid rocks from the Fullen (1–10) and Skållberget (11).

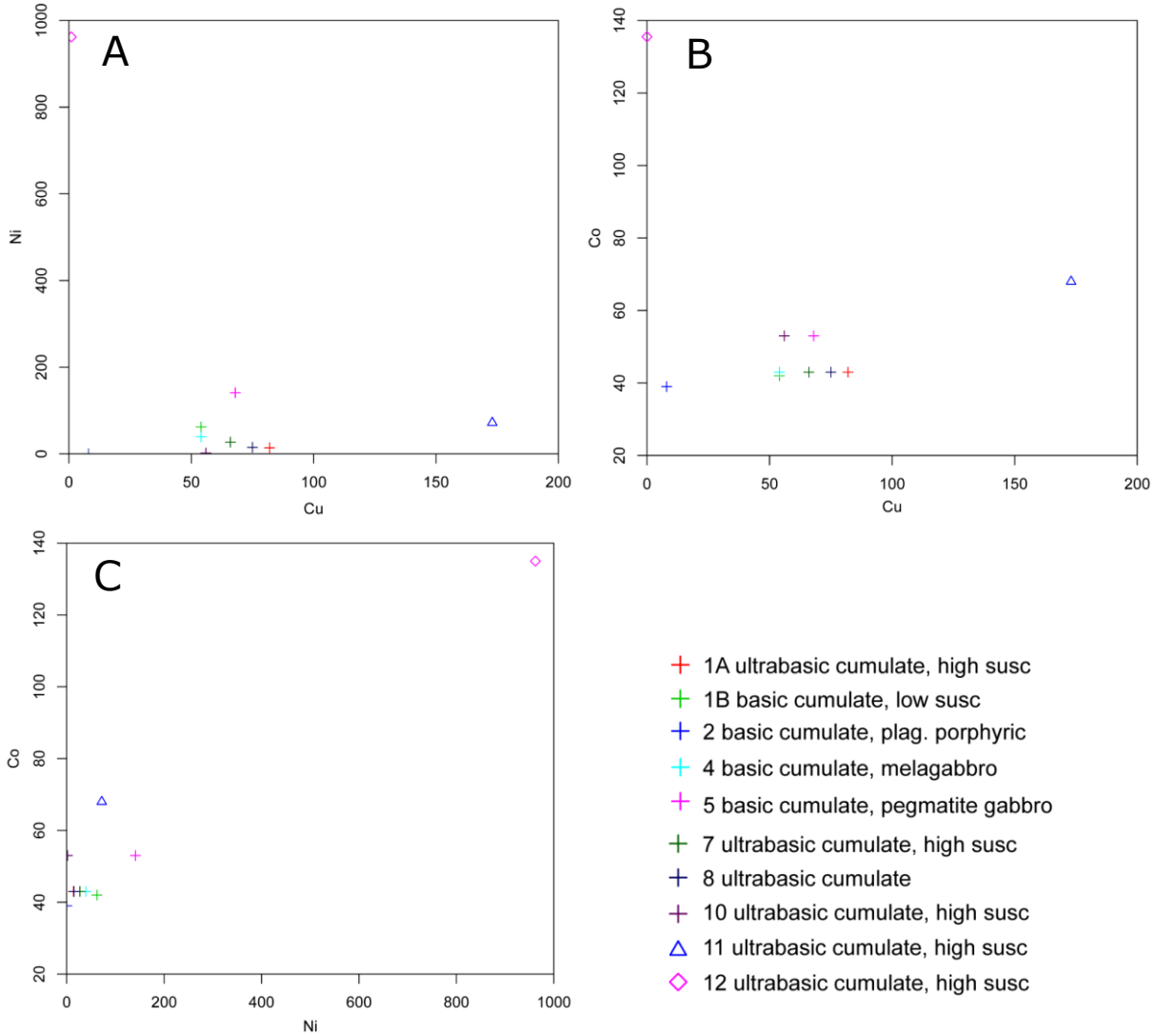

Figure 59. Plots of lithogeochemical data from the gabbroid rocks from the Fullen (1–10), Skållberget (11) and Furulund (12) intrusions. All values in ppm. **A.** Copper versus nickel. **B.** Copper versus cobalt. **C.** Nickel versus cobalt.

Table 7. Lithogeochemical analyses for samples from the Fullen, Skållberget and Furulund intrusions.

	1A UB	1B BC	2 BC	4 MG	5 PG	7 UB	8 UB	10 UB	11 UB	12 UB
SiO2	43.5	46.5	45.0	45.6	50.9	44.4	43.8	44.1	42.3	36.3
Al2O3	18.05	17.05	15.7	14.8	8.93	17.7	16.45	15.8	15.0	1.78
Fe2O3	16.3	13.55	16.8	16.15	9.77	14.9	16.7	17.95	18.95	14.05
CaO	11.55	11.25	10.15	9.71	13.2	12.4	11.7	11.55	11.35	0.74
MgO	5.76	7.27	5.43	6.01	14.1	6.23	6.18	5.73	8.02	34.3
Na2O	1.85	1.75	2.48	2.48	1.18	1.78	1.54	1.71	1.08	0.03
K2O	0.3	0.33	0.4	0.63	0.43	0.34	0.31	0.34	0.32	0.08
TiO2	1.42	0.83	1.85	1.75	0.45	1.38	1.98	1.46	1.21	0.07
MnO	0.24	0.29	0.3	0.25	0.17	0.21	0.24	0.21	0.2	0.2
P2O5	0.41	0.21	0.63	0.59	0.1	0.59	0.7	0.17	0.02	0.01
Cr	30	150	10	90	910	60	30	20	20	3560
Ni	14	62	0.2	39	141	27	15	1.7	72	962
Cu	82	54	8	54	68	66	75	56	173	1.3
Au	0.002	0.001	<0.001	0.001	0.002	0.001	<0.001	<0.001	0.002	<0.001
Pt	<0.005	<0.005	<0.005	<0.005	<0.005	<0.005	<0.005	<0.005	<0.005	<0.005
Pd	0.001	0.002	0.001	0.001	0.002	0.001	<0.001	0.001	<0.001	0.001
Co	43	42	39	43	53	43	43	53	68	135
Pt:Pd	N.A.	N.A.	N.A.	N.A.	N.A.	N.A.	N.A.	N.A.	N.A.	N.A.
mg#	41.2	51.5	39.0	42.4	74.1	45.3	42.3	38.7	45.6	82.9
Co#	30.9	26.6	82.6	31.6	20.2	31.6	32.3	47.9	21.7	12.3
Ni#	14.6	53.4	2.4	41.9	67.5	29.0	16.7	2.9	29.4	99.9
Ni/Cu	0.17	1.15	0.03	0.72	2.07	0.41	0.2	0.03	0.42	962
S/Se	4 330	6500	8 000	5 330	1 000	4 000	8 000	9 000	6 300	1 000
Sb	<0.05	<0.05	<0.05	0.05	<0.05	<0.05	0.06	0.05	0.06	0.07
As	0.2	0.3	0.1	0.3	0.2	0.2	0.3	0.3	1.4	0.9

Co# = 100*Co/(Co+Ni+Cu), Ni# = 100*Ni/(Ni+Cu), mg# = 100* MgO/(FeO+MgO) [mol%]
UB = ultrabasic cumulate, BC = basic cumulate, MG = melanocratic gabbro, PG = pegmatitic gabbro.
Sample 11 = Skållberget and 12 = the Karlsborg mine, Furulund.

Table 8. Normative values for the Fullen, Skållberget and Furulund intrusions according to CIPW.

	1A UB	1B BC	2 BC	4 MG	5 PG	7 UB	8 UB	10 UB	11 UB	12 UB
Q	2.559	4.326	4.374	4.321	3.527	2.52	4.895	4.742	3.119	0
C	0	0	0	0	0	0	0	0	0	0.323
Or	1.773	1.95	2.364	3.723	2.541	2.009	1.832	2.009	1.891	0.473
Ab	15.654	14.808	20.985	20.985	9.985	15.062	13.031	14.47	9.139	0.254
An	40.061	37.693	30.525	27.39	17.8	39.302	37.057	34.432	35.136	3.606
Di	7.778	11.232	7.861	8.653	35.842	10.651	7.409	12.978	13.099	0
Hy	10.743	12.904	9.883	10.96	18.509	10.582	11.961	8.258	13.907	29.057
Ol	0	0	0	0	0	0	0	0	0	39.515
Mt	0	0	0	0	0	0	0	0	0	0.414
Ilm	0.205	0.312	0.452	0.155	0.316	0.07	0	0	0	0.133
Hm	16.301	13.551	16.801	16.151	9.771	14.901	16.701	17.951	18.952	13.766
Tn	3.221	1.634	3.957	4.095	0.696	3.297	4.861	3.584	2.97	0
Ap	0.971	0.497	1.492	1.397	0.237	1.397	1.658	0.403	0.047	0.024
Py	0.244	0.244	0.15	0.3	0.037	0.3	0.406	0.355	0.338	0.019
Sum	99.51	99.15	98.84	98.13	99.26	100.09	99.81	99.18	98.60	87.58

UB = ultrabasic cumulate, BC = basic cumulate, MG = melanocratic gabbro, PG = pegmatitic gabbro.
Sample 11 = Skållberget and 12 = the Karlsborg mine, Furulund.

Sulphide mines at Kuså, Gaddebo and Brunnsjöberget

In both the multi-element diagram and the REE diagram, the sulphide mineralised samples analysed from Kuså and Gaddebo show similar characteristics (figs. 60, 61). In the multi-element diagram, only Zr shows a significant difference between the samples. Here the Muttogruvan 2 sample differs due to its positive anomaly whereas the other samples have negative anomalies (fig. 60). Large negative anomalies are seen for Nb, P and Ti while more subtle negative anomalies are observed for La and Ce. Positive anomalies are seen for Pb. The characteristic strong negative anomalies for Nb and positive Pb anomalies are indications that the rocks may have originated in a subduction-related environment. The REE diagram shows a weak fractionation-controlled enrichment of the light REEs with a relatively flat curve for the heavy REEs. This is interpreted to indicate that there were no residual garnets in the source rock of the original magmas (fig. 61). The Brunnsjöberget, Hedemora data and additional geophysical surveying and measurements are found in Claeson et al. (2018, 2019). Only samples anomalous in PGEs are plotted in some figures here for comparison.

The analyses from the Kuså, Mutto, Illingsberg, and Gaddebo mines show very weak elevations of As and Sb, which possibly indicates a minor contamination of the basic magma from sulphide-bearing sediments (table 9). The sulphide mine at Brunnsjöberget has no elevated values of As and Sb and thus resembles the results from the Flinten intrusion (table 9).

The analyses of sulphide-mineralised gabbro and sulphide-mineralised gabbro pegmatite were plotted in ternary diagrams to document fractionation and variation of some elements, which are important for interpretation of ore genesis and interesting for exploration for this type of sulphide ore (fig. 62). The data are also plotted in bivariate plots (fig. 63).

The ratio between Pt and Pd is lower in the samples from the Flinten intrusion and the Brunnsjöberget intrusion compared with the samples from Kuså gruva 2 and Gaddebo mines (tables 4 and 9). The sample from Gaddebo mines deviates the most (fig. 62).

In a comparison between the different deposits, the Flinten and the Brunnsjöberget intrusions have more in common with each other than with other deposits/mines in this study. This is possibly related to how the formation of the Cu-Ni-PGE anomalous parts occurred. However, additional data and analysis would need to be conducted before any firm conclusions about their petrogenesis could be drawn.

Normative values for the Kuså, Gaddebo, and Brunnsjöberget samples, according to CIPW dry and wet systems, are presented in tables 10 and 11.

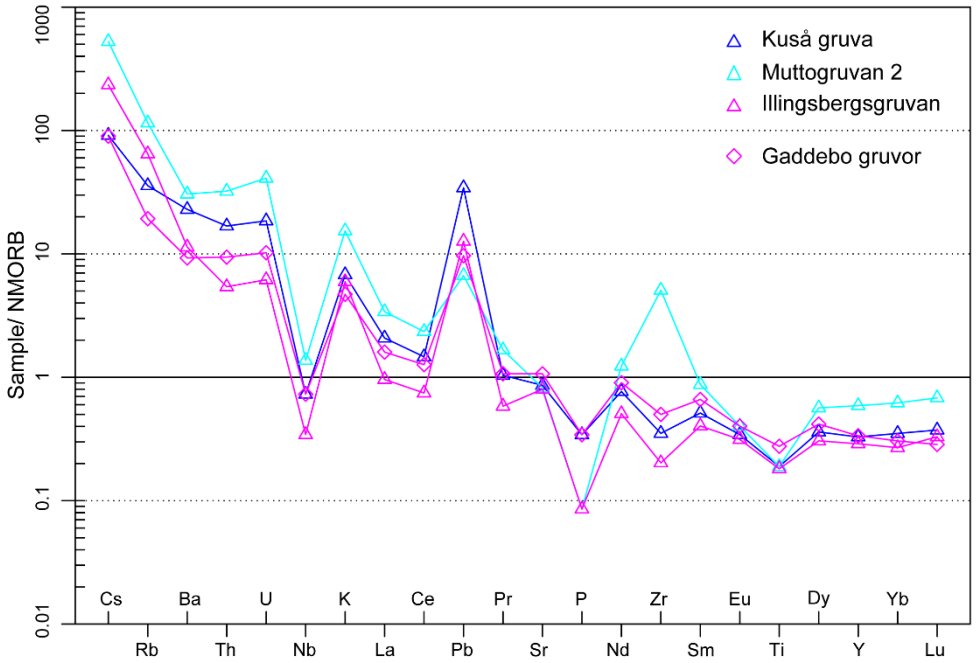

Figure 60. Multi-element diagram of mineralised, gabbroid rocks from the mines at Kuså and Gaddebo. Normalising values for N-MORB from Sun & McDonough (1989).

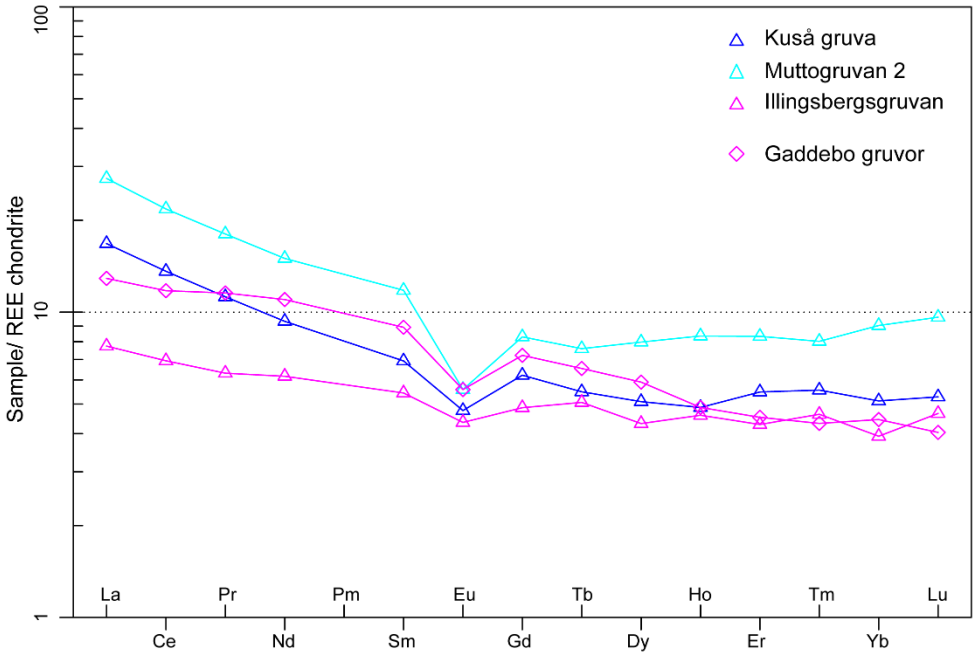

Figure 61. REE diagram of mineralised, gabbroid rocks from the mines at Kuså and Gaddebo. Normalising values for chondrite from Boynton (1984).

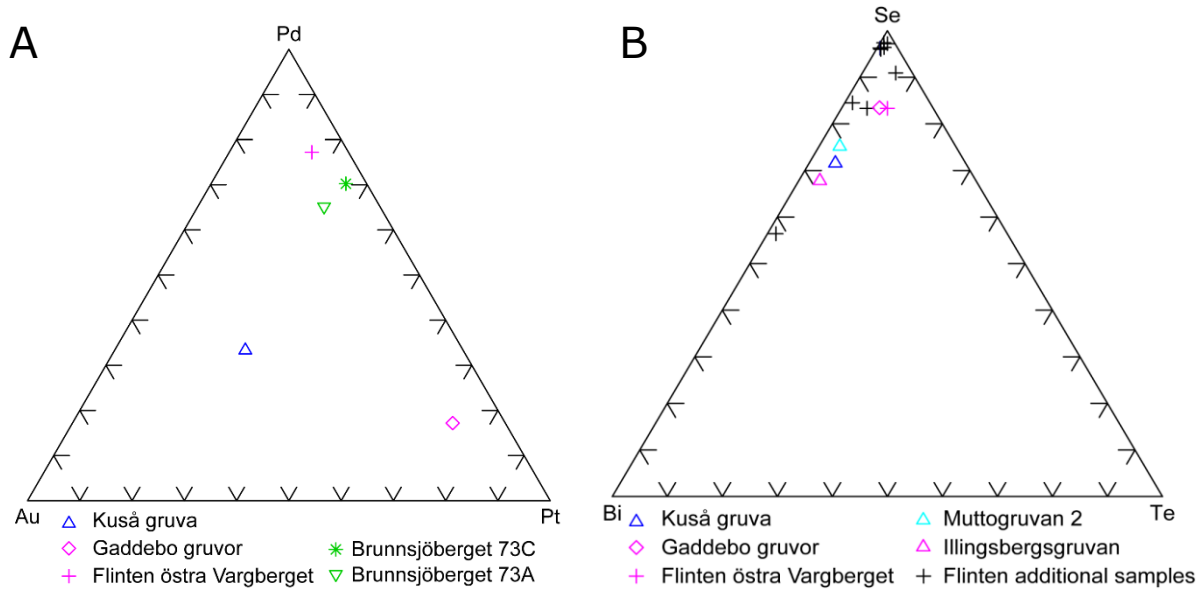

Figure 62. Ternary diagram of mineralised, gabbroid rocks from the mines at Flinten, Kuså, Gaddebo, and Brunnsjöberget. **A.** Au-Pd-Pt and **B.** Bi-Se-Te.

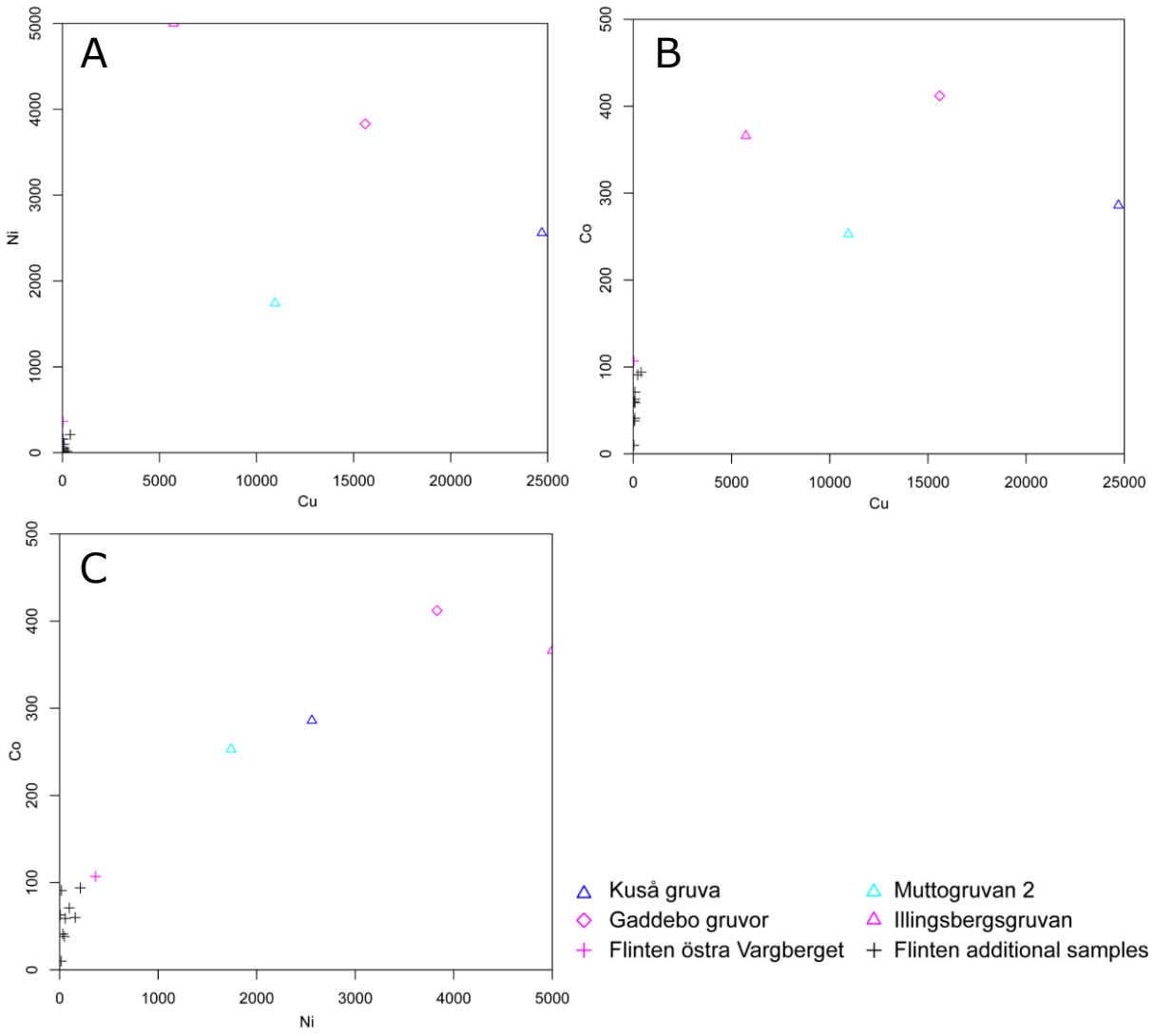

Figure 63. Plots of lithogeochemical data from the Flinten intrusion and mines at Kuså and Gaddebo. All values in ppm. **A.** Copper versus nickel. **B.** Copper versus cobalt. **C.** Nickel versus cobalt.

Table 9. Selected lithogeochemical results for Ni-Cu-(PGE) sulphide mines and Brunnsjöberget.

	23 Kuså	24 Mutt	25 Illi	30 Gadd	Brun73A	Brun73C
SiO2	42.6	47	42.8	38	45.6	42.6
Al2O3	6.2	6.59	5.68	5.17	7.18	8.91
Fe2O3	21.7	20	21.1	26.5	9.55	13.25
CaO	8.55	6.33	7.07	10.15	17.85	15.3
MgO	13.8	12.65	17.7	11.05	15.6	13.6
Na2O	0.67	0.67	0.31	0.62	0.25	0.33
K2O	0.49	1.11	0.43	0.34	0.04	0.08
TiO2	0.24	0.24	0.23	0.35	0.27	0.28
MnO	0.22	0.21	0.18	0.12	0.15	0.13
P2O5	0.04	0.01	0.01	0.04	0.005	0.03
Cr	1 390	420	440	1 470	1 410	930
Ni	2 560	1 740	5 000	3 830	785	1 990
Cu	24 700	10 950	5 730	15 600	2 080	6 000
Au	0.045	0.03	0.045	0.096	0.058	0.082
Pt	0.027	<0.005	<0.005	0.694	0.131	0.531
Pd	0.036	0.002	0.007	0.164	0.353	1.445
Co	286	253	366	412	60.1	155.5
Pt:Pd	1:1.33	N.A.	N.A.	1:0.24	1:2.69	1:2.72
mg#	55.7	55.6	62.4	45.2	76.4	67.0
Co#	1.0	2.0	3.3	2.1	2.1	1.9
Ni#	9.4	13.7	46.6	19.7	27.4	24.9
Ni/Cu	0.1	0.2	0.9	0.2	0.4	0.3
S/Se	2770	3900	3480	4190	2890	2990
Sb	0.07	0.09	<0.05	0.24	0.025	0.07
As	20	3.5	0.9	3.7	0.05	0.3

Co# = 100*Co/(Co+Ni+Cu), Ni# = 100*Ni/(Ni+Cu), mg# = 100* MgO/(FeO+MgO) [mol%]

Table 10. Normative values for Ni-Cu-(PGE) sulphide mines and Brunnsjöberget according to CIPW.

	23 Kuså	24 Mutt	25 Illi	30 Gadd	Brun73A	Brun73C
Q	4.461	10.705	2.632	3.574	0	0
Or	2.896	6.56	2.541	2.009	0.236	0.473
Ab	5.669	5.669	2.623	5.246	2.115	2.792
An	12.463	11.696	12.837	10.32	18.351	22.594
Di	22.463	14.639	16.636	30.011	53.89	40.586
Hy	23.964	24.726	36.381	13.614	6.049	11.292
Ol	0	0	0	0	5.487	2.644
Ilm	0	0	0	0	0	0
Hm	21.702	20.002	21.102	26.502	9.551	13.251
Tn	0.589	0.589	0.565	0.859	0.663	0.687
Ap	0.095	0.024	0.024	0.095	0.012	0.071
Py	0.372	0.355	0.304	0.203	0.254	0.22
Sum	94.67	94.96	95.64	92.43	96.61	94.61

Table 11. Normative values for Ni-Cu-(PGE) sulphide mines and Brunnsjöberget according to CIPW with hornblände.

	23 Kuså	24 Mutt	25 Illi	30 Gadd	Brun73A	Brun73C
Q	3.129	12.831	1.883	1.84	0	0
Ab	5.669	5.669	2.623	5.246	0	0
An	12.462	11.695	12.836	10.319	18.35	22.593
Wo	0	0	0	4.873	11.431	6.734
Ilm	0	0	0	0	0	0
Hm	21.702	20.002	21.102	26.502	9.551	13.251
Ap	0.095	0.024	0.024	0.095	0.012	0.071
Py	0.372	0.355	0.304	0.203	0.254	0.22
Bi	4.154	9.41	3.645	2.882	0.339	0.678
Hbl	42.392	28.043	31.655	40.122	61.271	53.039
Sum	89.98	88.03	74.07	92.08	101.21	96.59

External lithogeochemical data for the sulphide mines at Kuså and Gaddebo

Rolling Road Exploration Sweden AB have two exploration permits at Kuså, no. 3 and no. 4 running until 2023–02–03 and 2023–04–29, respectively. The no. 3 permit refers to cobalt, gold, silver, copper, zinc, lead, nickel, ruthenium, rhodium, palladium, osmium, iridium, and platinum. The no. 4 permit to cobalt, gold, silver, copper, nickel, ruthenium, rhodium, palladium, osmium, iridium, and platinum. At Kuså no. 1, Northern Lion Gold Sweden AB had an exploration permit in 2005–2008 regarding copper. Lithogeochemical data from waste rock samples were reported. Ragnar Metals Ltd. had exploration permits (nickel, copper) for Kuså no. 2 during the years 2013 to 2016, but no data are reported.

Ragnar Metals Ltd. had an exploration permit for Gaddebo no. 3 until 2020–10–30, which was positioned in parts at the historic sulphide mine. The permit referred to nickel, iron, copper, and lead. Rolling Road Exploration Sweden AB has an exploration permit for Gaddebo no. 4 until 2023–08–28, which is positioned adjacent to but outside of the area of Gaddebo no. 3. The permit refers to cobalt, gold, silver, copper, nickel, ruthenium, rhodium, palladium, osmium, iridium, and platinum. Expired permits have belonged to Dannemora Mineral AB (Gaddebo 2007–2013, Gaddebo no. 2 2008–2014, both related to nickel. In connection with these, Dannemora Mineral AB performed ground magnetometry, core drilling and mapping of these, as well as lithogeochemical analyses of drill cores and waste rock.

Levels of gold up to 0.47 ppm, platinum 0.68 ppm and palladium 0.58 ppm are reported from Gaddebo, only gold from Kuså and then at low levels around 0.06 ppm. Figure 64 shows parts of the analysis results received from the above-mentioned surveys and deposited at the SGU. Cobalt-bearing pentlandite is the probable cause of the positive linear relationship between Co and Ni in these sulphide mines and not olivine, as suggested earlier in the text for the ultrabasic rocks in the sample from the Karlsborg mine, Furulund intrusion (fig. 64C).

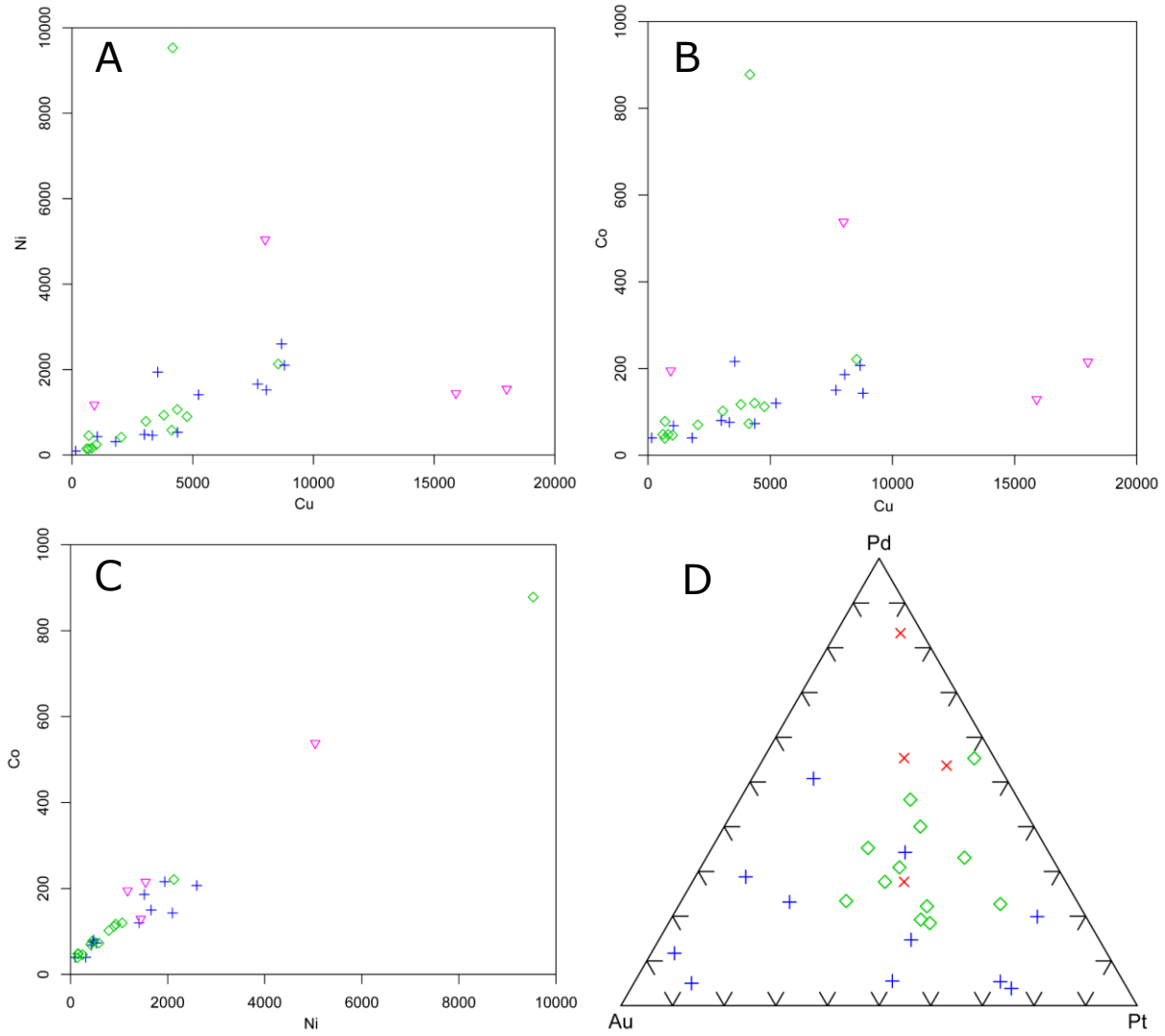

Figure 64. Plots of external lithogeochemical data from sulphide mines at Gaddebo (blue pluses and green diamonds show values from drill cores, and red crosses values from waste rock, analyses only for Au, PGE) and Kuså (light purple triangles show values from waste rock). **A.** Copper versus nickel. **B.** Copper versus cobalt. **C.** Nickel versus cobalt. **D.** Ternary diagram Au-Pd-Pt. All values in ppm.

DISCUSSION AND CONCLUSIONS

The mafic intrusions in the Bergslagen region show promising evidence that both base metals like nickel and copper along with PGE may occur in economically significant concentrations. However, not much is known about the extent of the mineralisations or the extractability of particular minerals or elements. Even though no PGE mining has occurred in the Bergslagen region, this study shows that there is potential, both in larger layered basic intrusions and in nickel-copper sulphide mines of the Bergslagen area. The known nickel-copper sulphide mines are often positioned in smaller, gabbroic intrusive bodies and thus show no apparent relation to the larger layered intrusions. However, to date, the geometry of these magmatic systems is unknown and therefore it is unknown if they might have any connection to larger magmatic bodies at greater depth.

Within this study, the geometry of the magmatic layering within both the Flinten and Fullen intrusions has been interpreted, based primarily on airborne magnetic field data and outcrop observations. Furthermore, the magnetic response of the layering has been modelled in 2-dimensions, and in the case of the Flinten intrusion 3-dimensions. Magnetic measurements made over a small focus area at the Fullen intrusion show excellent correlation between the orientation of the magnetic anomalies and magmatic layering in outcrop, fully supporting these interpretations. At the Flinten intrusion, however, the observations and magnetic measurements from a small focus area show a more complex relationship. This indicates that although the layering geometry interpreted from airborne data at Flinten is likely to be representative on a large scale, it can have a more complex geometry when considering a smaller scale. The characterization of the layering of these intrusions, albeit on a large scale, can be useful information for future geophysical and geological investigations. For example, it provides a means for predicting the orientation of any potential stratabound sulphide deposits which could be associated with PGEs and precious metals. This can be useful to design and optimise future investigation methods, such as ground-based electromagnetic measurements.

Based on the airborne and ground-based electromagnetic measurements presented in this study, several zones with lower resistivity values than their surroundings have been highlighted. In some cases, these zones appear to lie subparallel with the interpreted direction of magmatic layering. Such areas could be of interest for further investigation.

An interpretation of the structure of the Flinten intrusion is presented in this study, based on the observed layering direction, airborne magnetic measurements, and gravity data. In this interpretation the intrusion is divided into five regions, which are interpreted to represent individual sub-intrusions. Based on their geophysical characteristics, these regions can be gathered into two groups (three northern regions and two southern regions), where the sub-intrusions within each group are interpreted to be coeval. 2- and 3-dimensional modelling of the gravity and magnetic data support this interpretation. This characterization could be interesting to explore further, as it could indicate systematic differences in the chemistry and physical properties within the different parts of the intrusion. However, it is important to note that before such an interpretation can be substantiated more data (e.g. geochemical and petrophysical samples) would need to be collected and analysed.

Further investigations of the basic intrusions within the Bergslagen region could include extensive ground-geophysical measurements, comprehensive lithogeochemical sampling and analyses, determination of minerals and their composition, texture, structural geology, and when a potential sulphide mineralisation is located even core drilling. However, such investigations were not performed as part of this project due to costs and time constraints.

The financial cost of this initial assessment of the economic potential of layered intrusions in the Bergslagen region has been relatively low. Despite this, the methods and approach applied in this report have proven to be effective in characterising the structure, chemistry, and physical properties of these intrusions and hence, would be good to utilize in future investigations of mafic intrusions, within Sweden or elsewhere. This study also provides an example of what can be achieved when the extensive data within SGU's databases are leveraged together with new data from relatively small scale but focused ground-based investigations.

REFERENCES

Boynton, W.V., 1984: Cosmochemistry of the Rare Earth Elements: Meteorite studies. *In* P. Henderson (ed.): *Rare earth element geochemistry. Elsevier Science B.V.,* 63–114.

Claeson, D., Antal Lundin, I., Sadeghi, M., Persson, S. & Jönsson, C., 2018: Sammanfattning av pågående verksamhet 2017. Berggrundsgeologisk undersökning, Ludvika, Bergslagen etapp1. SGU-rapport 2018:12. Sveriges geologiska undersökning, 1–66.

Claeson, D., Sadeghi, M., Jönberger, J., Persson, L. & Bastani, M., 2019: Sammanfattning av pågående verksamhet 2018. Berggrundsgeologisk undersökning, Ludvika, Bergslagen etapp1. SGU-rapport 2019:16. Sveriges geologiska undersökning, 1–72.

De la Roche, H., Leterrier, J., Grandclaude, P. & Marchal, M., 1980: A classification of volcanic and plutonic rocks using R_1R_2-diagram and major-element analyses – Its relationships with current nomenclature. *Chemical Geology 29*, 183–210.

Ehlers, K., Grove, T.L., Sisson, T.W., Recca, S.I. & Zervas, D.A., 1992: The effect of oxygen fugacity on the partitioning of nickel and cobalt between olivine, silicate melt, and metal. *Geochimica et Cosmochimica Acta 56*, 3733–3743.

Ferré, C.E., Maes, S.M. & Butak, K.C., 2009: The magnetic stratification of layered mafic intrusions: Natural examples and numerical models. *Lithos 111*, 83–94.

Ferris, J., Johnson, A. & Storey, B., 1998: Form and extent of the Dufek intrusion, Antarctica, from newly compiled aeromagnetic data. *Earth and Planetary Science Letters 154*, 185–202.

Filén, B., 1990: PGE-prospektering i Sverige 1985–1990. *PRAP 90026*, Sveriges geologiska AB, 1–67.

Filén, B., Ekström, M., Lundmark, L.-G. & Renberg, A., 1989: PGE-prospektering 1989. *PRAP 89061*, Sveriges geologiska AB, 1–17.

Filén, B., Lundmark, L.-G., Renberg, A. & Åkerman, C., 1988: PGE-Ni-prospektering 1988. *PRAP 88066*, Sveriges geologiska AB, 1–25.

Finn, C., Zientek, M.K., Bloss, B.R., Wintzer, N.E. & Parks, H.L., 2013: Geophysical imaging of the Stillwater complex and relation to platinum group element exploration. *Geological Society of America Abstracts with Programs* 45 (7), 277.

Finn, A.C., Bedrosian, P.A., Cole, J.C., Khoza, T.D. & Webb, S.J., 2015: Mapping the 3D extent of the Northern Lobe of the Bushveld layered mafic intrusion from geophysical data. *Precambrian Research 268*, 279–294.

Geijer, P., 1917: Falutraktens berggrund och malmfyndigheter. *Sveriges geologiska undersökning C 275,* 1–316.

Granar, L. & Henkel, H., 1981: Sammanställning och tolkning av mätresultat från fältövningen 1981 mm över indikationen vid Sparvguldsberget i området 13 G 5-6 b-c. *BRAP 81421*, Sveriges geologiska undersökning, 1–62.

Grip, E., 1961: Geology of the nickel deposit at Lainejaur in northern Sweden and a summary of other deposits in Sweden. *Sveriges geologiska undersökning C 577,* 1–79.

Hammergren, P., 1982: Sparvguld. *BRAP 82523*, Sveriges geologiska undersökning, 1–3.

Herzberg, C., Vidito, C. & Starkey, N.A., 2016: Nickel–cobalt contents of olivine record origins of mantle peridotite and related rocks. *American Mineralogist 101*, 1952–1966.

Högdahl, K., Sjöström, H. & Bergman, S., 2009: Ductile shear zones related to crustal shortening and domain boundary evolution in the central Fennoscandian Shield. *Tectonics 28*, 1–18.

Irvine, T.N., & Baragar, W.R.A., 1971: A guide to the chemical classification of common volcanic rocks. *Canadian Journal of Earth Sciences 8*, 523–548.

Janousek, V., Farrow, C.M. & Erban, V., 2006: Interpretation of whole-rock geochemical data in igneous geochemistry: Introducing Geochemical Data Toolkit (GCDkit). *Journal of Petrology 47*, 1255–1259.

King, A., 2007: Review of Geophysical Technology for Ni-Cu-PGE deposits. *Proceedings of Exploration 07: Fifth Decennial International Conference on Mineral Exploration,* 647–665.

Kulling, O. & Hjelmqvist, S., 1948: Beskrivning till kartbladet Falun. *Sveriges geologiska undersökning Aa 189,* 1–184.

Lindholm, T., 1990: Flinten djupmorän-och bergkaxprovtagning. *PRAP 90007*, Sveriges geologiska undersökning, 1–4.

Löfstrand, G., 1903: Slättbergs och Kuso nickelgrufvor. *Geologiska Föreningen i Stockholm Förhandlingar 25,* 103–122.

Maes, S.M., Tikoff, B., Ferré, C.E., Brown, P.E. & Miller, J.D., 2007: The Sonju Lake layered intrusion, northeast Minnesota: Internal structure and emplacement history inferred from magnetic fabrics. *Precambrian Research 157*, 269–288.

Magnusson, N.H., 1973: *Malm i Sverige 1. Mellersta och södra Sverige*. Almqvist & Wiksell, Stockholm. 1–320.

McEnroe, S.A., Brown, L.L. & Robinson, P., 2009: Remanent and induced magnetic anomalies over a layered intrusion: Effects from crystal fractionation and magma recharge. *Tectonophysics 478*, 119–134.

Nilsson, G., 1985: Nickel-copper deposits in Sweden. *In* H. Papunen & G.I. Gorbunov (eds.): Nickel-copper deposits of the Baltic Shield and Scandinavian Caledonides. *Geological Survey of Finland Bulletin 333,* 313−362.

Pirajno, F., 2009: *Hydrothermal Processes and Mineral Systems*. Springer, 1–1250.

Ripa, M., Kampmann, T.C. & Hellström, F.A., 2017: SIMS U-Pb zircon geochronology at the Kuså Ni-Cu deposit, south-central Sweden. *GFF 139*, 233–240.

Sun, S.S. & McDonough, W.F., 1989: Chemical and isotopic systematic of oceanic basalts: implications for mantle composition and processes. *In* A.D. Saunders & M.J. Norry (eds.): *Magmatism in ocean basins. Geological Society of London, Special Publication 42,* 313–345.

Stephens, M.B., Ripa, M., Lundström, I., Persson, L., Bergman, T., Ahl, M., Wahlgren, C.-H., Persson, P.-O. & Wickström, L., 2009: Synthesis of the bedrock geology in the Bergslagen region, Fennoscandian shield, south-central Sweden. *Sveriges geologiska undersökning Ba 58,* 1–259.

Wik, N.-G., Albrecht, L., Bergman, S., Kübler, L. & Sundberg, A., 2009: Malmer, industriella mineral och bergarter i Gävleborgs län*., Rapporter och meddelanden 130,* Sveriges geologiska undersökning, 1–310.

Wik, N.-G., Stephens, M.B. & Sundberg, A., 2006: Malmer, industriella mineral och bergarter i Uppsala län. *Rapporter och meddelanden 124,* Sveriges geologiska undersökning, 1–223.

Zakrzewski, M.A., 1989: Sperrylite from the Ni-Cu sulphide deposit of Kuså, Sweden. *Geologiska Föreningens i Stockholm Förhandlingar 111,* 100.